TÉCNICO LISBOA

Thymus architecture in primary immunodeficiency and leukemogenesis

Mariana Esteves Ávila

Thesis to obtain the Master of Science Degree in

Biological Engineering

Supervisors: Dr. Vera Sofia Correia Martins

Dr. Nuno Filipe Santos Bernardes

Examination Committee

Chairperson: Prof. Cláudia Alexandra Martins Lobato da Silva

Supervisor: Dr. Vera Sofia Correia Martins

Member of the Committee: Dr. Nuno Miguel de Oliveira Lages Alves

October 2018

Preface

The work presented in this thesis was performed at Instituto Gulbenkian de Ciência (Oeiras, Portugal), during the period February-September 2018, under the supervision of Dr. Vera Martins. The thesis was co-supervised at Instituto Superior Técnico by Dr. Nuno Bernardes.

Declaration

I declare that this document is an original work of my own authorship and that it fulfils all the requirements of the Code of Conduct and Good Practices of the Universidade de Lisboa.

Acknowledgements

I consider myself a lucky person for having so many special people in my life that helped me through these five years of learning and growth as a person, so this section is dedicated to them.

My supervisor Vera Martins, for all the support, orientation, corrections, patience and teaching about this beautiful world of immunology;

My supervisor Nuno Bernardes for the support and counseling;

Luna Ballesteros-Arias, Carolina Alves, Vasco Correia, Rafael Paiva, Camila Ramos, Mayra Martinez-Lopez and Ana Teresa Pais, my laboratory group colleagues, for helping me with my first steps in the laboratory and to make me feel like I was part of the group. Your support was crucial and I knew that with you I would never feel lost. Your kindness and support through all this months was really touching and I feel that I have made good friends in this experience. Rafael, I want to thank you specially for being so patient and available to help me with my corrections;

Gabriel, Nuno and Hugo from the Advanced Imaging Facility for helping me with the microscopy and with all the problems that I had with the images acquisition and treatment;

Joana, from the Histopathology Unit, that was an angel with all the thymus sectioning that I asked her to do. I know I asked her for too much, but she never said no to me;

The Flow Animal House Facility and the Flow Cytometry Facility, thank you for providing all the mice and the help with the cytometer.

Catarina Costa, Inês Brilhante, Inês Ferreira, Mafalda Santos: You were my “family” during this five years and with you I felt that I would never be alone. We got through so much together, we laughed, we cried, we studied, we celebrated. You were my “home” when I felt homesick. Thank you for your friendship, that will now be forever;

My family, but especially my mother and father. Thank you for always teaching me how to fight for my goals, for giving me the chance to study and to always give me the best conditions possible during these 5 years. Without your love, friendship, and unconditional support, none of this was possible.

This thesis is dedicated to all of them, but also to my aunt Natal, who I miss a lot. She was amazing, one of the strongest persons I have known, and always put family first. I chose to work on this topic because it is very touching for me since I relate it to the way she left us. Thank you for inspiring me to contribute with studies on the cancer field.

Abstract

T lymphocyte development takes place in the thymus and relies on the constant seeding by bone marrow-derived progenitors. After arrival into the thymus, these progenitors commit to the T lymphocyte lineage and further differentiate to originate T lymphocytes. This is a rather complex process in which thymocytes migrate throughout the thymus, and according to the specific differentiation stage at which they are, occupy defined niches where they receive the necessary signals for further progression. Thymic epithelial cells (TEC) create these specialized niches in the thymus and are therefore essential for T lymphocyte development. Indeed, defects in the development of TEC impact T lymphocytes. The opposite is also true, and cell-autonomous defects in T lymphocyte development impact TEC development. This work has addressed the architecture of the thymus, i.e. its cellular structure in immunodeficiency and during leukemogenesis. Specifically, I analyzed histologically the thymus of immunodeficient mice and found that defects in T lymphocyte development led to impairments in TEC differentiation. Furthermore, using a model that involves thymus transplantations, we have analyzed the progression of a normal thymus during leukemogenesis. We observed that thymus structure is fully conserved while thymopoiesis is normal, but this changes with time, when pre-leukemic cells emerge and progress to T-cell acute lymphoblastic leukemia. Taken together, results show that defects in T lymphocyte development lead to impairments in TEC differentiation. Progression towards leukemia impacts both T cells and TEC. Further research is needed to clarify which of the described abnormalities precedes the other.

Keywords: T cell development, thymus development**,** thymic epithelial cells, primary immunodeficiencies, thymus autonomy, T-cell acute lymphoblastic leukemia.

Resumo

O desenvolvimento de linfócitos T ocorre no timo e depende da constante colonização de progenitores derivados da medula óssea. Após chegada ao timo, estes progenitores restringem-se à linhagem de linfócitos T e diferenciam-se para originarem os mesmos. Isto é um processo complexo no qual timócitos migram no timo, e de acordo com o estadio de diferenciação ocupam nichos específicos onde recebem os sinais essenciais para continuar a diferenciar-se. As células epiteliais do timo (TEC) estabelecem estes nichos e são, portanto, essenciais para o desenvolvimento de linfócitos T. Defeitos no desenvolvimento das TEC impactam nos linfócitos T. Analogamente, defeitos celulares autónomos no desenvolvimento de linfócitos T também influenciam o desenvolvimento das TEC. Este trabalho abordou a arquitectura do timo, i.e., a sua estrutura celular em imunodeficiência e no desenvolvimento de leucemia. Especificamente, analizei histologicamente o timo de ratinhos imunodeficientes e constatei que defeitos no desenvolvimento de linfócitos T causaram deficiências na diferenciação das TEC. Inclusivamente, usando um modelo que envolve transplantes de timo, analizámos a progressão de um timo normal durante o desenvolvimento de leucemia. Observámos que a estrutura do timo é conservada enquanto a timopoiese é normal, mas altera-se com o tempo, à medida que células pré-leucémicas emergem e progridem para leucemia linfoblástica aguda de células T. Globalmente, os resultados mostram que defeitos no desenvolvimento de linfócitos T causam deficiências na diferenciação das TEC e a progressão para leucemia impacta mutuamente nas células T e nas TEC. É necessária mais pesquisa para clarificar qual das anormalidades descritas precede a outra.

Palavras-chave: Desenvolvimento de linfócitos T, desenvolvimento do timo, células epiteliais do timo, imunodeficiências primárias, autonomia do timo, leucemia linfoblástica aguda de células T.

Contents

Figure Index

Abbreviations

Bcl-2- B-cell lymphoma 2

CCL17- C-C motif ligand 17

CCL19- C-C motif ligand 19

CCL21- C-C motif ligand 21

CCL25- C-C motif ligand 25

CCR7- C-C receptor 7

CCR9- C-C receptor 9

cTECs- Cortical thymic epithelial cells

CXCL12- C-X-C motif chemokine 12

DCs- Dendritic cells

DLL4- Delta-like 4 ligand

DN 1- Double Negative 1

DN 2- Double Negative 2

DN 2a- Double Negative 2 early

DN 2b- Double Negative 2 late

DN 3- Double Negative 3

DN 3a- Double Negative 3 early

DN 3b- Double Negative 3 late

DN 4- Double Negative 4

DP- Double Positive

ETP- Early T-cell precursor

FBS- Fetal bovine serum

FACS- Fluorescence-activated cell sorting

Foxn1- Forkhead box protein N1

IGC- Instituto Gulbenkian de Ciência

IL-7- Interleukin-7

IL-7r- Interleukin-7 receptor

IL-7rα- Interleukin-7 receptor α chain

ILC- Innate lymphoid cells

Intercellular adhesion molecule 1- ICAM-1

ISP- Immature Single Positive

ITAM- Immunoreceptor tyrosine-based activation motif

JAK3- Janus-activated kinase 3

K5- Keratin 5

K8- Keratin 8

MALTs- Mucosa-associated lymphoid tissues

MHC- Major Histocompatibility Complex

mTECs- Medullary thymic epithelial cells

NK- Natural killer

OCT- Optimal cutting temperature

PBS- Phosphate-buffered saline

PGE- Promiscuous gene expression

Rag- Recombination-activating gene

RT- Room temperature

SCID- Severe combined immunodeficiency

SP- Single Positive

T-ALL- T-cell acute lymphoblastic leukemia

TCR- T cell receptor

TECs- Thymic epithelial eells

TEPs- Thymic epithelial cell progenitors

TRAs- Tissue-restricted antigens

Treg- Regulatory T cells

TSPs- Thymic seeding progenitors

V(D)J- Variable Diversity Joining

VCAM-1- Vascular cell adhesion protein 1

WT- Wild-type

XSCID- X-linked severe combined immunodeficiency

γc- Common cytokine receptor γ chain

Introduction

The Adaptive Immune System

The immune system is responsible for the recognition and elimination of pathogens, and of abnormal cells, including those that can lead to cancer. It can be subdivided in the adaptive and the innate immune systems. Although this subdivision is somewhat artificial because the two systems interconnect, it eases their study because they differ for some very general principles. While the innate immune responses to pathogens are developed after recognition of conserved patterns, adaptive immune responses are based on the recognition of specific antigens. Additionally, the adaptive immune system has immunological memory, i.e., after the first interaction with a pathogen, B and T lymphocytes are capable of recognizing it as a reinvasion, mounting a faster and more efficient immunological response [1][2].

The cellular components of the innate immune system include macrophages, granulocytes, and natural killer (NK) cells. These cells have pattern recognition receptors encoded by genes inherited from the parents and do not undergo somatic rearrangements. The adaptive immune system is composed of B and T lymphocytes. In contrast with the cells of the innate immune system, B and T lymphocytes are special in the sense that they undergo somatic recombination of the loci that encode for the B and T cell receptors (BCR and TCR), respectively. These are the receptors that make each cell highly specific (every cell has one receptor with one specificity), but the pool of cells is so large, that altogether they are highly diverse. Although similar, B and T lymphocytes are not the same, and differ in the type of receptor, how they recognize the antigens, and in the mechanism of action. B lymphocytes recognize antigens by direct binding, while T lymphocytes require the antigens to be presented in a complex of a short peptide-Major Histocompatibility Complex (MHC) at the surface of antigen-presenting cells (APCs). These peptides are fragments of larger peptides or proteins. Before this interaction T lymphocytes are called naïve T lymphocytes and have low functionality.

T lymphocytes can be broadly sub-divided into three groups: cytotoxic, helper and regulatory T lymphocytes. Cytotoxic T lymphocytes create immune responses against cells infected with intracellular pathogens or against aberrant cells. Infected cells display the antigens of the pathogen in their MHC complexes, and these can be recognized by the TCR of cytotoxic T lymphocytes, which kill the infected cells directly. T helper lymphocytes recognize foreign antigens that were uptaken by phagocytosis and are displayed in peptide-MHC complexes by APCs. Then, T helper lymphocytes activate other cells of the immune system such as macrophages or B lymphocytes. The macrophages will eliminate the infected cells through phagocytosis. B lymphocytes will differentiate into plasma cells and produce antibodies that bind to the foreign antigens. These antibodies mediate the immune response in one of three mechanisms: neutralization, opsonization or complement activation. They can inactivate virus particles and bacterial cells; they can be recognized by the macrophages or neutrophils that will ingest and destroy them; or the antibodies together with complement proteins will cause the formation of pores that lead to the lysis of bacteria. Lastly, regulatory T lymphocytes (Treg) are

responsible for limiting the immune response. The end of the immune response happens when Tregs produce inhibitory cytokines that limit the proliferation and activity of the effector T lymphocytes and also when they interact with dendritic cells (DCs) stimulating these cells to produce enzymes that are toxic to T lymphocytes near them. Treg lymphocytes are also fundamental in preventing autoimmunity [2][3][4].

T Lymphocytes

T lymphocytes are derived from bone marrow progenitors and develop in the thymus, a primary lymphoid organ located in the thorax, above the heart. Histologically, the thymus is divided into an outer cortex and an inner medulla. In ontogeny, thymus organogenesis starts at embryonic day 9 and originates from the third pharyngeal pouch, a pocket of the foregut endodermal tube [5].

Two main lineages of T lymphocytes develop in the thymus: $\alpha\beta$ and $\gamma\delta$ T lymphocytes. These two lineages differ in the structure of their T-cell receptor (TCR) and function differently. While $\alpha\beta$ T lymphocytes have a TCR composed by a α and β chain, $\gamma\delta$ T lymphocytes have a TCR with a γ and a δ chain. It is proposed that $\gamma\delta$ T lymphocytes have different antigen-recognition properties and their role in the immune system is still not clear. This thesis focuses on $\alpha\beta$ T cells only.

T cells have an antigen receptor present in their surface that is termed T-cell receptor (TCR). The TCR is a heterodimeric protein composed by variable α and β chains, CD3 chains and accessory ζ chains (Fig. 1). Only after TCR-antigen interaction do T cells become effector T lymphocytes, and according to their function, they have different activities in the immune system. The identification and classification of αβ T lymphocytes can be made according to surface markers. If they express a CD8 co-receptor at their cell surface, they are termed cytotoxic T lymphocytes and are activated when their TCR interacts with peptides present in cells that express the MHC class-I. If they express a CD4 co-receptor at the cell surface, they are termed helper and are activated by the interaction between their TCR and the peptide-MHC complex class-II, present in the APCs [2]. Most regulatory T cells also express CD4.

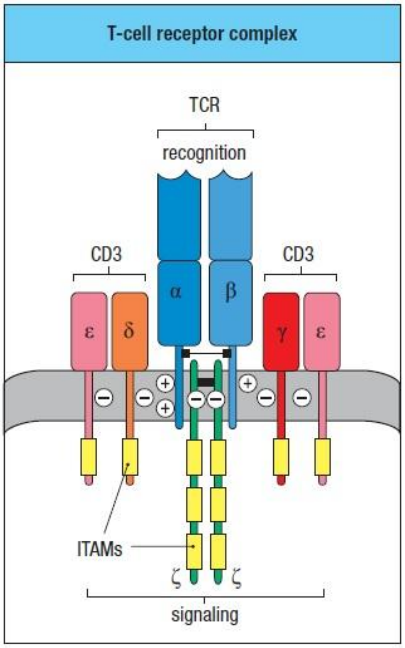

Figure 1- Structure of the TCR from αβ T lymphocytes. The αβ TCR is composed by one α and one β glycoprotein chains, two ζ chains and two CD3 complexes, each composed by one ε chain and a δ or γ chain, respectively. Figure taken from [2].

T Lymphocyte Development

T lymphocyte development relies on a life-long seeding of the thymus by pluripotent hematopoietic progenitors of bone marrow origin. These cells enter the thymus at the cortico-medullary junction, through postcapillary venules. Chemokines and adhesion molecules are important for the seeding and the migration of the cells within the thymus. The earliest population of T lymphocyte precursors (thymocytes) that can be identified in the thymus are still not committed to the T lymphocyte lineage and maintain the potential to give rise to natural killer cells (NK), dendritic cells (DCs), B cells and macrophages [6][7]. Only after reaching the thymus these progenitors commit to the T lymphocyte lineages and lose B lymphocyte potential [8].

Thymocytes can be subdivided in different stages of differentiation based on the expression of the CD4 and CD8 surface markers, namely $CD4^-CD8^-$ double negative (DN), $CD4^+CD8^+$ double positive (DP) and $CD4^+CD8^-$/ $CD4^-CD8^+$ single positive (SP). The most immature ($CD4^-CD8^-$) DN thymocytes can be further subdivided in DN1 to DN4 based on the differential expression of CD25 and CD44. DN1 are a heterogeneous population that contains the early T cell precursor (ETP), that express high levels of CD117. ETP ($CD44^+CD25^-CD117^+$) differentiate into DN2 ($CD44^+CD25^+CD117^{int}$)), then into DN3 ($CD25^+CD44^{lo/-}CD117^-$), and DN4 ($CD25^-CD44^-CD117^-$), and those into $CD4^+CD8^+$ double positive cells. The latter down-regulate either CD8 or CD4 at the end of the differentiation process, becoming $CD4^+CD8^-$ or $CD4^-CD8^+$ single positive (SP) cells, respectively (Fig. 2).

ETP reside at the cortico-medullary junction for approximately 10 days. They result directly from the proliferation that follows Notch1 signaling and their consequent commitment to the T cell

lineage. It is known that the ligand essential for this signaling pathway, in the thymus, is delta-like 4 (DLL4), which is expressed by the thymic epithelial cells (TECs) [9][10]. After this differentiation stage, the cells migrate into the thymic cortex and are at the DN2 stage, where gene rearrangement of the γ, δ and β loci of the T-cell receptor begins. The DN2 stage can be divided into DN2a ($CD4^-CD8^-CD44^+CD25^+CD117^{hi}$) and DN2b ($CD4^-CD8^-CD44^+CD25^+CD117^{int}$) and while differentiating from one stage to the other, T cell lineage commitment is completed through the expression of the tumor suppressor Bcl11b, with loss of NK cell potential. This is accompanied by the downregulation of CD117 expression. Bcl11b is also essential for cell survival [11].

The transition from the DN2b to the DN3 stage ($CD25^+CD44^{lo/-}CD117^-$) is accompanied by migration of the cells through the cortex towards the subcapsular zone. At the same time, they undergo an additional lineage decision between the αβ or γδ T cell lineage fate. The αβ lineage is more sensitive to Notch signaling than the γδ lineage [12][13]. At this point, Notch1 signaling is required while recombination of the locus encoding the TCR β chain take place. This recombination is somatic and occurs through rearrangement of Variable, Diversity and Joining (V(D)J) gene segments. Recombination activating genes -1 and -2 (*Rag*1 and *Rag*2) mediate this process and only cells that successfully rearrange the β chain transit from the DN3-early to the DN3-late stage. The pre-TCR is composed by a successfully rearranged TCRβ chain, an invariant pre-TCRα (pTα), and CD3 [14].

While migrating back through the cortex, thymocytes progress to the DN4 stage ($CD24^+CD25^-CD44^-CD117^-$) and after pre-TCR signaling cells upregulate CD4 and CD8. At this point thymocytes mature to the Double Positive (DP) stage where recombination of the locus encoding the TCR α chain, with rearrangements of the V and J segments takes place [15]. After the correct assembly, the αβTCR will be tested for its capacity to recognize self-peptide-MHC complexes. Only those cells that can recognize self will be positively selected and progress differentiation. The majority of thymocytes fail positive selection and die by neglect at this stage. Those thymocytes that were positively selected, will have self-MHC-restricted TCRs, and commit to become either CD4 ($CD4^+CD8^-$) or CD8 T cells ($CD4^-CD8^+$). Single positive thymocytes migrate into the medulla and are tested for the level of affinity of their TCRs for self-antigens (Fig. 2). All thymocytes recognizing self with a strong affinity are negatively selected. Only thymocytes with TCRs that recognize and are tolerant to self survive and are exported from the thymus as naïve CD4 or CD8 T cells. After T lymphocyte development, the cells are exported to secondary lymphoid organs, such as the spleen, lymph nodes and mucosa-associated lymphoid tissues (MALTs).

While success of T lymphocyte development is essential for a healthy individual, failure to do so can have severe consequences. The scope of such problems is broad and can go from primary immunodeficiencies, in which the immune system is non-functional, to autoimmunity, in which the immune system reacts against self, or leukemia, in which cancer evolves from thymocytes

or T lymphocytes [14].

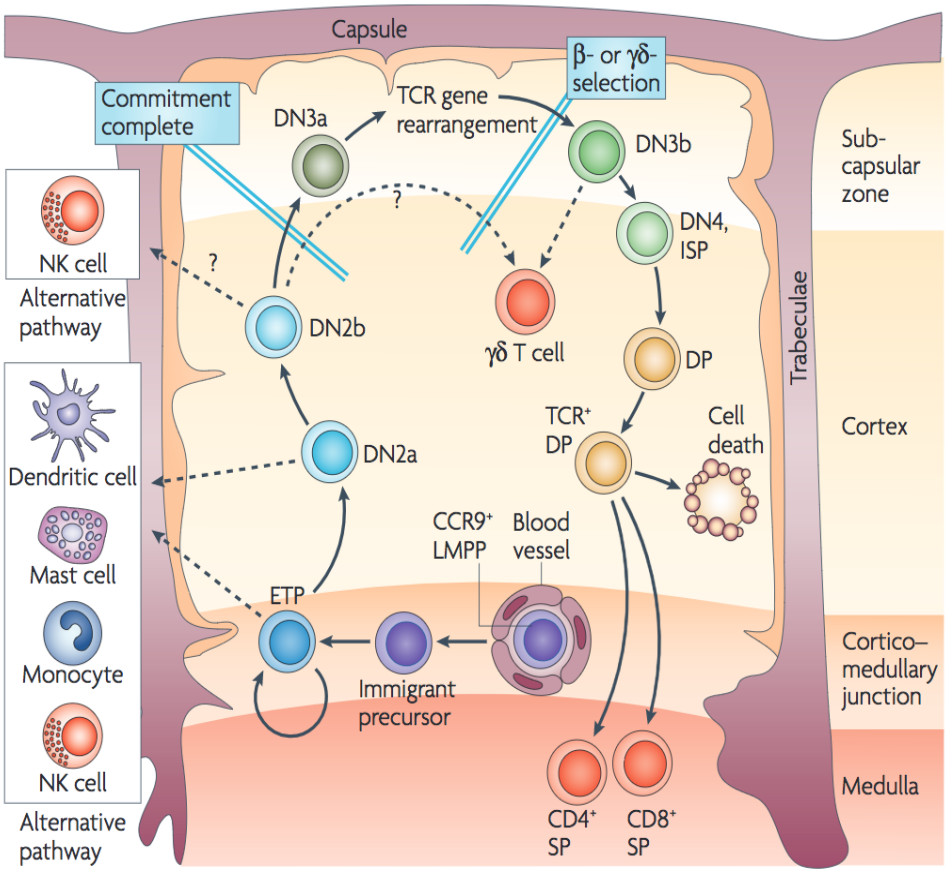

Figure 2- Overview of T lymphocyte development. The migration pattern of thymocytes in the thymus is associated with different stages of commitment, development and selection. Progenitors of bone marrow origin enter the thymus at the cortico-medullary junction. Following this stage, cells differentiate to DN2 and migrate through the cortex towards the subcapsular zone, where most DN3 thymocytes accumulate. $CD4^+CD8^+$ double positive cells (DP) occupy the majority of the cortex and are submitted to positive selection. CD4 or CD8 single positive (SP) thymocytes migrate into the medulla, where they undergo negative selection, and from where they are exported to the periphery. Figure taken from [5].

Thymic Epithelial Cells

The thymic stroma is composed by fibroblasts, macrophages, mesenchymal, endothelial, epithelial and dendritic cells. In particular, thymic epithelial cells (TECs) are essential to T cell development since they express the signaling molecules and produce the survival factors that constitute the different microenvironments necessary for several stages of differentiation. It is well-accepted that the migration pattern of thymocytes is associated with their progressive differentiation, and that migration enables them to occupy the correct niches where they are provided with the correct signals, essential for differentiation.

The thymic epithelium originates from the endoderm of the third pharyngeal pouch and requires Forkhead box protein N1 (Foxn1). Studies using *Foxn1*^{nu} mice, which have a defect in *Foxn1*, revealed that thymus organogenesis is profoundly abrogated and TEC fail to differentiate. As a consequence of the lack of thymic epithelium, T lymphocytes also fail to develop [16]. Indeed, it

is known that Foxn1 is required for TEC identity at all ages. Within TECs, cortical thymic epithelial cells (cTECs) are present in the cortex and medullary thymic epithelial cells (mTECs) in the medulla. These two cell subsets arise from thymic epithelial cell progenitors (TEPs) in the early thymus anlage and several models of differentiation have been suggested, in which the progenitors have bipotent potential to give rise to the two lineages [17]. These two subsets can be distinguished by the differential expression of markers such as keratin 8 (K8), Ly51 or β5t by cTECs and keratin 5 (K5), MTS10, by mTECs [18].

Cortical TECs are essential in the most immature stages of T cell development. Expression of chemokines such as CCL21 and CXCL12 by cTECs mediates the migration of progenitors to the cortico-medullary junction and the beginning of T cell production. Expression of DLL4 by TEC is essential for Notch1 signaling, that leads to commitment to the T cell lineage. Expression of IL-7 and Kit ligand are essential for survival and proliferation. Transition from ETP to the DN2 stage happens in cortical niches, and the cells migrate through the cortex in response to the gradient of CCL25 generated by cTEC, with the help of adhesion molecules like VCAM-1 and E-cadherin by the thymocytes. Following this gradient, thymocytes progress to the DN 3 stage of differentiation, that accumulate at the subcapsular zone. While migrating back to the cortex and differentiating into the double positive stage, IL-7, CCL25, intercellular adhesion molecule 1 (ICAM-1) and MHC are also necessary. At this point, thymocytes undergo positive selection as the consequence of interaction between TCR and self peptide-MHC complexes, expressed by cTECs. Positively selected thymocytes become single positive and migrate into the medulla in response to the chemokine gradient of the C-C motif ligand 17 (CCL17), C-C motif ligand 19 (CCL19) and C-C motif ligand 21 (CCL21). Thymocytes undergo, then, negative selection as result of the interaction with mTECs and dendritic cells, where the avidity of the TCR for self-antigens is tested [19][20].

Positive and Negative Selection

Thymocytes expressing unique TCRs have to be tested for efficacy and safety before they can leave the thymus as naïve T cells. Some of these cells express TCRs that fail to recognize self peptide-MHC complexes. These cells are, therefore, unable to mount immune responses. Other T cells have TCRs that react with high avidity to self antigens, having the potential of eliciting autoimmune responses. These cells are eliminated in the thymus to ensure that the resulting T cells are capable of mounting an efficient immune response without harming the organism. Both positive and negative selection rely on the strength of interaction between TCR and the peptide-MHC complexes presented by the APCs, such as cTECs, mTECs and DCs. These cells express both MHC class I and MHC class II (Fig. 3).

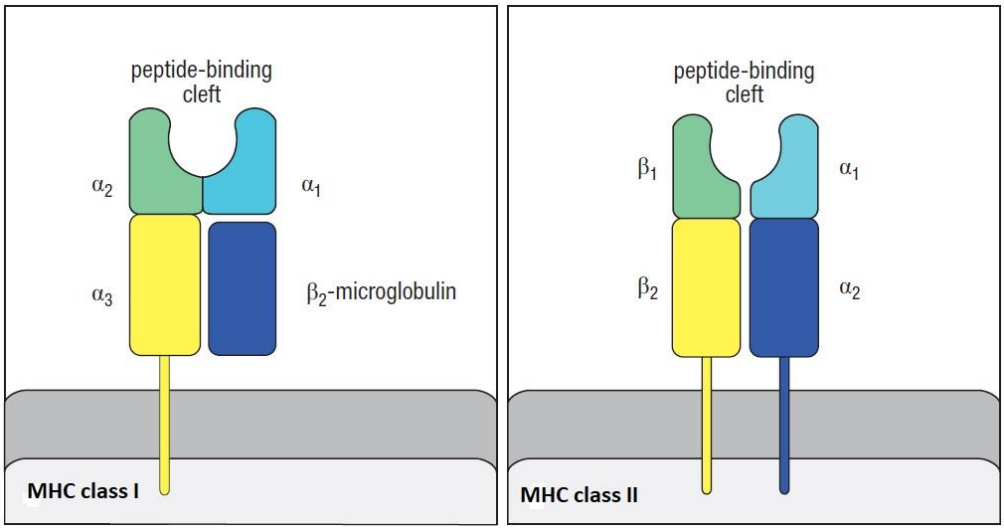

Figure 3- Structure of the major histocompatibility complex class I and class II. The MHC class I molecule is composed by a transmembranar α chain, divided in domain α_1, α_2 and α_3. This α chain is bound non-covalently to β_2-microglobulin that is non-transmembranar. The peptide-binding cleft is open in one end and closed in the other. In contrast to the MHC class I, MHC class II is composed of a transmembranar α chain with α_1 and α_2 domains, and a β chain, composed by β_1 and β_2 domains, and both α and β chains are transmembranar. Another difference comparing to the MHC class I is that the peptide-binding cleft is open at both ends. Figure taken from [2].

Positive selection is the first checkpoint for TCR affinity and is mediated by cTECs. Double positive thymocytes that have TCRs with low affinity for peptide-MHC complexes expressed by the cTECs die by neglect. Intermediate interaction between the TCR and peptide-MHC complexes will lead to the differentiation into the $CD4^+$ single positive or $CD8^+$ single positive lineage, accordingly to with which MHC class the TCRs react. Interaction between TCRs and MHC class I lead to downregulation of CD4 and thymocytes become $CD8^+$ single positive T cells. On the other hand, if the TCRs interact with MHC class II, downregulation of CD8 occurs and thymocytes become $CD4^+$ single positive T cells. During positive selection, more than 90% of the thymocytes die by neglect [21][22].

If thymocytes successfully go through positive selection, $CD4^+$ and $CD8^+$ single positive cells migrate to the medulla and undergo negative selection, mediated by mTECs and DCs. The peptides that are presented in the thymus can be ubiquitous, but also tissue-restricted antigens (TRAs) are expressed. TRAs are typically expressed by limited tissues at the periphery. In the thymus, the expression of TRAs is regulated by the autoimmune regulator (Aire) and Fezf2 by mTECs. Furthermore, TRAs are also cross-presented by dendritic cells, which thereby also contribute to negative selection to TRAs. Interaction of TCRs with self-antigens above a certain threshold will lead to the elimination of the thymocytes by apoptosis. This phenomenon is called central tolerance. Nevertheless, some few cells can escape negative selection and are exported to the periphery. These are controlled in the periphery by mechanisms of peripheral tolerance that include Treg [22][23].

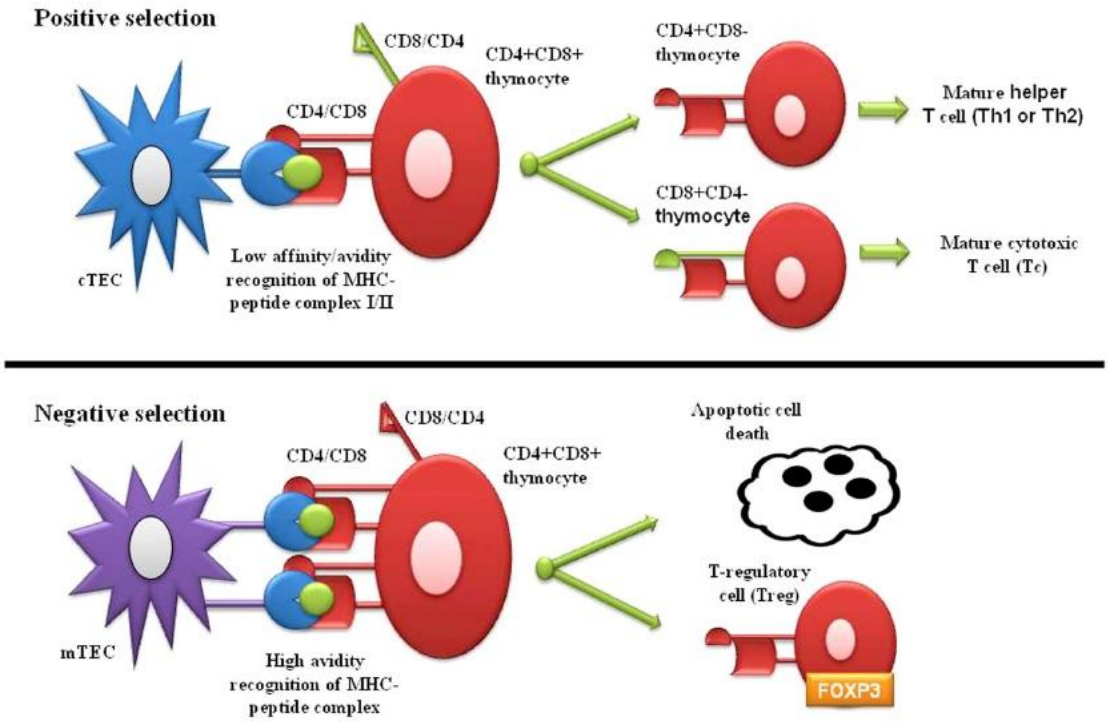

Figure 4- Selection steps during differentiation of thymocytes. In the cortex, $CD4^+CD8^+$ double positive thymocytes which have TCRs with intermediate affinity for peptide-MHC complexes undergo positive selection and become $CD4^+$ or $CD8^+$ single positive cells. The positively selected SP cells migrate to the medulla. Thymocytes with high avidity of the TCRs for peptide-MHC complexes are considered autoreactive and die by apoptosis during negative selection. In the process of negative selection Tregs are also generated. Figure from [24].

Primary immunodeficiency

Immunodeficiencies result from defects in the immune system. These can be divided in primary and secondary immunodeficiencies. Primary immunodeficiencies result from genetic defects leading to loss of immune cells or affecting their function, while in secondary immunodeficiencies these defects are due to external factors such as bacterial or viral infections, drugs that induce immunosupression, etc. Among the primary immunodeficiencies, severe combined immunodeficiency (SCID) is a disease in which more than one lineage of cells of the immune system is compromised. Patients with SCID require bone marrow or hematopoietic stem cell transplantation to survive [25]. These are rare diseases that manifest at young age. There are several forms, which can be divided into categories according to the cellular deficiency, i.e. absence of T, B and NK cells, and the genetic defect that causes the disease. The most common form is X-linked SCID (XSCID) which is $T^-B^+NK^-$ SCID and is characterized by few or even absent T and NK cells and results from defects in the γc gene. The common γc chain is part of the receptor for several cytokines, namely interleukin (IL-) 4, IL-7, IL-9, IL-15 and IL-21 (Fig. 5).

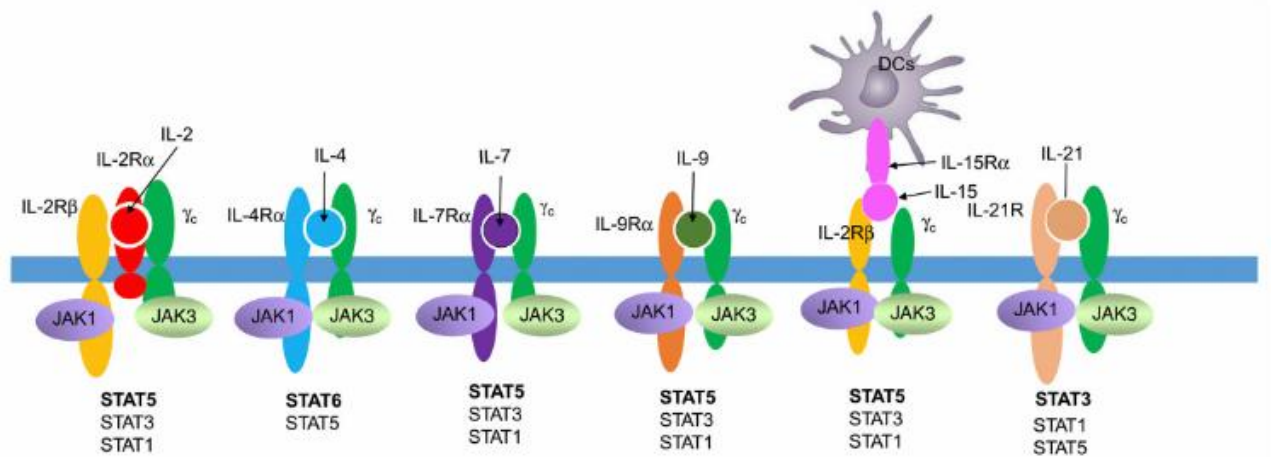

Figure 5- Common gamma chain (γ_c) cytokines and receptors. IL-2r, IL-4r. IL-7r, IL-9r, IL-15r and IL-21r are all composed by one γ chain and a specific α in their structure (IL2r and IL-15r have additionally a beta subunit). The receptors mediate signaling transduction by Janus-activated kinases (JAK) 1 and 3, which signal further through signal transducer and activator of transcription (STAT) proteins. Figure from [26].

The result of the deficiency in γc, differs between mice and humans. Specifically, patients have a $T^-B^+NK^-$ XSCID phenotype, i.e. B lymphocyte development is normal and only B cell function is affected (due to lack of T cell help). However, mice have a $T^-B^-NK^-$ XSCID phenotype, i.e. in addition to the defect in T and NK cell development they are also severely impaired in B lymphocyte development [27]. The defect in T lymphocyte development is caused by lack of IL-7. The defect in NK cells is caused by lack of IL-15 signaling. Since Janus-activated kinase 3 (JAK3) is downstream of γc signaling, patients and mice with mutations in JAK3 have the same phenotype as XSCID.

Patients with loss-of-function mutations in *IL-7r alpha chain (IL-7rα)* have $T^-B^+NK^+$ SCID. In mice, the B lymphocyte lineage is also affected. Therefore, IL-7 signaling is required for T and B cell development in mice. This differs in humans lacking functional *IL-7rα*, who have normal B cell numbers [28][29].

Other genes that are crucial for T and B cell development are *Rag1* and *Rag2*. These genes are necessary for recombination of the loci encoding for T- and B cell receptors. Therefore, loss-of-function mutations in *Rag 1* and *Rag 2* result in the absence of both T and B cells both in mice and humans. This is an extremely rare condition in humans. However, there are mutations in humans for *Rag1/2* that encode for hypomorphs and are responsible for Omenn syndrome. This syndrome is characterized by an oligoclonal $\alpha\beta$TCR repertoire, absence of circulating B lymphocytes and Tregs, which altogether are responsible for autoimmune reactions [30][31]. The several types of SCID in humans are summarized in Table 1.

Table 1- Lymphocyte phenotype of several types of SCID due to different genetic defects.

Genetic defect	T cells	B cells	NK cells
Common γ chain	-	+	-
JAK3	-	+	-
IL-7rα	-	+	+
Rag1/2	-	-	+

T-cell Acute Lymphoblastic Leukemia

T-cell acute lymphoblastic leukemia (T-ALL) is an aggressive blood cancer, characterized by aberrant production and proliferation of immature lymphocytes termed blasts [32]. Chromossomal translocations as well as cooperating mutations that lead to overexpression of oncogenes are among the causes of T-ALL.

Examples of factors involved in all subgroups of T-ALL are NOTCH1 and IL-7R. Gain-of-function mutations in *NOTCH1* are found in over 50% of the T-ALL cases in humans. A rare chromosomal translocation of the C-terminal region to the TCRB locus, t(7;9)(q34;q34.3), was found in some patients and was the first evidence that the aberrant Notch signaling was related to T-ALL. This leads to a dominant-active and ligand-independent form of NOTCH1. NOTCH1 is involved in T-cell lineage commitment and survival, being activated or suppressed at different stages of T-lymphocyte development. In T-ALL, NOTCH1 activates the *MYC* oncogene, leading to proliferation of the leukemic cells [14][33][34]. Deregulation in IL-7 signaling is also considered to be implicated in some cases of T-ALL. IL-7 is essential for survival and regulates proliferation during T-cell development, through the upregulation of B-cell lymphoma 2 (Bcl-2), responsible for inhibiting apopotosis and downregulating $p27^{Kip1}$, an inhibitor of cell-cycle progression. Therefore, abnormal IL-7 signaling can lead to increased proliferation of the cells, since the regulation of *Bcl-2* and $p27^{Kip1}$ is suppressed. Furthermore, gain-of function mutations of *IL-7Rα* have also been reported in human T-ALL [35].

Nevertheless, T-ALL is a heterogeneous disease and can be subgrouped according to the expression of specific genes. The largest subgroup is defined by expression of *TAL1* and the *LMO2* [36]. *TAL1* is an oncogenic transcription factor required for the specification of blood lineage and maturation of hematopoietic stem cells. Its expression decreases as T-cell development progresses. *TAL1*, together with E-proteins and *LMO2* can form regulatory complexes. Chromossomal translocations and somatic mutations result in an abnormal expression of this transcription factor and lead to T-ALL. Abnormalities in this transcription factor are present in between 40-60% of the cases of this disease [36]. Also, in mice, the overexpression of *Lmo2* has been shown to promote self-renewal of developing T cells and accumulation of mutations leading to the transformation of cells into leukemic cells. [37].

Thymus turnover versus thymus autonomy and leukemia

T cell development relies on the constant influx of bone marrow progenitors into the thymus and is characterized by high cellular turnover. Thymus transplantation experiments can be used to study a number of aspects related to T lymphocyte development, in particular those related to the dynamic nature of thymopoiesis. Transplants of wild-type thymi under the kidney capsule of wild-type mice demonstrated that the total replenishment of thymocytes takes around four weeks [38] (Fig. 6).

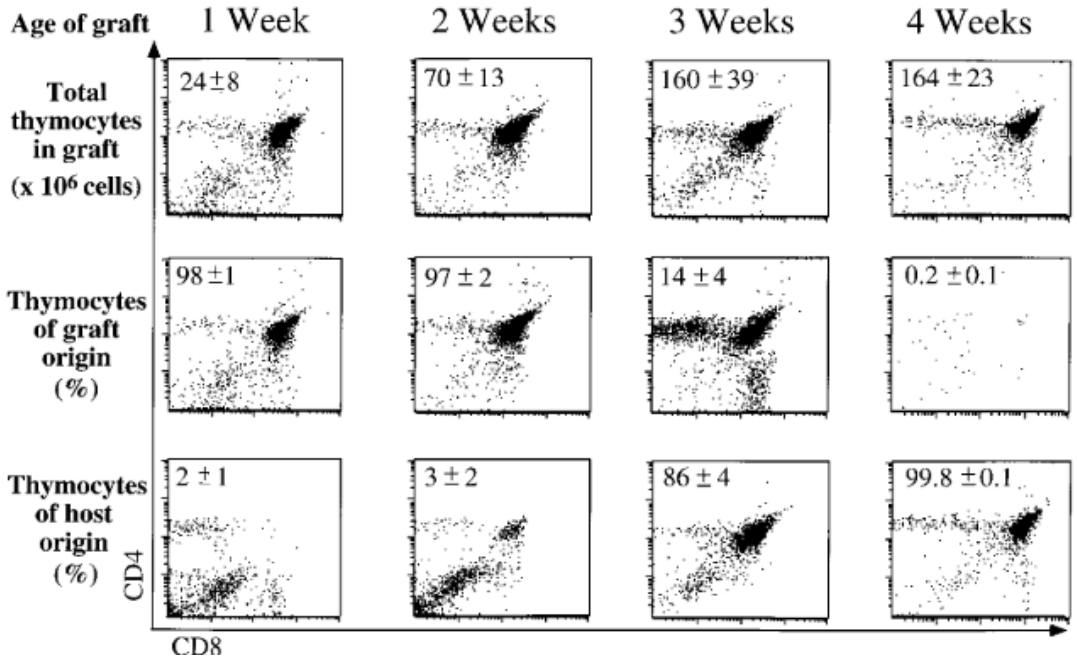

Figure 6- Thymocytes of graft origin are fully replaced within 4 weeks by host thymocytes. Wild type newborn thymi were grafted into wild type mice and cells from the grafts were stained for CD4 and CD8 and analyzed by flow cytometry. The top row shows cells gated in total thymocytes. In the middle and bottom row, cells were gated on thymocytes of graft or host origin, respectively. Grafts were analyzed at the indicated time points. Numbers on the the plots correspond to average cell numbers of the indicated population +/- standard deviation. Figure taken from [38].

Classical experiments of transplantation of wild-type thymi into SCID or *Rag2*$^{-/-}$ mice, have shown that the wild-type thymus graft exports one single wave of T cells and then stops. This led to the generalized idea that thymocytes were short-lived cells and lacked the capacity to self-renew, which became a dogma of thymus and T cell biology. This dogma was challenged by work of two independent labs, which have shown that the thymus can maintain T lymphocyte production independently of bone marrow contribution under specific conditions [39][40]. Performing thymus transplants of wild-type newborn thymi into *Rag2*$^{-/-}\gamma c^{-/-}Kit^{W/Wv}$ recipients, which are devoid of progenitors capable of colonizing the thymus, T lymphocytes of donor origin continued to be produced and exported for unexpectedly long time (Fig. 7). These results showed that, under specific conditions, thymocytes can become long-lived and acquire self-renewal capacity [39].

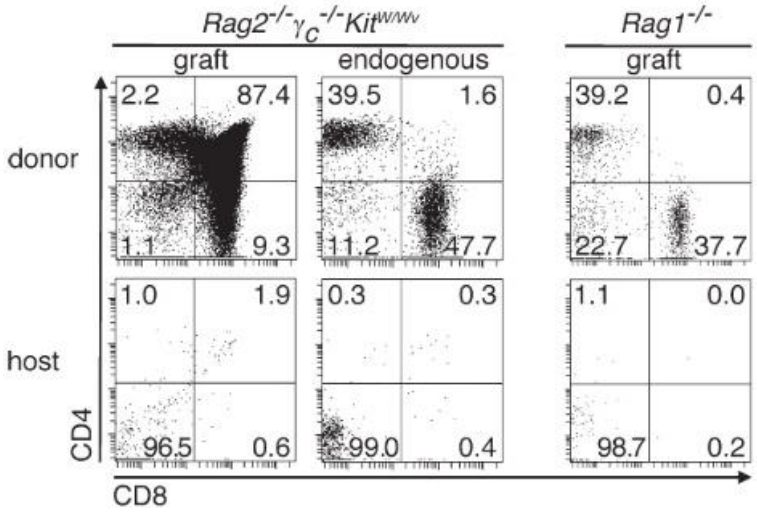

Figure 7- T lymphocyte development persists even in the absence of thymus seeding by bone marrow progenitors. Newborn wild-type thymi were transplanted under the kidney capsule of the indicated recipients and analyzed by flow cytometry 9–11 weeks (left) or 6 weeks later (right). Cells were gated in donor origin (upper row) or host origin (bottom row). The endogenous thymus of the same mouse is shown as a control (middle). In the right column are the analyses of wild-type newborn thymi grafted into *Rag1*$^{-/-}$ recipients (analyzed 6 weeks after transplant). Figure taken from [39].

Since thymus autonomy developed from grafts into *Rag2*$^{-/-}\gamma c^{-/-}$*Kit*$^{W/Wv}$ hosts, new experiments were designed to identify the mutation that was permissive for thymus autonomy. Transplants of wild-type newborn thymi into *Rag2*$^{-/-}\gamma c^{-/-}$, *Rag2*$^{-/-}$*IL-7r*$^{-/-}$, $\gamma c^{-/-}$ and *IL-7r*$\alpha^{-/-}$ recipients revealed autonomous T-cell development, opposite thymi grafted into *Rag2*$^{-/-}$ or *Kit*$^{W/Wv}$. These experiments revealed a key role for the presence of IL-7r in the T lymphocyte progenitors of donor origin [39][40][41]. Indeed, thymus autonomy leads to the development of T cells with a diverse TCR repertoire and capable of conferring immune protection to the host against infections [40][42].

Thymus autonomy leads to T-ALL in *Rag2*$^{-/-}\gamma c^{-/-}$*Kit*$^{W/Wv}$, *Rag2*$^{-/-}\gamma c^{-/-}$ and in $\gamma c^{-/-}$ recipients. These leukemias appear from 4 months after transplant onwards and have a CD8^{+} immature single positive/double positive-like phenotype both in spleen, bone marrow and in thymus grafts (Fig. 8). T-ALLs that emerged from these experimental setups were similar to T-ALL in humans. In 80% of the cases, gain-of function mutations in *Notch1* were present, and *Tal1* and *Lmo2* were upregulated [41].

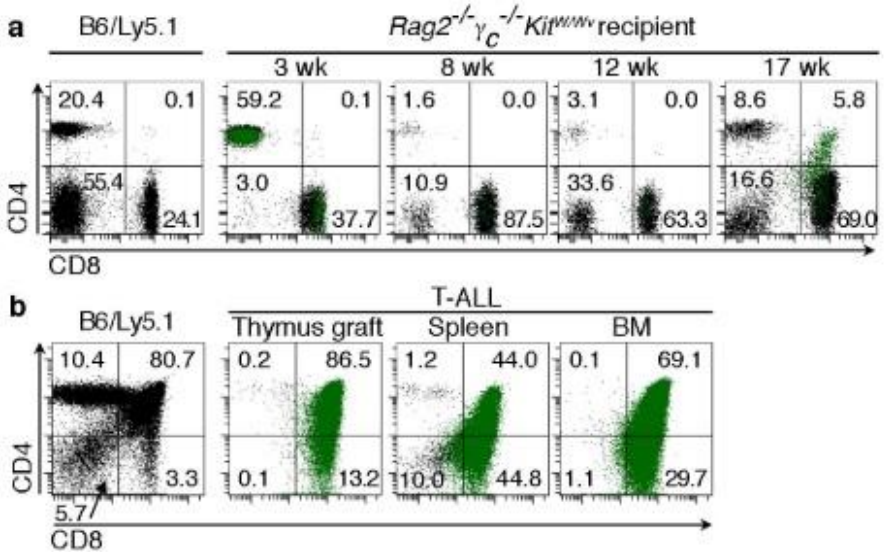

Figure 8- Development of T-ALL following thymus autonomy. Wild type thymi were grafted into *Rag2*$^{-/-}$ $\gamma c^{-/-}$*Kit*$^{W/Wv}$ recipients. a) Blood was analyzed by flow cytometry at the indicated timepoints (in weeks, wk) post-transplantation. B6/Ly5.1 is shown as control (left). b) Representative example of a T-ALL that developed at week 18 after transplant from *Rag2*$^{-/-}$ $\gamma c^{-/-}$*Kit*$^{W/Wv}$ recipients. The thymus graft, spleen and bone marrow were analyzed by flow cytometry. B6/Ly5.1 thymus is shown as a control. Figure adapted from [41].

Aim of the project

The thymus stroma, in particular the thymic epithelium, is responsible for providing the specific niches in which T lymphocytes differentiate. Likewise, thymocytes impact on the differentiation of T lymphocytes. Several examples of thymus crosstalk have been described in the literature. These include cases in which a defect in TEC leads to impaired T lymphocyte development, and the opposite, in which defects in T lymphocyte development impact on TEC structure and differentiation. The aim of this thesis is to address the structure of the thymus, i.e. its architecture, in two conditions of disease that emerge from defects in T lymphocyte development: immunodeficiency and in leukemogenesis. The two are linked in the experimental approach chosen, which involves thymus transplants into immunodeficient recipients. Two main objectives are proposed, as follows:

Objective 1: Study of the thymus architecture in primary immunodeficiencies

Objective 2: Study of the thymus architecture in leukemogenesis:

- From thymus autonomy to T-ALL
- Progression of thymus autonomy in a *Rag2*$^{-/-}$ background
- Thymus autonomy in multiple IL-7-unresponsive hosts

Most analyses used immunohistology, as this enables us to visualize the organization of the cells, the composition of the thymus, and the relative position of all cells in the organ.

Results

Thymus architecture in primary immunodeficiencies

During T lymphocyte development, thymocytes go through several stages of differentiation. To characterize the different cell populations in the thymus of wild type and immunodeficient mice, fluorescence-activated cell sorting (FACS) analysis was performed in thymocytes isolated from wild type, $\gamma c^{-/-}$, *IL-7r*$\alpha^{-/-}$, *IL-7*$^{-/-}$, *Rag2*$^{-/-}$, *Rag2*$^{-/-}$*IL-7r*$\alpha^{-/-}$ and *Rag2*$^{-/-}\gamma c^{-/-}$ thymi. In a wild type thymus the cells proceed from the double negative stage ($CD4^-CD8^-$) to the double positive stage ($CD4^+CD8^+$) ending the differentiation process at the single positive stage ($CD4^+CD8^-$ or $CD4^-CD8^+$). The majority of the cells are at the double positive stage (Fig. 9A). The same populations could be observed in $\gamma c^{-/-}$, *IL-7r*$\alpha^{-/-}$ and *IL-7*$^{-/-}$ mice but thymi have a decrease in cell number (Fig. 9C), which is due to lack of IL-7 signaling, essential for cell proliferation and survival especially at the double negative stage. As expected, all *Rag*-deficient thymi lack double positive and single positive thymocytes (Fig. 9A). Within the $CD4^-CD8^-$ double negative (DN) cell populations, differential expression of cell-surface markers CD44 and CD25 can be used to identify four stages of T cell development, namely DN 1 ($CD44^+CD25^-$), DN 2 ($CD44^{+/lo}CD25^+$), DN 3 ($CD44^{-/lo}CD25^+$) and DN 4 ($CD44^-CD25^-$) cells. The majority of the cells are at the DN 3 stage. All immature stages from DN 1 to DN 4 are present in the thymus of $\gamma c^{-/-}$, *IL-7r*$\alpha^{-/-}$ and *IL-7*$^{-/-}$ mice. As expected the *Rag2*$^{-/-}$ thymus shows an accumulation of cells at the DN 3, consistent with the developmental block at this stage (Fig. 9B). This phenotype is exacerbated in the *Rag2*$^{-/-}$*IL-7r*$\alpha^{-/-}$ and *Rag2*$^{-/-}\gamma c^{-/-}$ thymi, resulting from combination of the developmental block at the DN 3 and the lack of IL-7 signaling (Fig. 9B).

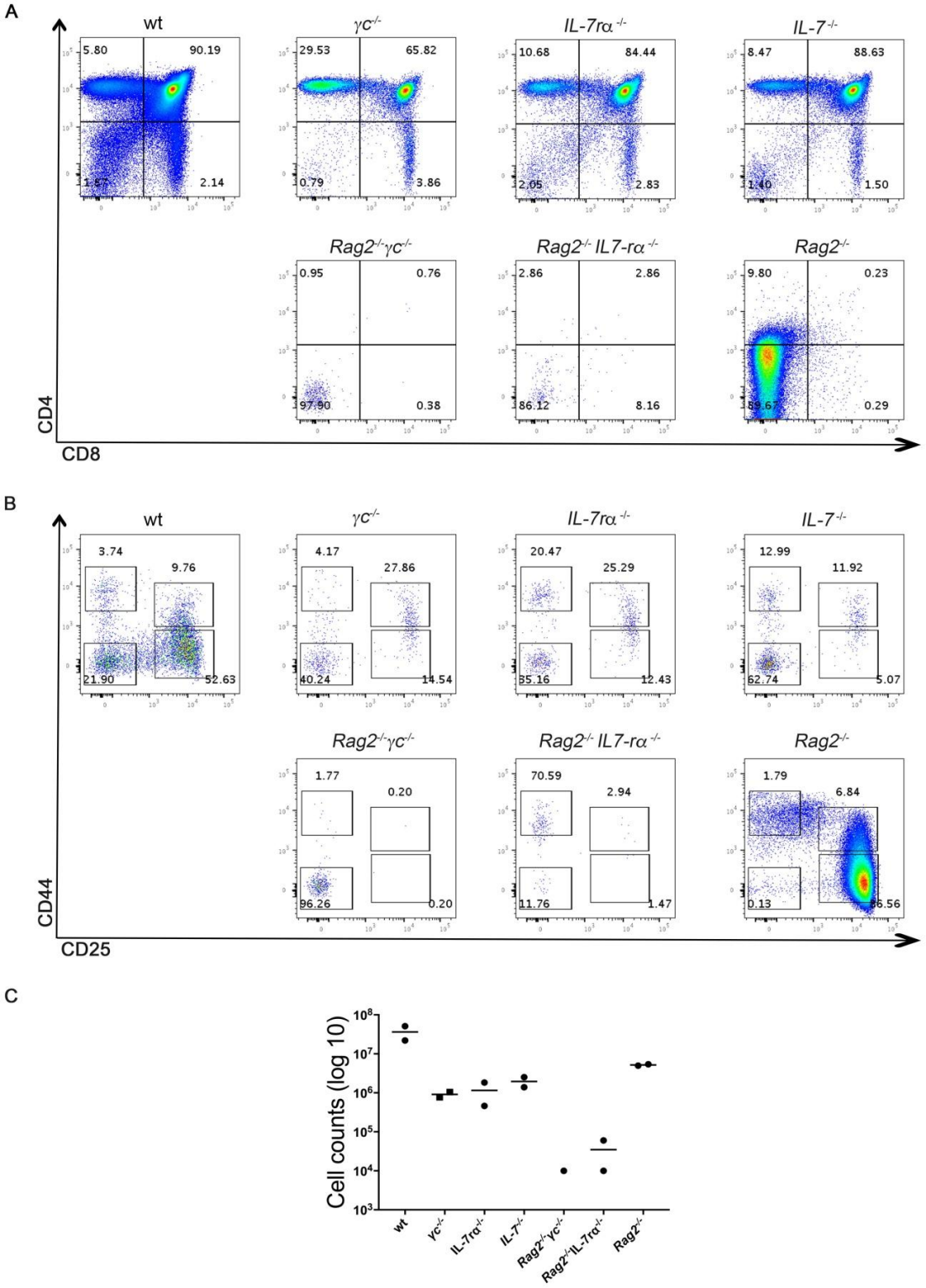

Figure 9- Differentiation stages of T cell development and thymocyte numbers in immunodeficient mice. Thymocytes from the indicated genotypes were analyzed by FACS for CD3ε, CD4, CD8, CD25 and CD44. SYTOX blue was used to exclude dead cells. (A) Expression of CD4 and CD8 in live thymocytes. (B) Cells in A were further gated on $CD4^-CD8^-CD3\varepsilon^-$ thymocytes and analyzed for the expression of CD44 and CD25. This experiment was performed once, using two animals from each genotype, 6 to 11 weeks of age. (C) Thymocyte counts from each immunodeficient mice. Cells from one of the *Rag2*$^{-/-}\gamma c^{-/-}$ thymus were below the detection limit.

Animals with the same genotypes were further analyzed by immunohistology to assess thymus structure. CD4 and CD8 identify the major populations of thymocytes and co-expression of the two markers defines $CD4^+CD8^+$ double positive thymocytes, which occupy the cortical region of the thymus in wild type, $\gamma c^{-/-}$, *IL-7r*$\alpha^{-/-}$ and *IL-7*$^{-/-}$ thymi. In all these thymi, $CD4^+$ and $CD8^+$ single positive thymocytes are located in the medulla, which can be further identified with basis on the presence of medullary thymic epithelial cells (mTEC), stained by cytokeratin 5 (K5) (Fig. 10A). The number of $CD4^+$ cells is bigger than the $CD8^+$ cells. As expected, all *Rag2* mutants lack double positive and single positive cells, consistent with the block in T cell development at the DN 3 stage. In these thymi, the thymus structure can only be identified with basis on the expression of K5 (and Dapi, not shown). The red staining outside the thymi corresponds to unspecific binding of the streptavidin to fat (Fig. 10A).

Beyond thymocytes, other cell populations were also analyzed, namely cortical thymic epithelial cells (cTECs), medullary thymic epithelial cells (mTECs) and dendritic cells (DCs). These cells were identified specifically by the expression of Keratin 8 (K8), Keratin 5 (K5) and CD11c, which stain mTECs, cTECs, and dendritric cells, respectively (Fig. 10B). A good separation between cortex and medulla could be observed, with basis on the differential expression of K5 and K8. Dendritic cells localized mainly in the medullary areas. Some TEC express both K5 and K8 (orange/yellow), which is thought to identify more immature cells, that are mostly restricted to the cortico-medullary junction [43]. The phenotype in $\gamma c^{-/-}$, *IL-7r*$\alpha^{-/-}$ and *IL-7*$^{-/-}$ thymi is identical to that of the wild type control, with a clear separation between cortex and medulla and the dendritic cells mainly localized in the medulla. However, these thymi had an increase in the proportion of TEC that co-expressed K5 and K8 in the cortical region. In all cases of *Rag2* deficiency, there were no medullary areas. Nevertheless, *Rag2*$^{-/-}$ thymi have TEC that are clearly positive for K5 but not K8, i.e. TEC that have the phenotype of mTEC (Fig. 10B). The thymus of *Rag2*$^{-/-}$*IL-7r*$\alpha^{-/-}$ and *Rag2*$^{-/-}\gamma c^{-/-}$ mice had a more severe phenotype, with a more compacted cellular structure than the *Rag2*$^{-/-}$, and with virtually all TEC co-expressing both K5 and K8 and presence of cysts. Also no dendritic cells could be identified in these sections.

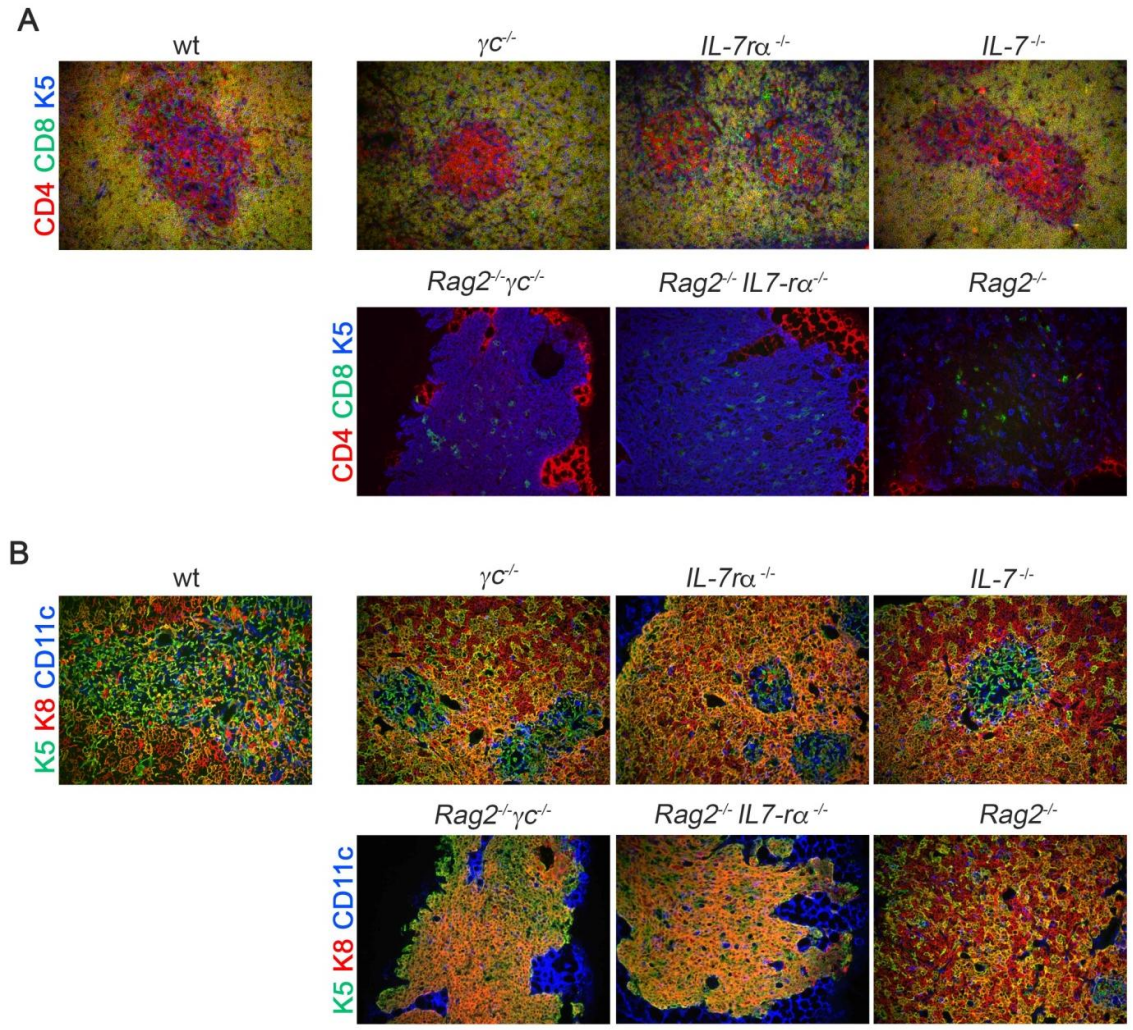

Figure 10- Thymus structure in mice with primary immunodeficiencies. Immunohistology of thymus sections of B6 wild type, $\gamma c^{-/-}$, *IL-7rα*$^{-/-}$, *IL-7*$^{-/-}$, *Rag2*$^{-/-}$, *Rag2*$^{-/-}$*IL-7rα*$^{-/-}$, and *Rag2*$^{-/-}\gamma c^{-/-}$ mice, as depicted. (A) Staining for CD4 (red), CD8 (green) and K5 (blue). (B) Staining for K5 (green), K8 (red) and CD11c (blue). Images were acquired in Leica DMRA2 microscope with the software MetaMorph using a 20x magnification. Photos of the split channels (Dapi, K5-Alexa 488, CD4-bio-Streptavidin Cy3, CD8-APC in (A) and Dapi, K5-Alexa 488, CD11c-PE, K8-Alexa 647 in (B)) are depicted in Figures 1 and 2 of the Appendix section. This experiment was performed with 8 mice from 5 to 8 weeks of age.

Thymus architecture: from thymus autonomy to T-ALL

Thymus autonomy is the capacity of the thymus to maintain its function of generating T lymphocytes independently of bone marrow contribution. It is switched on in thymi that are deprived of competent progenitors and can be studied in a setting of thymus transplantation. If prolonged, thymus autonomy is permissive to the development of T-ALL. Thymus transplants were performed in the lab using newborn wild type donors transplanted into *Rag2*$^{-/-}\gamma c^{-/-}$ adult recipients (Fig. 11).This experimental condition was always compared with wild type thymi transplanted into wild type recipients and wild type thymi that were not transplanted. In all cases, the origin of the cells, i.e. whether they were of donor or host origin could be determined with basis on the differential expression of CD45.1 and CD45.2 (Fig. 11). To analyze the structure of the thymus during thymus autonomy, and determine whether it changes during the course of development of T-ALL, grafts were analyzed at several timepoints after

transplantation, namely 28 days after transplant, an early stage of thymus autonomy, 9 weeks after transplant, a later stage of autonomy/pre-leukemic stage and a final timepoint, when T-ALL has already developed (Fig. 11).

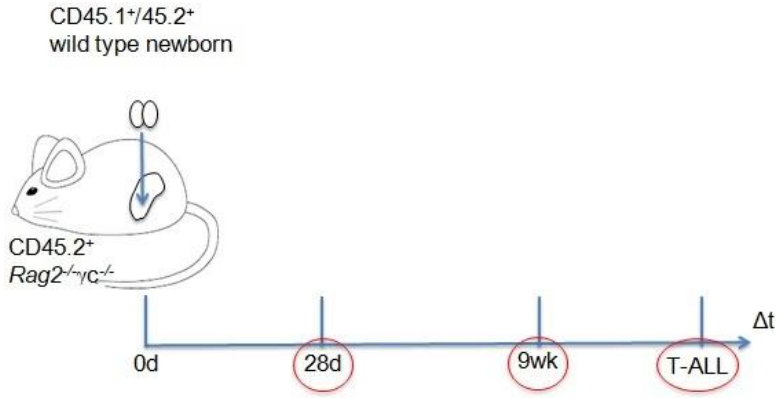

Figure 11- Representative scheme of the transplant model and timepoints of analyses selected. Wild type newborn thymi were transplanted under the kidney capsule of *Rag2*$^{-/-}$ $\gamma c^{-/-}$ mice. B6 wild type non-transplanted thymi as also as wild type newborn grafts from wild type recipients served as a staining control. The grafts were analyzed 28 days and 9 weeks after transplant and at a timepoint in which the development of T-cell acute lymphoblastic leukemia already happened.

The earliest timepoint analyzed was day zero, corresponding to thymi from newborn mice, which were not transplanted. These were compared to adult thymi. Both newborn and adult thymi had a similar distribution of thymocytes, with double positive thymocytes present in the cortex and single positive cells localized in the medulla (Fig. 12A). Furthermore, medullary areas can be distinguished from cortical areas, with staining for K5 in the medulla and for K8 in the cortex and with dendritic cells predominantly present in the medullas. (Fig. 12B).

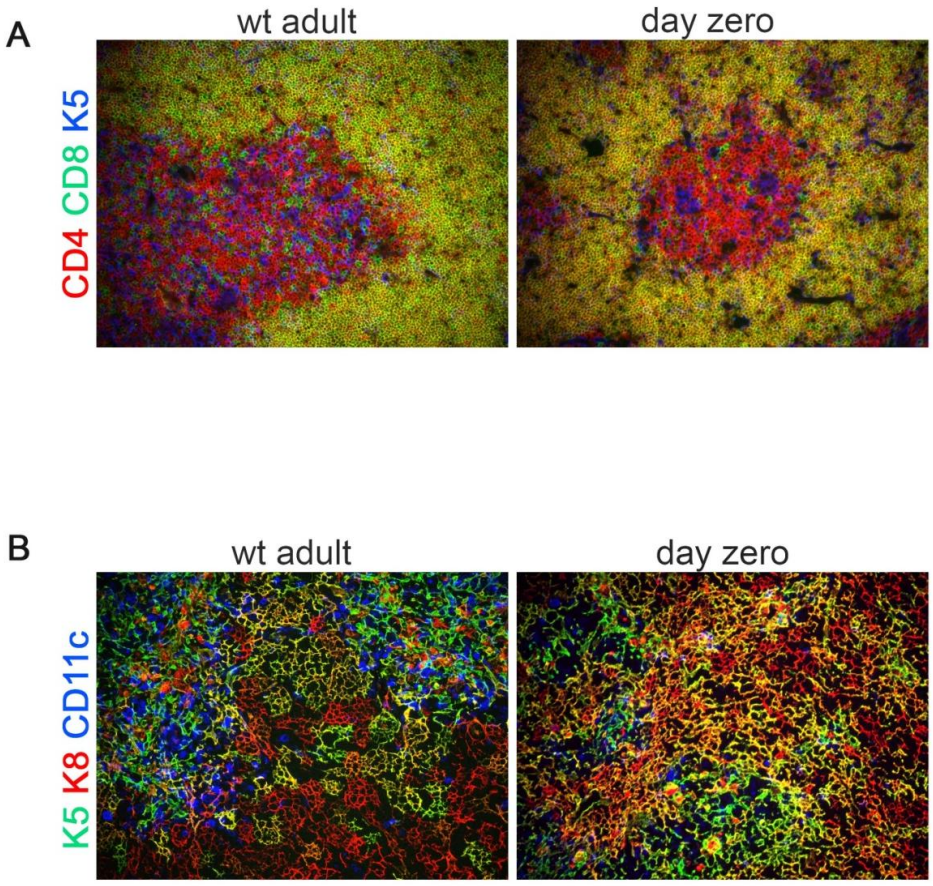

Figure 12- Thymic architecture of the newborn thymus. Immunohistology of thymus sections of wild type newborn (day 0) and adult thymus. (A) Staining for CD4 (red), CD8 (green) and K5 (blue). (B) Staining for K5 (green), K8 (red) and CD11c (blue). Images were acquired in Leica DMRA2 microscope with the software MetaMorph using a 20x magnification. Photos of the split channels (Dapi, K5-Alexa 488, CD4-bio-Streptavidin Cy3, CD8-APC in (A) and Dapi, K5-Alexa 488, CD11c-PE, K8-Alexa 647 in (B)) are depicted in Figure 3 of the Appendix section. This experiment was performed with 2 mice of 0 and 8 weeks of age.

Day 28 after transplant

Twenty eight days after transplant corresponds to a timepoint in which thymus turnover has mostly taken place in a wild type scenario. However, if a wild type thymus was grafted into a *Rag2*$^{-/-}\gamma c^{-/-}$ recipient, we consider that 28 days after transplant corresponds to an early stage of thymus autonomy. Wild type thymi that were transplanted into wild type recipients are identical to thymi that were not transplanted. CD4^{+}CD8^{+} double positive cells localized in the cortex, and CD4^{+} and CD8^{+} single positive cells are in the medullas, further identified by K5-positive mTECs. During autonomy, this structure is kept and the only difference is an increase in the proportion of CD8^{+} single positive thymocytes in the medulla (Fig. 13A,B), consistent with our previous work, by FACS [39]. In addition, TEC staining and the localization of dendritic cells is identical in all tested conditions (Fig. 13C,D). The only difference that could be detected in thymus autonomy was that medullary areas were larger than in control conditions in which thymus turnover took place (Fig. 13B,D).

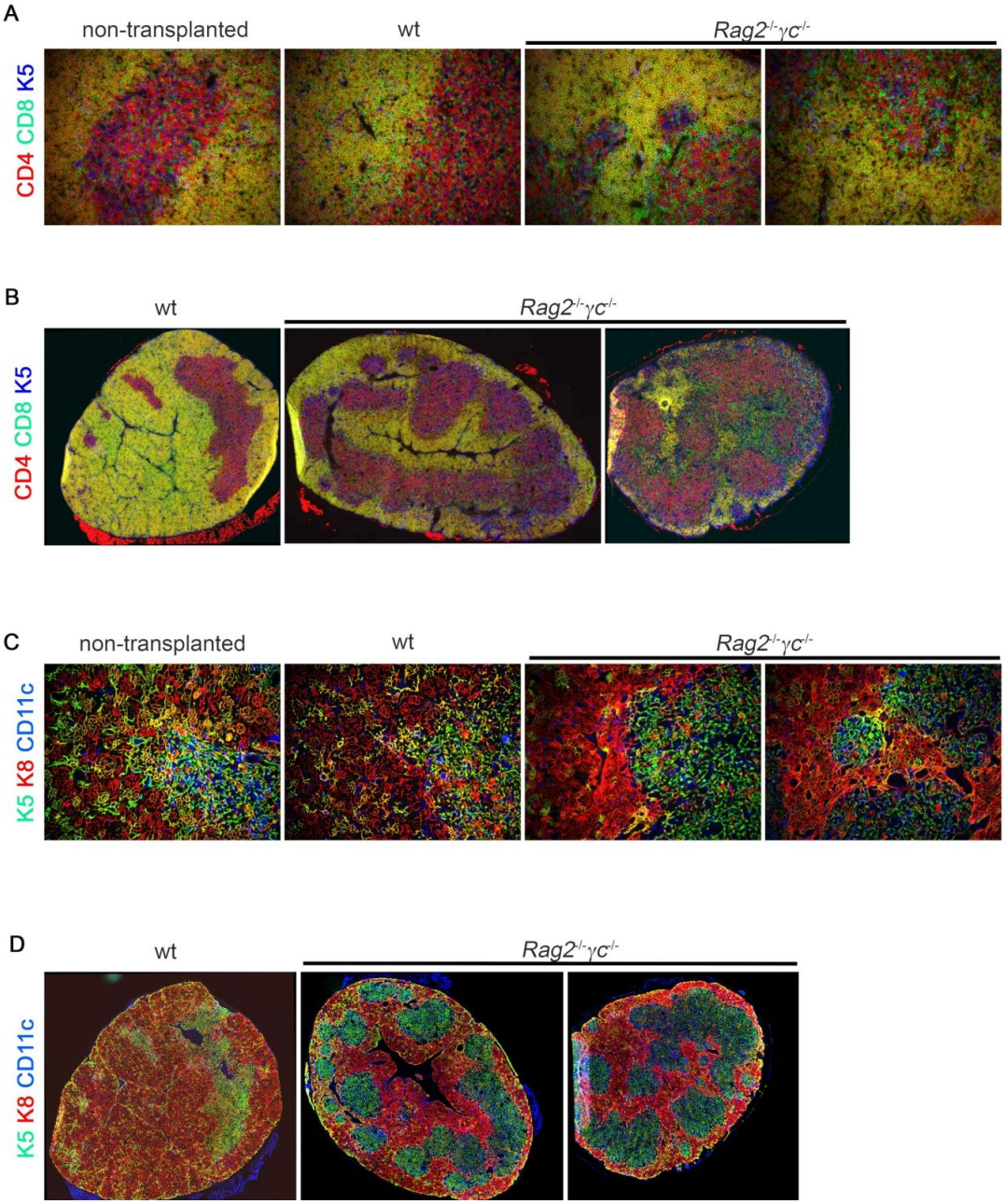

Figure 13- The phenotype of the thymus is maintained during early stages of thymus autonomy. Wild type newborn thymi were grafted under the kidney capsule of adult recipients (wild type or *Rag2*$^{-/-}\gamma c^{-/-}$, as indicated) and analyzed 28 days later by immunohistology for the indicated markers. Wild type B6 thymus was used as staining control. (A, B) Staining for CD4 (red), CD8 (green) and K5 (blue), as depicted. (C,D) Staining for K5 (green), K8 (red) and CD11c (blue), as depicted. Images were acquired in Leica DMRA2 microscope with the software MetaMorph using a 20x magnification (A, C) and in Nikon High Content Screening microscope with the software Nikon Elements for the overview of the sections, also using a 20x magnification (B, D). Photos of the split channels (Dapi, K5-Alexa 488, CD4-bio-Streptavidin Cy3, CD8-APC in (A,B) and Dapi, K5-Alexa 488, CD11c-PE, K8-Alexa 647 in (C,D)) are depicted in Figures 4 and 5 of the Appendix section. This experiment was performed with 12 mice.

Week 9 after transplant

Wild type thymi that were transplanted into wild type recipients and wild type non-transplanted thymi have the same phenotype. The cortical areas harbor $CD4^+CD8^+$ double positive cells, while the presence of $CD4^+$ and $CD8^+$ single positive cells is almost restricted to the medullas,

identified by the cells that express K5. The majority of the grafts are broadly normal, characterized by having a similar phenotype to a wild type case. A second phenotype was also identified, corresponding to exhausted thymi, in which thymopoiesis was no longer supported. In the latter case no more $CD4^+CD8^+$ double positive thymocytes were found, and large areas of keratin staining only were visible. In those thymi, circulating $CD4^+$ or $CD8^+$ single positive cells were present in areas resembling former medullas (Fig. 14A, 14B).

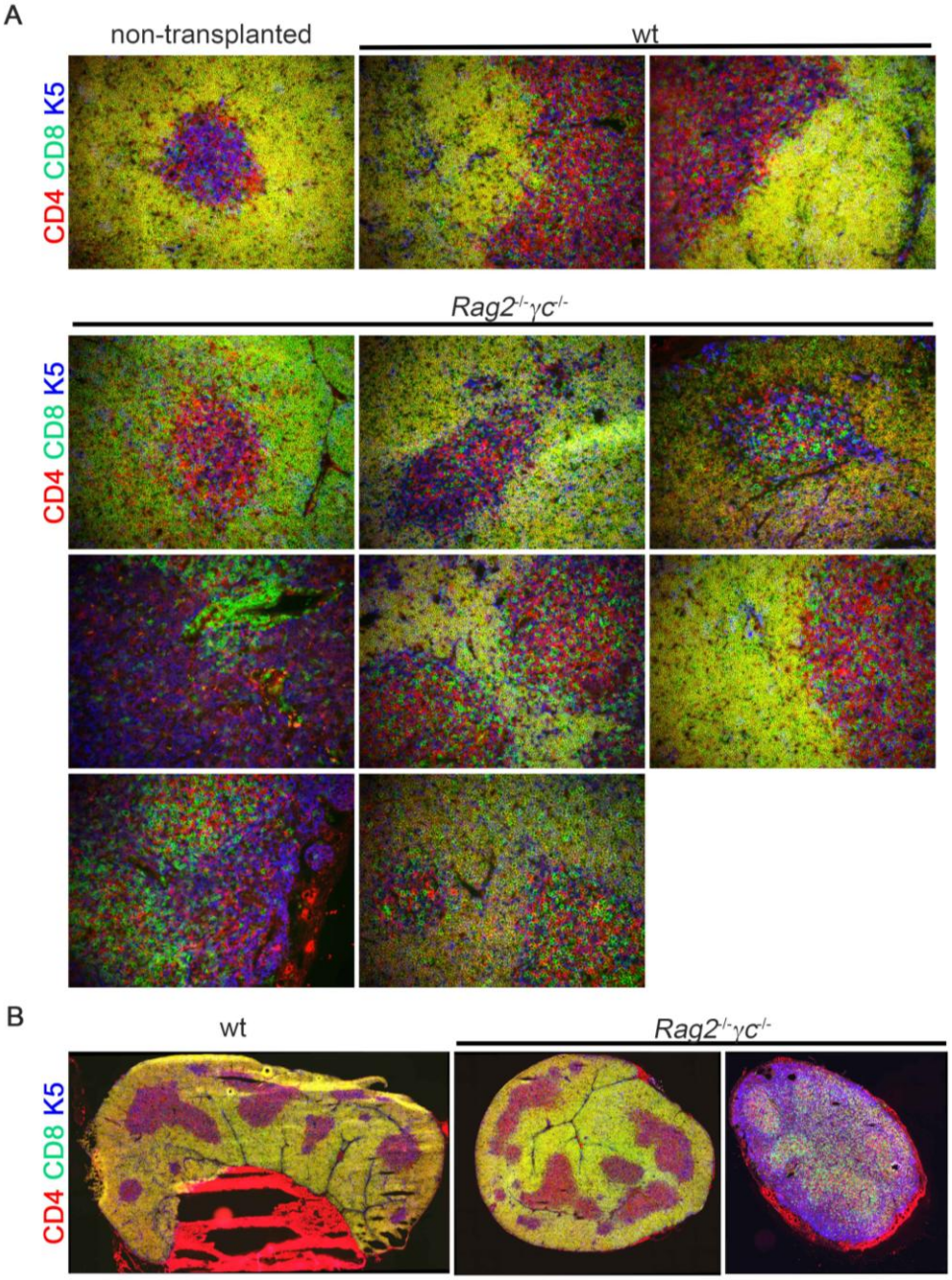

Figure 14- Thymus structure is maintained in thymus autonomy nine weeks after transplant. Wild type newborn thymi were grafted under the kidney capsule of adult recipients (wild type or *Rag2*$^{-/-}\gamma c^{-/-}$, as indicated) and analyzed 9 weeks later by immunohistology for the indicated markers. Wild type B6 thymus was used as staining control. (A, B) Staining for CD4 (red), CD8 (green) and K5 (blue). Images were acquired in Leica DMRA2 microscope with the software MetaMorph using a 20x magnification (A) and in Nikon High Content Screening microscope with the software Nikon Elements for the overview of the sections, also using a 20x magnification (B). Photos of the split channels (Dapi, K5-Alexa 488, CD4-bio-Streptavidin Cy3, CD8-APC) are depicted in Figures 6 and 7 of the Appendix section. This experiment was performed with 11 mice.

Figures 14 and 15 correspond to the same thymus grafts and the identical position in the two figures belong to the same graft. Analysis of TEC and dendritic cells also had some variation between thymi in autonomy. Some were identical to the control conditions, while others had some major changes. Even grafts in which T lymphocyte development appeared normal (Fig. 14) could have changes in the epithelium, i.e. medulla and cortex could be easily identified but many cTECs that co-expressed K5 and K8, suggestive that the loss of cellularity in thymocytes occurring in autonomy particularly impacts on the cortical epithelium. The most extreme cases, corresponding to exhausted thymi correspond to a minority. These maintained the separation between cortex and medulla but the proportion of cells co-expressing K5 and K8 was increased in the cortex. Dendritic cells maintain their normal localization in the medullas (Fig. 15A). Examples of micrographs of whole thymus sections are shown for thymus grafts with active thymopoiesis and exhaustion (Fig. 15B).

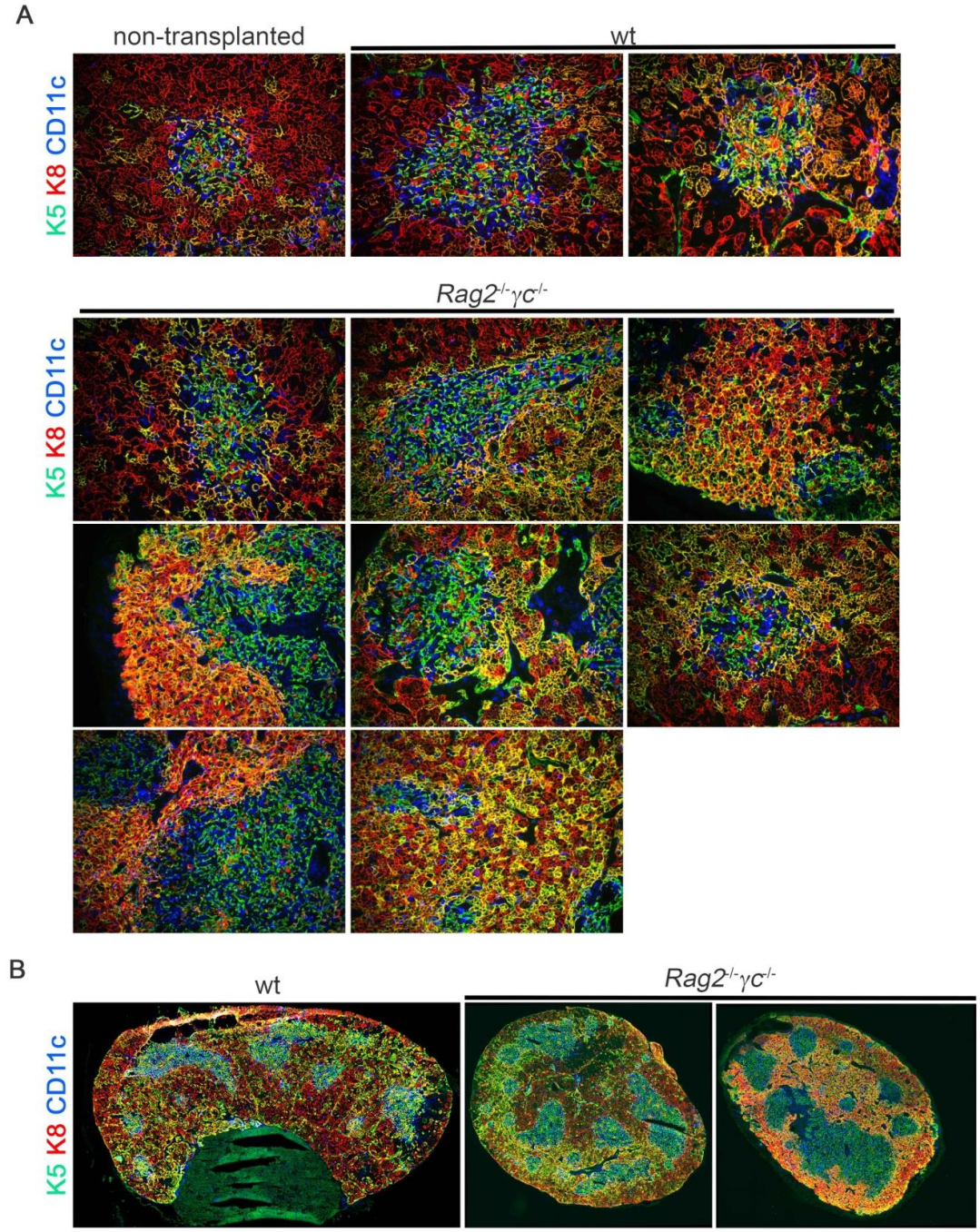

Figure 15- In thymus autonomy, 9 weeks after transplant, the cTECs lose their identity. Sections of the same grafts shown in Figure 14 were stained for K5 (green), K8 (red) and CD11c (blue). Images were acquired in Leica DMRA2 microscope with the software MetaMorph using a 20x magnification (A) and in Nikon High Content Screening microscope with the software Nikon Elements for the overview of the sections, also using a 20x magnification (B). Photos of the split channels (Dapi, K5-Alexa 488, CD11c-PE, K8-Alexa 647) are depicted in Figures 8 and 9 of the Appendix section.

T-cell Acute Lymphoblastic Leukemia

T-ALL samples were analyzed by flow cytometry and I reanalyzed the files of the same samples posteriorly analyzed by immunohistology. Leukemic cells present an immature phenotype, expressing both CD4 and CD8, resembling the expression profile of thymocytes in a normal thymus but never found outside the thymus of a healthy mouse. The extent of CD4 or CD8

intensity differed from sample to sample, i.e. two of the T-ALL samples were $CD4^+CD8^+$ double positive and $CD8^+$ immature single positive, while in the other the majority of the cells were $CD4^+CD8^+$ double positive (Fig. 16A). This fits the staining observed by immunohistology, in which grafts showed varying intensities of the staining for CD4 and CD8 between samples (Fig. 16B). No normal structure was found, and the segregation between medulla and cortex was lost. Instead, an apparent organ destruction took place and epithelial areas were largely absent. The dendritic cells are still present but are scattered through all the tissue (Fig. 16C).

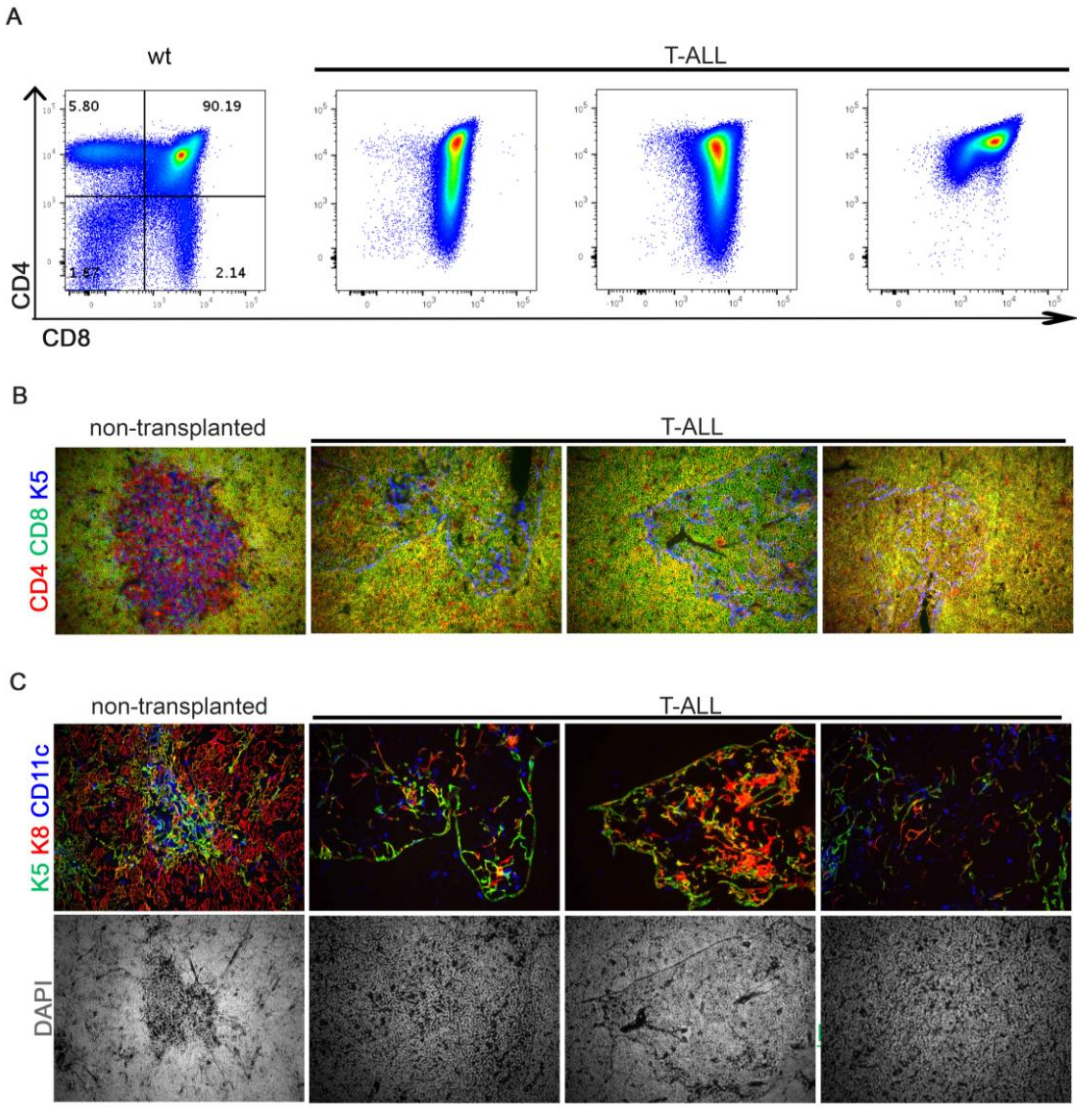

Figure 16- T-ALL is characterized by organ destruction with loss of the epithelium. (A) Thymocytes isolated from a wild type B6 adult and the thymus grafts in three T-ALL samples were analyzed by flow cytometry for the expression of CD4 and CD8. Thymocytes were stained with anti-CD3ε, anti-CD4, anti-CD8, and with SYTOX blue to exclude the dead cells. (B, C) Immunohistology in thymus sections of wild type adult thymus and grafts of T-ALL. Wild type B6 thymus was used as staining control..(B) Immunohistology of the thymus sections with staining for CD4 (red), CD8 (green) and K5 (blue). (C) Immunohistology of the thymus sections with staining for K5 (green), K8 (red) and CD11c (blue). Staining for Dapi is in grey, staining the nuclei of the cells. Images were acquired in Leica DMRA2 microscope with the software MetaMorph using a 20x magnification. Photos of the split channels (Dapi, K5-Alexa 488, CD4-bio-Streptavidin Cy3, CD8-APC in (B) and Dapi, K5-Alexa 488, CD11c-PE, K8-Alexa 647 in (C)) are depicted in Figure 10 of the Appendix section. FACS experiment was performed with 5 mice, while immunohistology experiment was performed with 6 mice.

Comparing the different timepoints of study, covering from day zero until 28 days after transplant, the distribution of T cells, TECs and dendritic cells was kept normal but the medullary areas became larger. From 28 days to 9 weeks after transplant, thymus architecture was maintained in terms of T cell development but some cTECs started to co-express K5 and K8. From 9 weeks on, grafts with autonomy present the same phenotype as in 28 days after transplant in terms of T cell distribution, but there is an enrichment in cTECs that are $K5^{+}K8^{+}$. In T-ALL there was tissue destruction with leukemic cells occupying the entire organ and TEC largely absent (Fig. 17A, 17B).

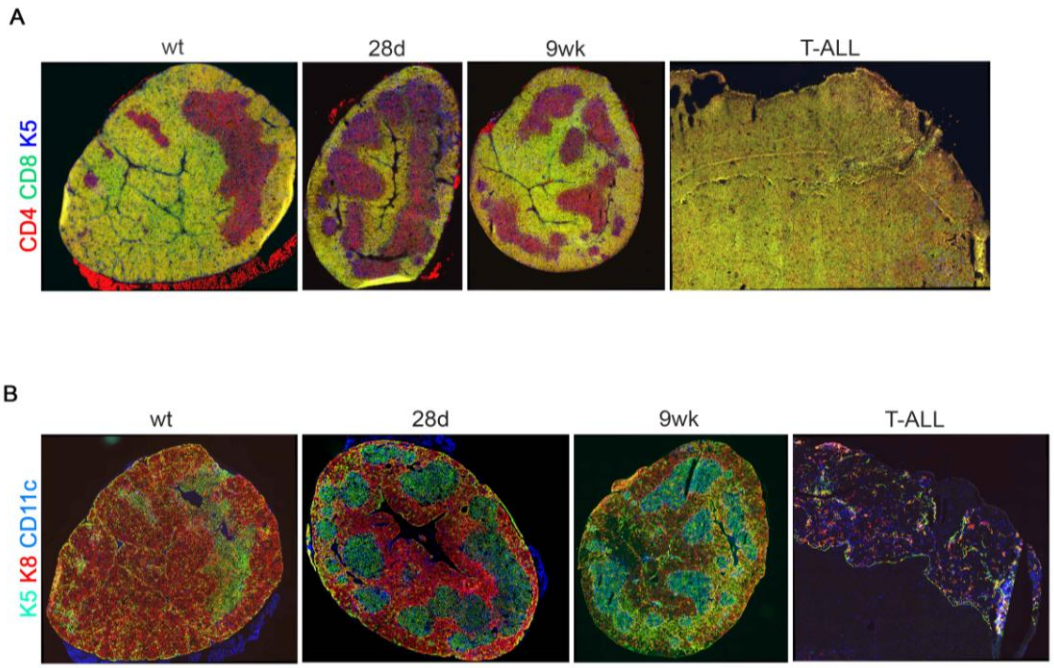

Figure 17- Progression from thymus autonomy to leukemogenesis has an impact in T cell development and epithelium. Wild type newborn thymi were grafted under the kidney capsule of adult recipients (wild type or *Rag2*$^{-/-}\gamma c^{-/-}$, as indicated) and analyzed 28 days, 9 weeks later and a timepoint in which T-ALL already developed by immunohistology for the indicated markers. (A) Staining for K5 (blue), CD4 (red) and CD8 (green). (B) Staining for K5 (green), K8 (red) and CD11c (blue). Images were acquired in Nikon High Content Screening microscope with the software Nikon Elements for the overview of the sections, using a 20x magnification. Photos of the split channels (Dapi, K5-Alexa 488, CD4-bio-Streptavidin Cy3, CD8-APC in (A) and Dapi, K5-Alexa 488, CD11c-PE, K8-Alexa 647 in (B)) are depicted in Figure 11 of the Appendix section.

Thymus architecture: Progression of thymus autonomy in a *Rag2*$^{-/-}$ background

T-ALL developed from wild type donor thymi as a consequence of prolonging thymus autonomy. Furthermore, T-ALL also developed from *Rag*$^{-/-}$ donor thymi, indicating that *Rag* is not necessary for leukemogenesis [41]. Since the transcriptome and the immunophenotype were identical between wild type and *Rag*-deficient T-ALL, we set to characterize the thymus of *Rag*$^{-/-}$ donors progressing towards T-ALL. Earlier timepoints, corresponding to those in which we study thymus autonomy in wild type thymi were also of interest to address, to characterize the parallel process in *Rag*$^{-/-}$ thymi. For this purpose, *Rag2*$^{-/-}$ thymi were transplanted under the kidney capsule of *Rag2*$^{-/-}\gamma c^{-/-}$ mice. Similarly, to the previous transplantation experiments, different timepoints were studied including 14, 28 days and 9 weeks after transplant (Fig. 18).

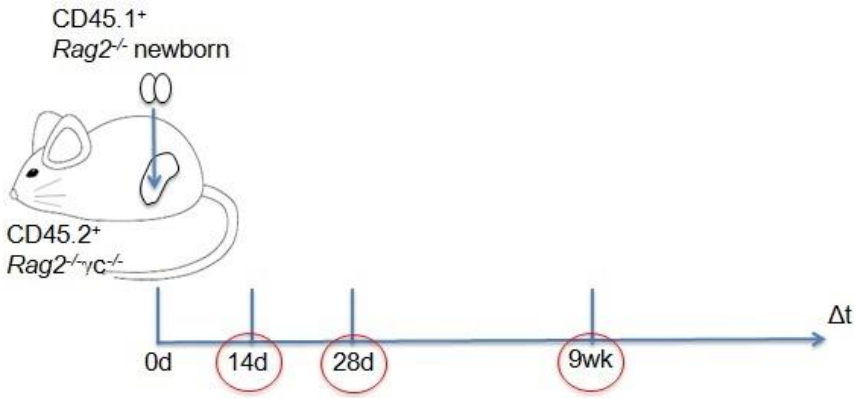

Figure 18- Representative scheme of the thymus transplantation model. *Rag2*$^{-/-}$ newborn thymi were transplanted under the kidney capsule of *Rag2*$^{-/-}\gamma c^{-/-}$ mice. Wild type B6 and *Rag2*$^{-/-}$ non-transplanted thymi served as a staining control. The grafts were analyzed 14 days, 28 days, and 9 weeks after transplant.

In *Rag2*$^{-/-}$ thymus there are no medullary areas, and K5 is expressed in many epithelial cells, scattered through the thymus (Fig. 19). Although some cells co-express K5 and K8, the majority of the epithelial cells only express either K5 or K8. The dendritic cells are also scattered throughout the organ. In all timepoints studied the lack of medullary areas and scatter of the DCs is constant and similar to the *Rag2*$^{-/-}$ control. Fourteen days after transplant, one of the grafts has a similar phenotype as the *Rag2*$^{-/-}$ thymus section, while in the other graft the majority of the cells are $K5^{+}K8^{+}$. Analyses of the grafts from 28 days and 9 weeks post-transplantation show the same heterogeneity as in day 14 after transplant, in which some grafts have TECs expressing K5 or K8 individually, while in others the tissue is marked by $K5^{+}K8^{+}$ cells (Fig. 19A). This can be better observed in the examples selected to show the complete thymus section. In general, the phenotype of the epithelium is maintained at every timepoint analyzed for the thymi in which thymocytes were still present (Fig. 19B).

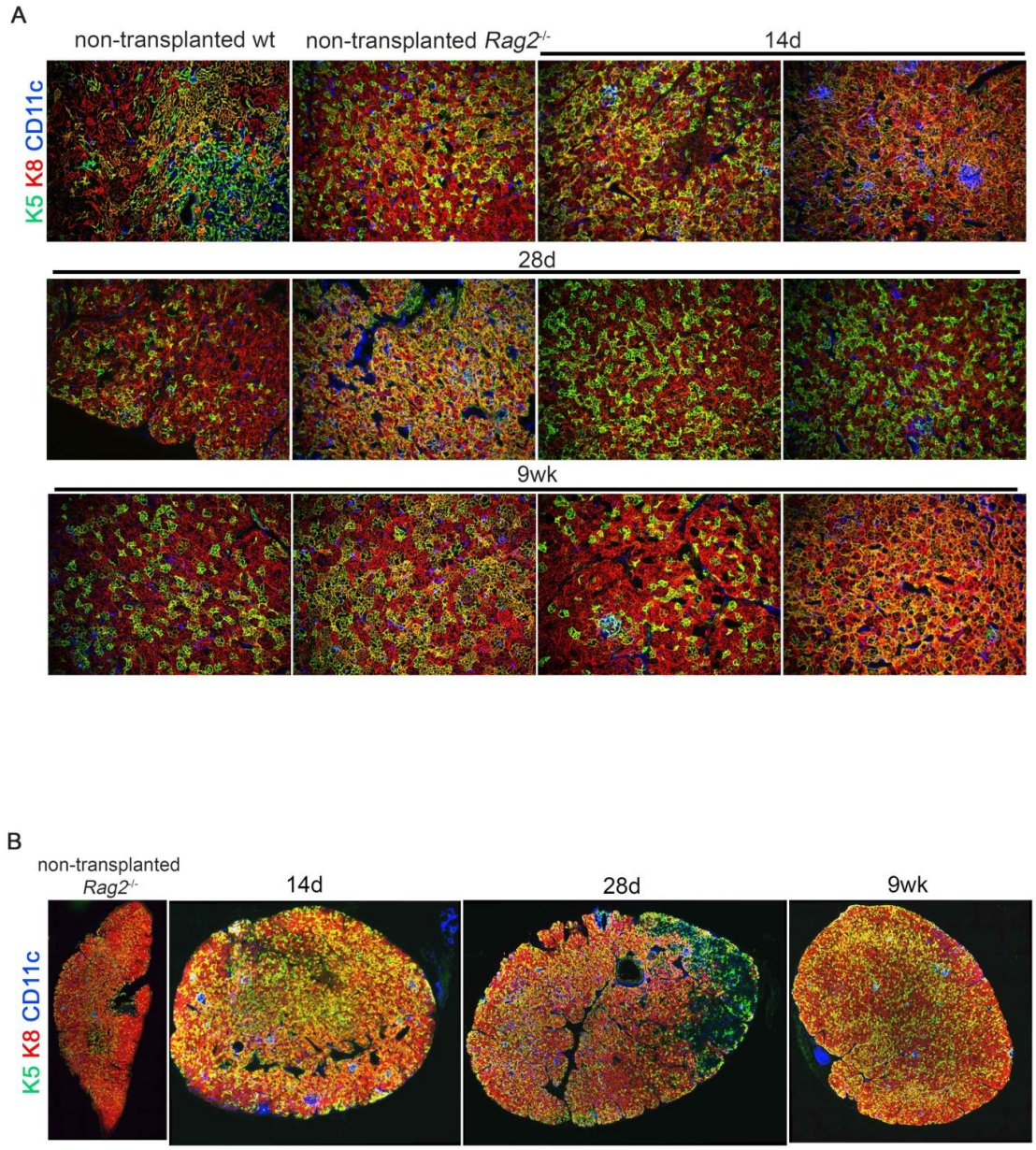

Figure 19- Thymic architecture in thymus autonomy from *Rag2*$^{-/-}$ donors. *Rag2*$^{-/-}$ newborn thymus were grafted under the kidney capsule of adult *Rag2*$^{-/-}\gamma c^{-/-}$ recipients and analyzed 14 days, 28 days and 9 weeks later by immunohistology for the indicated markers. Wild type B6 and *Rag2*$^{-/-}$ thymus were used as staining control. (A, B) Staining for K5 (green), K8 (red) and CD11c (blue). (A) Images were acquired in Leica DMRA2 microscope with the software MetaMorph using a 20x magnification. (B) The same samples in A were also acquired in a Nikon High Content Screening microscope with the software Nikon Elements, using a 20x magnification and one representative example of every timepoint is shown. Photos of the split channels (Dapi, K5-Alexa 488, CD11c-PE, K8-Alexa 647) are depicted in Figures 12 and 13 of the Appendix section. This experiment was performed with 13 mice.

Since *Rag2*$^{-/-}$ thymocytes cannot rearrange the TCRβ cannot progress beyond the double negative 3 stage. Therefore, no $CD4^+CD8^+$ double positive or single positive thymocytes could be detected in the thymus sections. As expected, the staining for K5 was scattered throughout the section, as no medullary areas organize in these thymi. In the thymus grafts (into *Rag2*$^{-/-}\gamma c^{-/-}$ recipients), this phenotype is maintained by 14 days post transplantation. Surprisingly, 28 days after transplant half of the grafts analyzed have double positive cells. No single positive

thymocytes were detected. By 9 weeks after transplant, all grafts analyzed presented cells co-expressing CD4 and CD8 (Fig. 20A). One example per timepoint was selected to show a complete thymus section and permit evaluating how the thymus evolves in the course from autonomy towards leukemia (Fig. 20B). The *Rag2*$^{-/-}$ thymus grafts are identical to thymi that were not grafted by day 14. By day 28 post-transplantation CD4^{+}CD8^{+} double positive cells emerge in half of the thymus grafts analyzed, and by 9 weeks after transplant all grafts analyzed had double-positive cells (Fig. 20A).

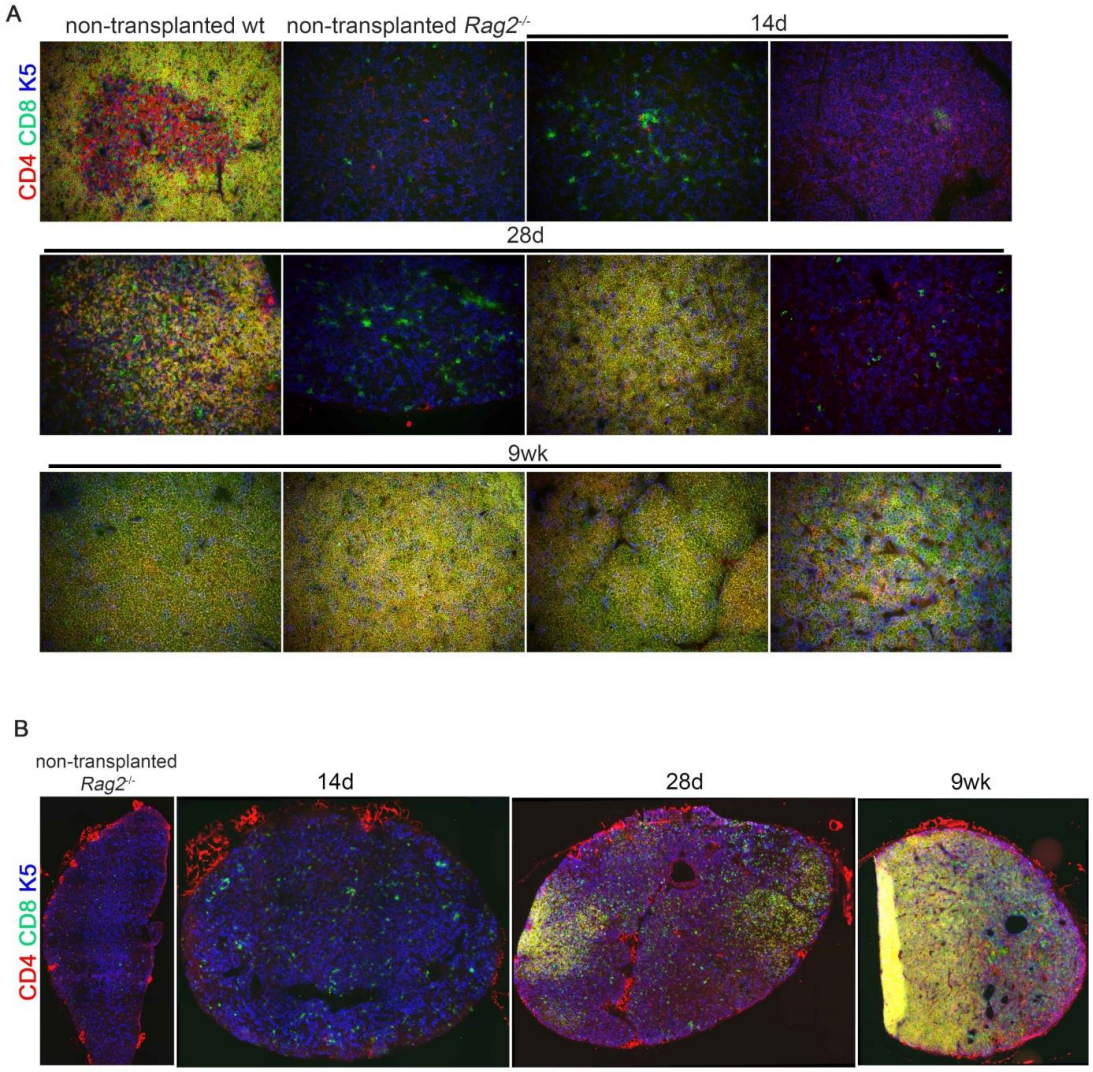

Figure 20- Double positive-like cells appear as thymus autonomy progresses in time. Sections of the same grafts shown in Figure 19 were stained for CD4 (red), CD8 (green) and K5 (blue). (A) Images were acquired in Leica DMRA2 microscope with the software MetaMorph using a 20x magnification. (B) The same samples in A were also acquired in a Nikon High Content Screening microscope with the software Nikon Elements, using a 20x magnification and one representative example of every timepoint is shown. Photos of the split channels (Dapi, K5-Alexa 488, CD4-bio-Streptavidin Cy3, CD8-APC) are depicted in Figures 14 and 15 of the Appendix section.

Thymus architecture: Thymus autonomy in multiple IL-7-unresponsive hosts

While deficiency in *Rag2* causes a developmental block at the double negative 3 stage and T cells fail to be generated, a deficiency in IL-7 signaling has a different impact in T cell differentiation. T cell development progresses through the several differentiation stages but leads to a marked decrease in the numbers of thymocytes. This leads to a dramatic decrease in the number of T cells produced. Former and current work by our lab shows that thymus autonomy can also arise in different recipients, with different genotypes, as long as they are unable to respond to IL-7. To study the structure of the thymus using different recipient mice, wild type newborn thymi were transplanted under the kidney capsule of *IL-7r*$\alpha^{-/-}$, $\gamma c^{-/-}$ and *Rag2*$^{-/-}$*IL-7r*$\alpha^{-/-}$ mice. Thymus structure was assessed 9 weeks after transplant (Fig. 21A).

Autonomy that arises from *IL-7r*$\alpha^{-/-}$, $\gamma c^{-/-}$ and *Rag2*$^{-/-}$*IL-7r*$\alpha^{-/-}$ can be characterized by a lymphocyte distribution similar to a wild type case, with double positive cells localized in the cortex and single positive cells in the medullas ($K5^+$ mTECs). The only differences are the enrichment of $CD8^+$ single positive cells in *IL-7r*$\alpha^{-/-}$ hosts (Fig. 21B).

One example showing the complete thymus section from each recipient was chosen and allows a clearer visualization of thymus autonomy maintenance in all recipients (Fig. 21C).

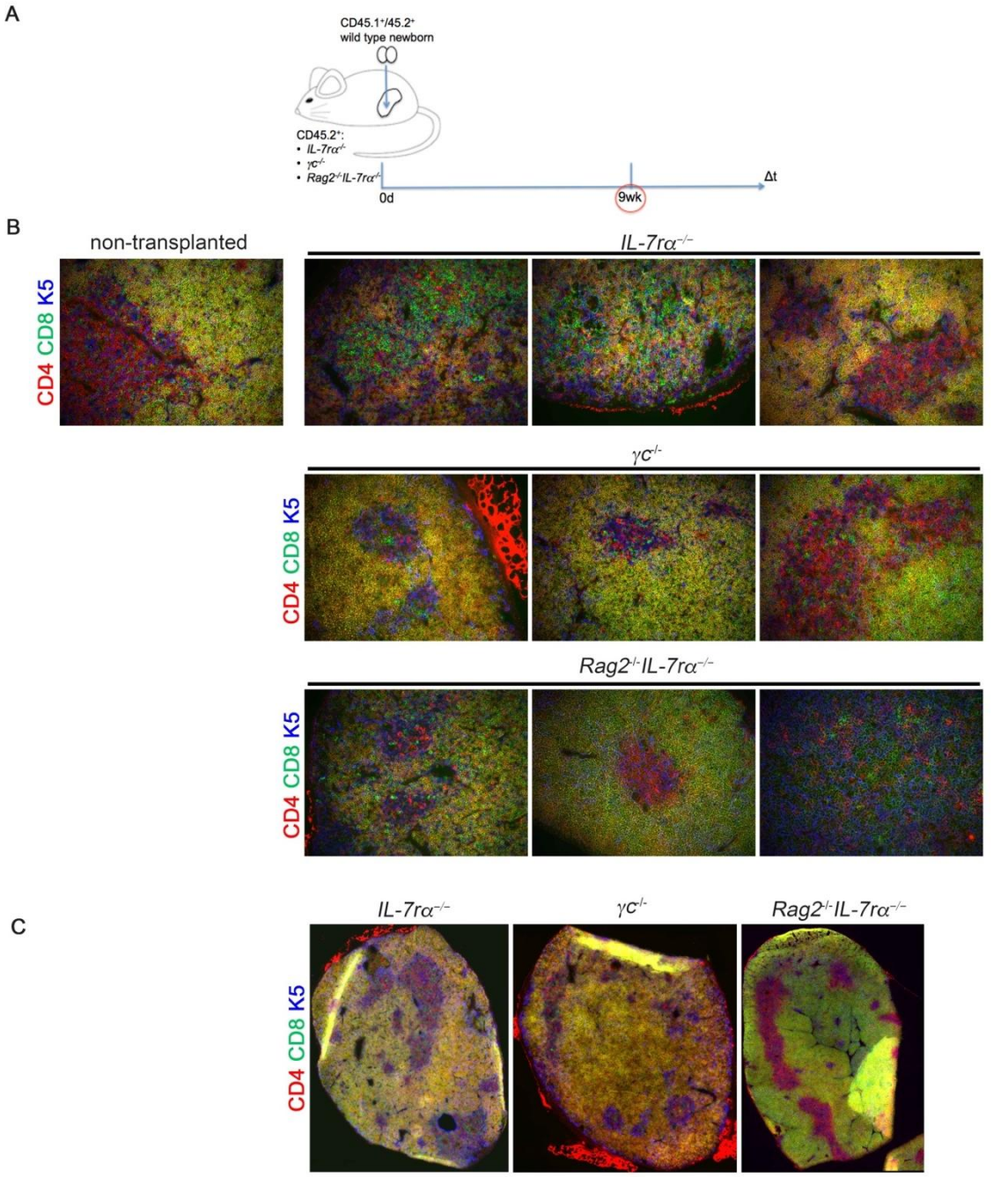

Figure 21- Thymus autonomy occurs from wild type donors grafted into *IL-7rα*$^{-/-}$, *γc*$^{-/-}$ and *Rag2*$^{-/-}$*IL-7rα*$^{-/-}$ recipients. (A) Representative scheme of the transplant model and timepoint studied using other recipients. Wild type B6 newborn thymi were transplanted into the following recipients: *IL-7rα*$^{-/-}$, *γc*$^{-/-}$ and *Rag2*$^{-/-}$*IL-7rα*$^{-/-}$ mice. The grafts were analyzed 9 weeks later by immunohistology for the indicated markers. Wild type B6 non-transplanted thymus was used as staining control. (B) Staining for CD4 (red), CD8 (green) and K5 (blue). Images were acquired in Leica DMRA2 microscope with the software MetaMorph using a 20x magnification. (B) The same samples in B were also acquired in a Nikon High Content Screening microscope with the software Nikon Elements, using a 20x magnification and one representative example of every timepoint is shown. Photos of the split channels (Dapi,K5- Alexa 488, CD4-bio-Streptavidin Cy3, CD8-APC) are depicted in Figures 16 and 17 of the Appendix section. This experiment was performed with 13 mice.

Thymic epithelial cells and dendritic cell distribution is similar in *IL-7rα*$^{-/-}$, *γc*$^{-/-}$ and *Rag2*$^{-/-}$*IL-7rα*$^{-/-}$ recipients. As previously reported with *Rag2*$^{-/-}$*γc*$^{-/-}$ recipients, these grafts present a good separation between cortex and medullas, with DCs mainly localized in the medullas. Additionally, in the majority of the grafts, some cTECs co-express K5^{+}K8^{+} (Fig. 22A).

The overview of one thymus section from each recipient leads to a better observation of phenotype similarities between the different recipients. (Fig. 22B).

Overall, the grafts analyzed from all 3 recipients resemble the phenotypes of thymus autonomy in *Rag2*$^{-/-}$*γc*$^{-/-}$ mice, indicating that the genotype of the host cells, so long as they cannot respond to IL-7, does not greatly impact on T cell development or thymic architecture during thymus autonomy.

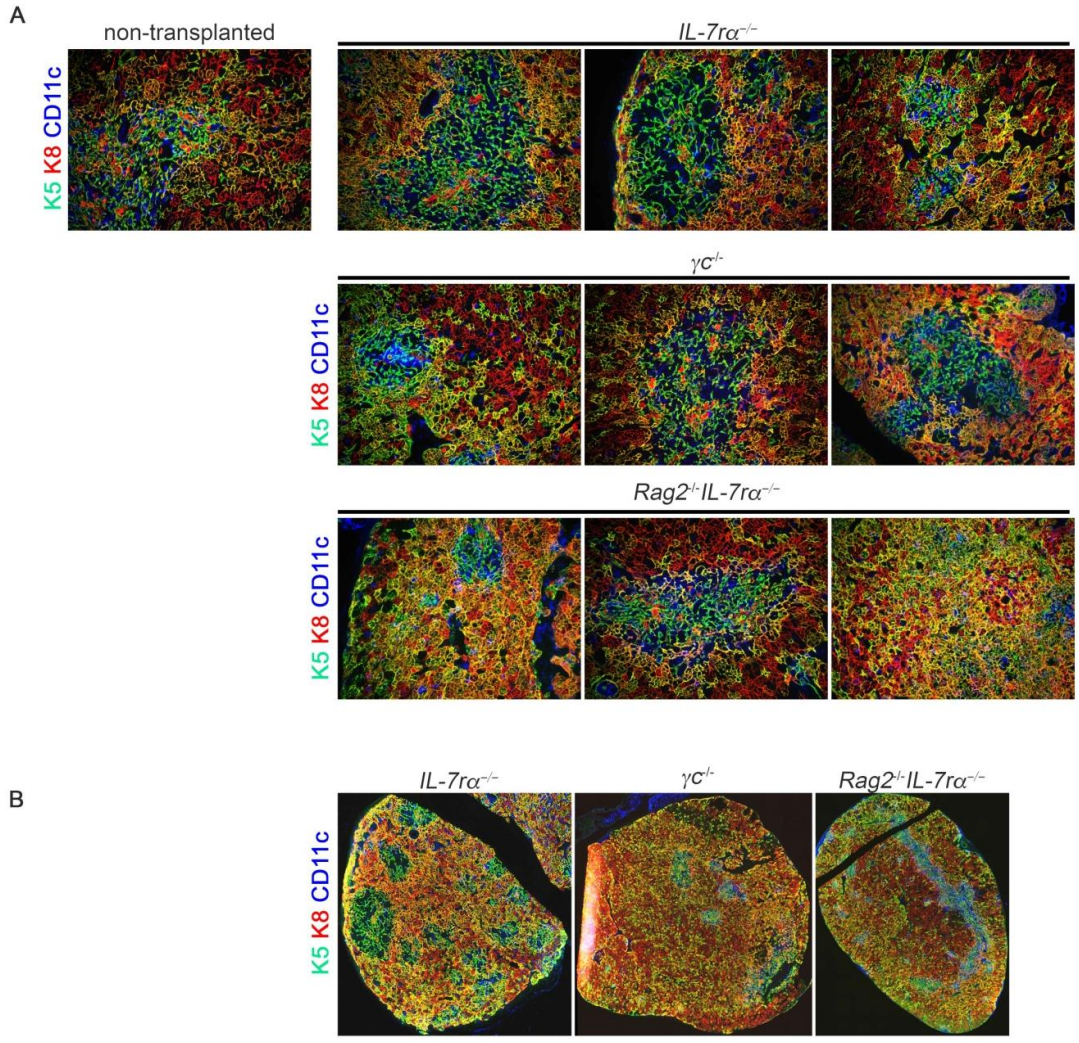

Figure 22- Nine weeks after transplant, cTECs lose their identity in *IL-7rα*$^{-/-}$, *γc*$^{-/-}$ and *Rag2*$^{-/-}$*IL-7rα*$^{-/-}$ recipients. Sections of the same grafts shown in Figure 21 were stained for K5 (green), K8 (red) and CD11c (blue). (A) Images were acquired in Leica DMRA2 microscope with the software MetaMorph using a 20x magnification. (B) The same samples in A were also acquired in a Nikon High Content Screening microscope with the software Nikon Elements, using a 20x magnification and one representative example of every timepoint is shown. Photos of the split channels (Dapi, K5-Alexa 488, CD11c-PE, K8-Alexa 647) are depicted in Figures 18 and 19 of the Appendix section.

Discussion

This work evaluated the architecture of the thymus in two extreme conditions: 1) in primary immunodeficiencies caused by defects of T lymphocyte development, and 2) during the progression that occurs from thymus autonomy to leukemia. The architecture of the thymus, i.e. the broad organization of the major cellular components of the thymus, was assessed by histology and focused on the composition and distribution of thymocytes, of TEC, and of dendritic cells. It was important to define the structure of the thymus in the immunodeficient mutants, as several were also used as recipients for the development of T-ALL.

As expected, all thymi with defects in the differentiation of T lymphocytes were dramatically reduced in cell numbers. While mutants for IL-7 or its receptor displayed a roughly normal distribution of thymocytes and TEC, *Rag* mutants had no cortex/medulla segregation [44][45]. This reflects the crosstalk that exists between developing T lymphocytes and TECs differentiation. *Rag2*$^{-/-}$ T cell precursors are unable to go beyond the double negative 3 stage during T lymphocyte development [14]. Accordingly, medullary areas are absent in the *Rag2*$^{-/-}$ thymus. This implicates that double positive and/or single positive thymocytes are required for the development of medullas. In the wild type thymus, TECs expressing both K5 and K8 are almost completely restricted to the cortico-medullary junction and identify a population of TEC progenitors [43]. As for *IL-7*$^{-/-}$, *IL-7r*$\alpha^{-/-}$ and $\gamma c^{-/-}$ thymi, the normal distribution of thymocytes is kept, and a good separation between cortical and medullary areas was observed. Nonetheless, a significant population of TECs in the cortical areas co-expressed K5 and K8, which is reminiscent of an immature TEC phenotype, possibly resulting from the reduced thymocyte number present in the cortex.

The architecture of the thymi in which thymus autonomy was active was identical to the normal thymi, in which progenitor colonization followed by turnover takes place at early stages post transplantation. However, with prolongation of autonomy in time TEC architecture starts to change. Specifically, cTECs begin to express both K5 and K8, consistent with the reduction of thymocyte number in these thymi. Interestingly, in the thymus grafts where donor T cell development ceased, the vast majority of cTECs co-expressed K5 and K8 and no lymphocytes were present in the cortex. Circulating T lymphocytes located in the medullary areas in such cases.

T-ALL eventually emerged, and leukemic cells co-expressed CD4 and CD8 to variable degrees. These accumulated in the thymus grafts causing tissue destruction that was obvious from the complete disruption of the network usually displayed by TEC.

Thymus autonomy occurs in *IL-7r*$^{-/-}$, $\gamma c^{-/-}$, *Rag2*$^{-/-}$*IL-7r*$^{-/-}$ and *Rag2*$^{-/-}\gamma c^{-/-}$ recipients. Since the hematopoietic progenitors in these mice differ in phenotype and in their capacity to respond to cytokines, it was interesting to compare whether that had any impact on thymus structure. No differences were detected between these recipients by 9 week-post-transplantation. Therefore,

IL-7 is the determinant factor for thymus autonomy while other γc cytokines have no impact in this process.

T-ALL also emerges from *Rag2*$^{-/-}$ donors [41]. Under the assumption that T-ALL is preceded by a period of thymus autonomy we confirmed that the phenotype of the *Rag2*$^{-/-}$ thymus is kept for some time, both in thymocytes and TEC. Thymi were characteristically devoid of medullary areas, the dendritic cells were scattered and most TEC expressed either K5 or K8 without an obvious organization. As soon as by 28 days post transplantation, thymocytes in half of the autonomous thymi co-expressed CD4 and CD8, which normally would never occur in *Rag2*$^{-/-}$ thymocytes. Nine weeks later, all thymi displayed the same phenotype. It is highly suggestive that this corresponds to a pre-leukemic state. This is similar to experiments of *Rag*-deficient mice exposed to sublethal doses of γ-radiation and developed double positive-like cells afterwards. The authors propose the existence of alternative pathways to β-selection that might enforce the differentiation from double negative to double positive in conditions of stress [46]. Although the experimental setup is not the same, it is conceivable that cells in thymus autonomy are under stress caused by self-renewal and excess proliferation. These could be responsible for the forced differentiation of the thymocytes into a double positive state.

In sum, thymus architecture is kept roughly normal during autonomy for the time in which thymopoiesis is normal but is reshaped over time as result of reduction of cellularity. The normal structure disappears in the leukemias, and the thymus is fully destroyed.

Future Work

The use of antibodies for K5, K8 and CD11c allowed for the visualization of the overall thymic stroma in situations of immunodeficiency, autonomy and T-ALL. The assessment of other markers such as Aire and MHC-II in mTECs might be of interest as they could be associated with the negative selection occurring during autonomy [47].

TECs produce many factors essential for thymocyte survival, proliferation and differentiation. To test whether TECs are playing a role in the progression of thymus autonomy, transcriptomic analyses in these cell subsets can be carried out. This could allow for the identification of changes in, for example, cytokines produced that could have a role in the persistence of thymocytes. We could then, generate *knock-out* mice for the genes of interest that are overexpressed or transgenic models of genes that are underexpressed, in comparison to wild type mice with thymus turnover. To test the relevance of such genes in thymus autonomy, we could transplant these thymi into *Rag2*$^{-/-}\gamma c^{-/-}$ mice and analyze for signs of thymus autonomy.

Materials and Methods

Mice

All mice used for the work described here were bred and kept at the mouse facility of Instituto Gulbenkian de Ciência (IGC). Strains that were kept and produced at the IGC were the C57BL/6J (B6, CD45.2^{+}), *IL-7*$^{-/-}$ and *Rag2*$^{-/-}$. The following strains were purchased from The Jackson Laboratory prior to establishing the respective colonies at IGC: B6.SJL-*Ptprc*^{a} Pep3^{b}/BoyJ (CD45.1^{+}), *IL-7r*$\alpha^{-/-}$ and $\gamma c^{-/-}$. *Rag2*$^{-/-}$ and *IL-7r*$\alpha^{-/-}$ mice were crossed to generate the *Rag2*$^{-/-}$*IL-7r*$\alpha^{-/-}$ line. *Rag2*$^{-/-}\gamma c^{-/-}$ mice were imported from Ulm, Germany, and rederived. All mice were bred and maintained in individually ventilated cages (IVCs) and in the specific pathogen free (SPF) area of the mouse facility. All animal experiments described here were approved by the Ethics Committee of the IGC – Fundação Calouste Gulbenkian and the Direção Geral de Alimentação e Veterinária (DGAV).

Thymus transplants

The thymi from newborn F1 donor mice (B6xB6.SJL) were isolated and the lobes were separated and kept in cold PBS. The recipient mice were anesthetized with Ketamin (100mg/kg) and Xylazine (16mg/kg). The surgery was performed in fully anesthetized animals (after pressing the paw to ensure that the mouse could not feel pain). Each recipient mouse received one thymus, transplanted under the kidney capsule, being each thymus lobe placed in each extremity of the kidney.

All transplants were executed by Rafael Paiva, a PhD student from the Lymphocyte Development and Leukemogenesis laboratory that is certified to do so.

Histology

Thymus grafts were isolated from the recipient mice at the specified time points and cryopreserved in OCT. The frozen blocks were stored at -80ºC until further use. The grafts were sectioned into 8 μm-thick slices by the Histopatology Unit of the IGC, using a Leica Cryostat CM 3050 S. The sections were collected onto glass slides, air dried and dehydrated in acetone for 10 minutes. The dehydrated and dried slides were stored at -80ºC.

Immunohistology

To proceed with the staining of the thymus sections, the slides were taken into new boxes in the cold to maintain the humidity-free environment. These were then allowed to reach room temperature. The sections were isolated using a PAP pen and rehydrated in PBS for at least 5 minutes. All blocking and staining steps were done in PBS/10%FBS in a humid environment. Blocking of the sections was performed together with the staining for DAPI (Sigma) with

114μg/ml mouse IgG (Jackson Laboratories) during 30 minutes. The staining with primary antibodies was carried out overnight at 4ºC. After washing 3 times for 5 minutes, sections were incubated for 30 minutes, at room temperature, with the secondary antibodies. All antibodies were purchased from Biolegend. The primary antibodies used were rabbit polyclonal anti-mouse Keratin 5 (Poly19055), mouse anti-Keratin 8-Alexa647 (1E8) and hamster anti-CD11c-PE (N418), or rat anti-CD4-bio (GK1.5) and rat anti-CD8-APC (53-6.7). The secondary antibodies used were α-Rabbit Alexa488 and Streptavidin-Cy3. After the incubation, the slides were washed again 3 times for 5 minutes. Stained slides were mounted with Fluoromount G (both from Southern Biotech and Invitrogen) and kept cold prior to image acquisition.

Microscopy

The images were acquired with a 20x magnification in both Leica DMRA2 microscope using the software MetaMorph and Nikon HCS microscope using Nikon Element, at the Advanced Imaging facility of the IGC. The image treatment was performed using FIJI/ImageJ and Adobe Photoshop CC 2018.

Flow cytometry

Organs were harvested and single-cell suspensions were prepared in cold PBS/10% FBS. Cells were counted with trypan blue exclusion using a Neubauer chamber. The cells were blocked with 11μg/ml mouse IgG (Jackson Laboratories) for 15 minutes and then stained for 30 minutes with the following antibodies: hamster anti-CD3ε APC-Cy7 (45-2C11), rat anti-CD4 PE (GK1.5), rat anti-CD4 PE-Cy7 (GK1.5), rat anti-CD8 FITC (from the Antibody Service of IGC, YTS169.4), rat anti-CD25 BV605 (PC61) and mouse anti-CD44 PerCP-Cy5.5 (A20). SYTOX blue was used to exclude dead cells (Molecular Probes). All antibodies were purchased from Biolegend, except for CD8-FITC, which was produced and labelled at the Antibody Service of the IGC. The samples were acquired on a BD Fortessa X-20 cell analyzer using a BD FACSDiva 8 software. Final analysis was performed using FlowJo.

References

[1] W. Ratajczak, P. Niedźwiedzka-Rystwej, B. Tokarz-Deptuła, and W. Deptuła, “Immunological memory cells,” *Cent. Eur. J. Immunol.*, vol. 43, no. 2, pp. 194–203, 2018.

[2] K. Murphy and C. Weaver, *Janeway ’ S 9 Th Edition*. 2017.

[3] F. A. Bonilla and H. C. Oettgen, “Adaptive immunity,” *J. Allergy Clin. Immunol.*, vol. 125, no. 2 SUPPL. 2, pp. S33–S40, 2010.

[4] S. Sakaguchi, K. Wing, Y. Onishi, P. Prieto-Martin, and T. Yamaguchi, “Regulatory T cells: How do they suppress immune responses?,” *Int. Immunol.*, vol. 21, no. 10, pp. 1105–1111, 2009.

[5] H.-R. Rodewald, “Thymus Organogenesis,” *Annu. Rev. Immunol.*, vol. 26, no. 1, pp. 355–388, 2008.

[6] E. V. Rothenberg, J. E. Moore, and M. A. Yui, “Launching the T-cell-lineage developmental programme,” *Nat. Rev. Immunol.*, vol. 8, no. 1, pp. 9–21, 2008.

[7] J. Halkias, H. J. Melichar, K. T. Taylor, and E. A. Robey, “Tracking migration during human T cell development,” *Cell. Mol. Life Sci.*, vol. 71, no. 16, pp. 3101–3117, 2014.

[8] K. Heinzel, C. Benz, V. C. Martins, I. D. Haidl, and C. C. Bleul, “Bone Marrow-Derived Hemopoietic Precursors Commit to the T Cell Lineage Only after Arrival in the Thymic Microenvironment,” *J. Immunol.*, vol. 178, no. 2, pp. 858–868, 2007.

[9] A. Wilson, H. R. MacDonald, and F. Radtke, “Notch 1-deficient common lymphoid precursors adopt a B cell fate in the thymus.,” *J. Exp. Med.*, vol. 194, no. 7, pp. 1003–12, 2001.

[10] U. Koch *et al.*, “Delta-like 4 is the essential, nonredundant ligand for Notch1 during thymic T cell lineage commitment,” *J. Exp. Med.*, vol. 205, no. 11, pp. 2515–2523, 2008.

[11] H. Y. Kueh *et al.*, “Asynchronous combinatorial action of four regulatory factors activates Bcl11b for T cell commitment,” *Nat. Immunol.*, vol. 17, no. 8, pp. 956–965, 2016.

[12] D. K. Shah and J. C. Zuniga-Pflucker, “An Overview of the Intrathymic Intricacies of T Cell Development,” *J. Immunol.*, vol. 192, no. 9, pp. 4017–4023, 2014.

[13] H. Hosokawa and E. V Rothenberg, “Initiation of T-Cell Development,” vol. 1, pp. 1–20, 2018.

[14] U. Koch and F. Radtke, “Mechanisms of T Cell Development and Transformation,” *Annu. Rev. Cell Dev. Biol.*, vol. 27, no. 1, pp. 539–562, 2011.

[15] C. H. Bassing, W. Swat, and F. W. Alt, “The mechanism and regulation of chromosomal V(D)J recombination,” *Cell*, vol. 109, no. 2 SUPPL. 1, pp. 45–55, 2002.

[16] H. J. Vaidya, A. Briones Leon, and C. C. Blackburn, “FOXN1 in thymus organogenesis and development,” *Eur. J. Immunol.*, vol. 46, no. 8, pp. 1826–1837, 2016.

[17] G. Anderson, P. J. L. Lane, and E. J. Jenkinson, “Generating intrathymic microenvironments to establish T-cell tolerance,” *Nat. Rev. Immunol.*, vol. 7, no. 12, pp. 954–963, 2007.

[18] N. L. Alves *et al.*, “Serial progression of cortical and medullary thymic epithelial microenvironments,” *Eur. J. Immunol.*, vol. 44, no. 1, pp. 16–22, 2014.

[19] Y. Takahama, “Journey through the thymus: Stromal guides for T-cell development and selection,” *Nat. Rev. Immunol.*, vol. 6, no. 2, pp. 127–135, 2006.

[20] H. T. Petrie and J. C. Zúñiga-Pflücker, “Zoned Out: Functional Mapping of Stromal Signaling Microenvironments in the Thymus,” *Annu. Rev. Immunol.*, vol. 25, no. 1, pp. 649–679, 2007.

[21] J. Abramson and G. Anderson, “Thymic Epithelial Cells,” *Annu. Rev. Immunol.*, vol. 35, no. 1, pp. 85–118, 2017.

[22] L. Klein, B. Kyewski, P. M. Allen, and K. A. Hogquist, “Positive and negative selection of the T cell repertoire: what thymocytes see and don’t see,” *Nat. Rev. Immunol.*, vol. 14, no. 6, pp. 377–391, 2016.

[23] B. Kyewski and L. Klein, “a Central Role for Central Tolerance,” *Annu. Rev. Immunol.*, vol. 24, no. 1, pp. 571–606, 2006.

[24] L. De Martino *et al.*, “APECED: A paradigm of complex interactions between genetic background and susceptibility factors,” *Front. Immunol.*, vol. 4, no. October, pp. 1–10, 2013.

[25] M. Christine and R. Warrington, “Primary immunodeficiency,” *Allergy Asthma Clin Immunol*, vol. 7, no. S1, pp. 1–8, 2011.

[26] R. Spolski, D. Gromer, and W. J. Leonard, “The γc family of cytokines: fine-tuning signals from IL-2 and IL-21 in the regulation of the immune response,” *F1000Research*, vol. 6, no. 0, p. 1872, 2017.

[27] W. J. Leonard, “Cytokines and immunodeficiency diseases,” *Nat. Rev. Immunol.*, vol. 1, no. 3, pp. 200–208, 2001.

[28] A. Puel, S. F. Ziegler, R. H. Buckley, and W. J. Leonard, “Defective IL7R expression in T-B+ NK+ severe combined immunodeficiency,” *Nat. Genet.*, vol. 20, no. 4, pp. 394–397, 1998.

[29] A. Puel and W. J. Leonard, “Mutations in the gene for the IL-7 receptor result in T-B+NK+ severe combined immunodeficiency disease,” *Curr. Opin. Immunol.*, vol. 12, no. 4, pp. 468–473, 2000.

[30] B. Corneo *et al.*, “Identical mutations in RAG1 or RAG2 genes leading to defective V (D) J recombinase activity can cause either T-B − severe combined immune deficiency or Omenn syndrome,” vol. 97, no. D, pp. 2772–2776, 2012.

[31] T. Niehues, R. Perez-Becker, and C. Schuetz, “More than just SCID-The phenotypic range of combined immunodeficiencies associated with mutations in the recombinase activating genes (RAG) 1 and 2,” *Clin. Immunol.*, vol. 135, no. 2, pp. 183–192, 2010.

[32] L. A. Pui CH, Robison L.L, “Acute lymphoblastic leukaemia,” *Lancet*, vol. 371, no. 9617, pp. 1030–1043, 22AD.

[33] C. Grabher, H. Von Boehmer, and A. T. Look, “Notch 1 activation in the molecular pathogenesis of T-cell acute lymphoblastic leukaemia,” *Nat. Rev. Cancer*, vol. 6, no. 5, pp. 347–359, 2006.

[34] A. P. Weng, “Activating Mutations of NOTCH1 in Human T Cell Acute Lymphoblastic Leukemia,” *Science (80-.).*, vol. 306, no. 5694, pp. 269–271, 2004.

[35] P. P. Zenatti *et al.*, “Oncogenic IL7R gain-of-function mutations in childhood T-cell acute lymphoblastic leukemia,” *Nat. Genet.*, vol. 43, no. 10, pp. 932–941, 2011.

[36] T. K. Tan, C. Zhang, and T. Sanda, “Oncogenic transcriptional program driven by TAL1 in T-cell acute lymphoblastic leukemia.,” *Int. J. Hematol.*, 2018.

[37] M. P. Mccormack, L. F. Young, S. Vasudevan, and C. A. De Graaf, “The Lmo2 Oncogene Initiates Leukemia in Mice by Inducing Thymocyte Self-Renewal,” no. February, pp. 879–884, 2010.

[38] S. P. Berzins, R. L. Boyd, and J. F. Miller, “The role of the thymus and recent thymic migrants in the maintenance of the adult peripheral lymphocyte pool.,” *J. Exp. Med.*, vol. 187, no. 11, pp. 1839–1848, 1998.

[39] V. C. Martins *et al.*, “Thymus-autonomous T cell development in the absence of progenitor import,” *J. Exp. Med.*, vol. 209, no. 8, pp. 1409–1417, 2012.

[40] L. Peaudecerf *et al.*, “Thymocytes may persist and differentiate without any input from bone marrow progenitors,” vol. 209, no. 8, pp. 1401–1408, 2012.

[41] V. C. Martins *et al.*, “Cell competition is a tumour suppressor mechanism in the thymus,” *Nature*, vol. 509, no. 7501, pp. 465–470, 2014.

[42] L. Peaudecerf, G. Krenn, P. Gonçalves, F. Vasseur, and B. Rocha, “Thymocytes self-renewal: A major hope or a major threat?,” *Immunol. Rev.*, vol. 271, no. 1, pp. 173–184, 2016.

[43] D. B. Klug, C. Carter, E. Crouch, D. Roop, C. J. Conti, and E. R. Richie, “Interdependence of cortical thymic epithelial cell differentiation and T-lineage commitment.,” *Proc. Natl. Acad. Sci. U. S. A.*, vol. 95, no. 20, pp. 11822–11827, 1998.

[44] F. Rucci *et al.*, “Abnormalities of thymic stroma may contribute to immune dysregulation in murine models of leaky severe combined immunodeficiency,” *Front. Immunol.*, vol. 2, no. MAY, pp. 1–13, 2011.

[45] V. Marrella, P. L. Poliani, L. D. Notarangelo, and A. Villa, “Rag defects and thymic stroma: Lessons from animal models,” *Front. Immunol.*, vol. 5, no. JUN, pp. 1–6, 2014.

[46] J. C. Zúñiga-Pflücker, D. Jiang, P. L. Schwartzberg, and M. J. Lenardo, “Sublethal γ-radiation induces differentiation of CD4-/CD8- into CD4+/CD8+ thymocytes without T cell receptor β rearrangement in recombinase activation gene 2-/- mice,” *J. Exp. Med.*, vol. 180, no. October, pp. 2–6, 1994.

[47] Y. Hamazaki, M. Sekai, and N. Minato, “Medullary thymic epithelial stem cells: role in thymic epithelial cell maintenance and thymic involution,” *Immunol Rev*, vol. 271, no. 1, pp. 38–55, 2016.

Appendix

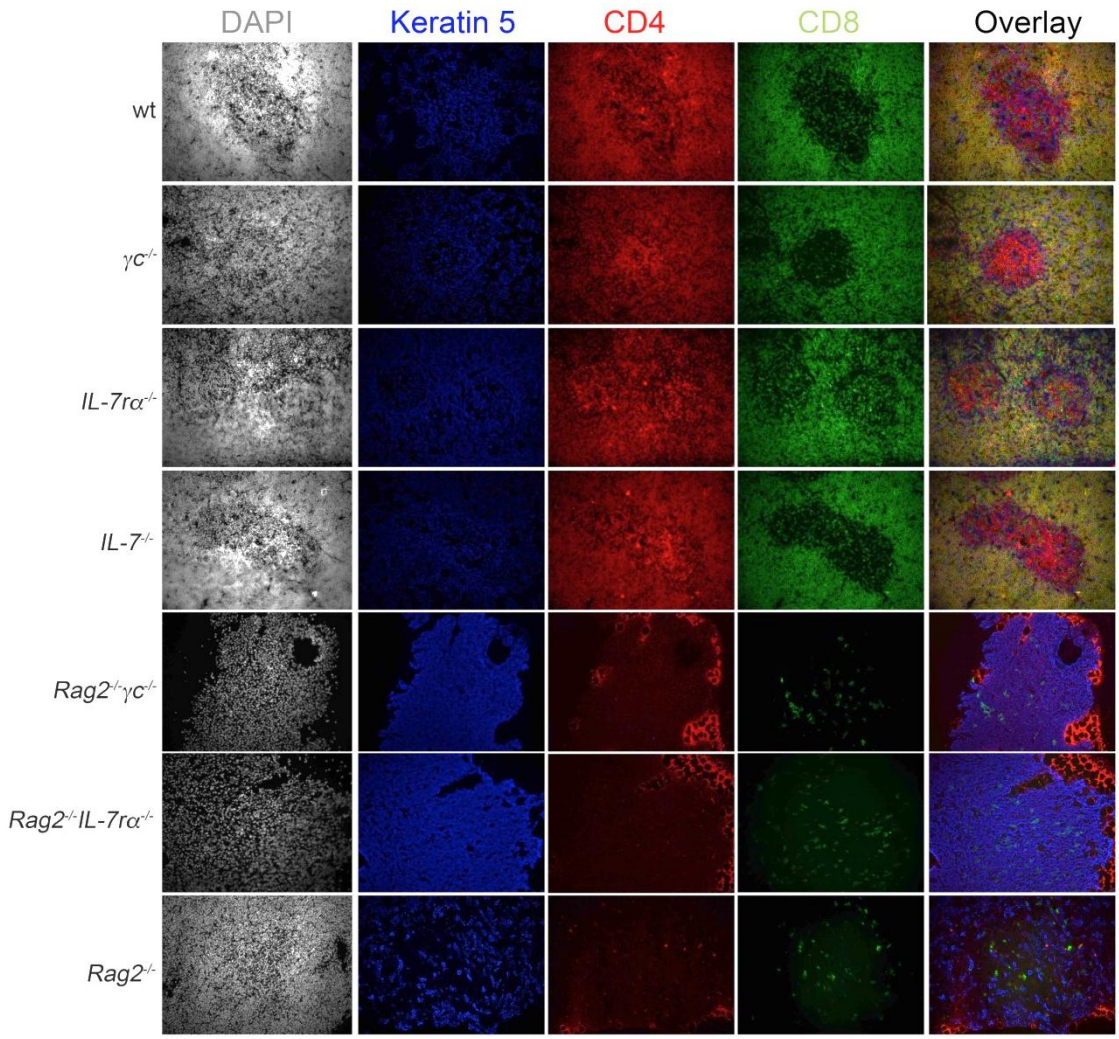

Figure 1- Photos of the split channels from immunohistology of thymus sections of B6 wild type, *γc*$^{-/-}$, *IL-7rα*$^{-/-}$, *IL-7*$^{-/-}$, *Rag2*$^{-/-}$, *Rag2*$^{-/-}$*IL-7rα*$^{-/-}$, and *Rag2*$^{-/-}$*γc*$^{-/-}$ mice, as depicted. Staining for Dapi is represented in grey, for K5-Alexa 488 in blue, for CD4-bio-Streptavidin Cy3 in red and for CD8-APC in green. In the right column are the overlays of all channels. Images were acquired in Leica DMRA2 microscope with the software MetaMorph using a 20x magnification.

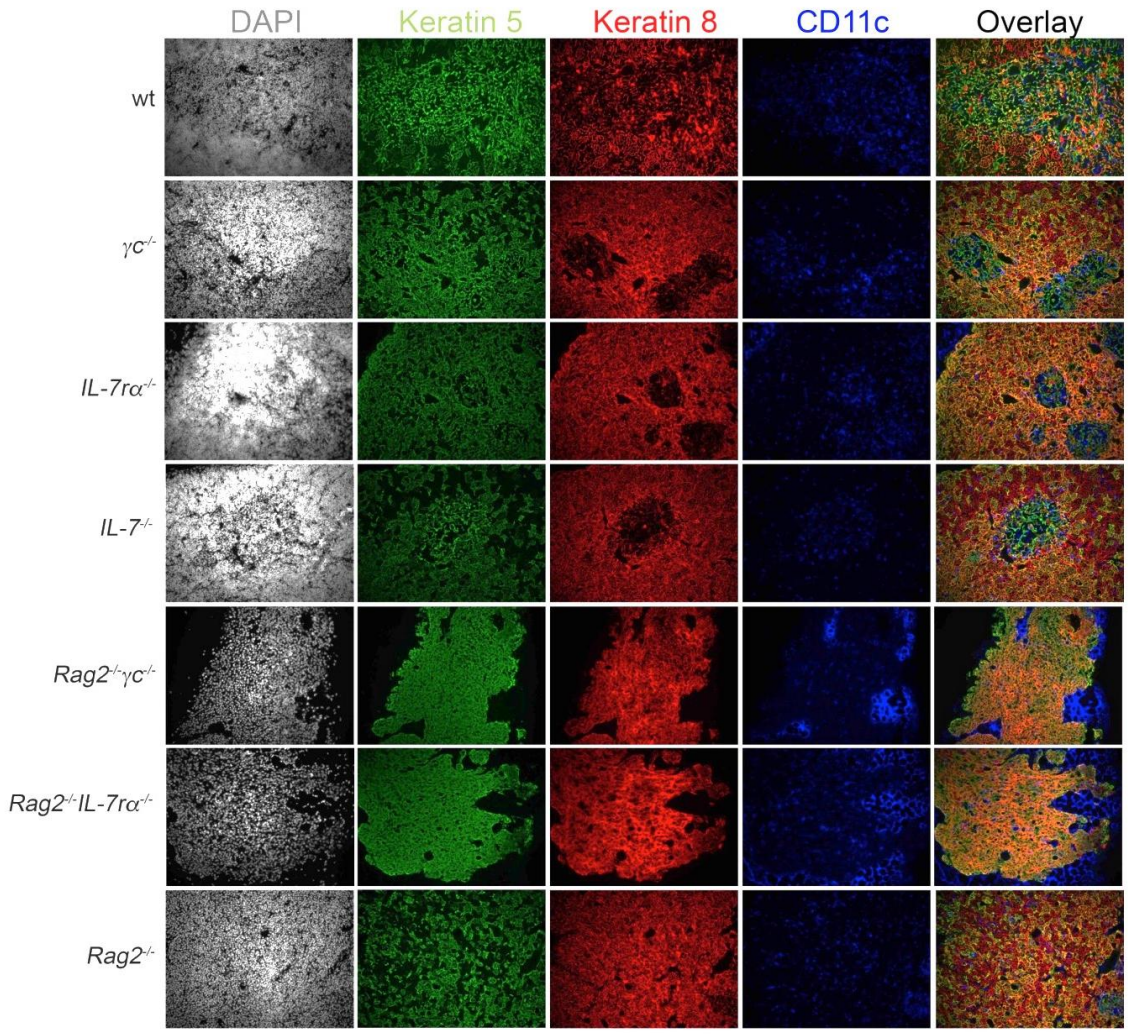

Figure 2- Photos of the split channels from immunohistology of thymus sections of B6 wild type, *γc*$^{-/-}$, *IL-7rα*$^{-/-}$, *IL-7*$^{-/-}$, *Rag2*$^{-/-}$, *Rag2*$^{-/-}$*IL-7rα*$^{-/-}$, and *Rag2*$^{-/-}$*γc*$^{-/-}$ mice, as depicted. Staining for Dapi is represented in grey, for K5-Alexa 488 in green, for K8-Alexa 647 in red and for CD11c-PE in blue. In the right column are the overlays of all channels. Images were acquired in Leica DMRA2 microscope with the software MetaMorph using a 20x magnification.

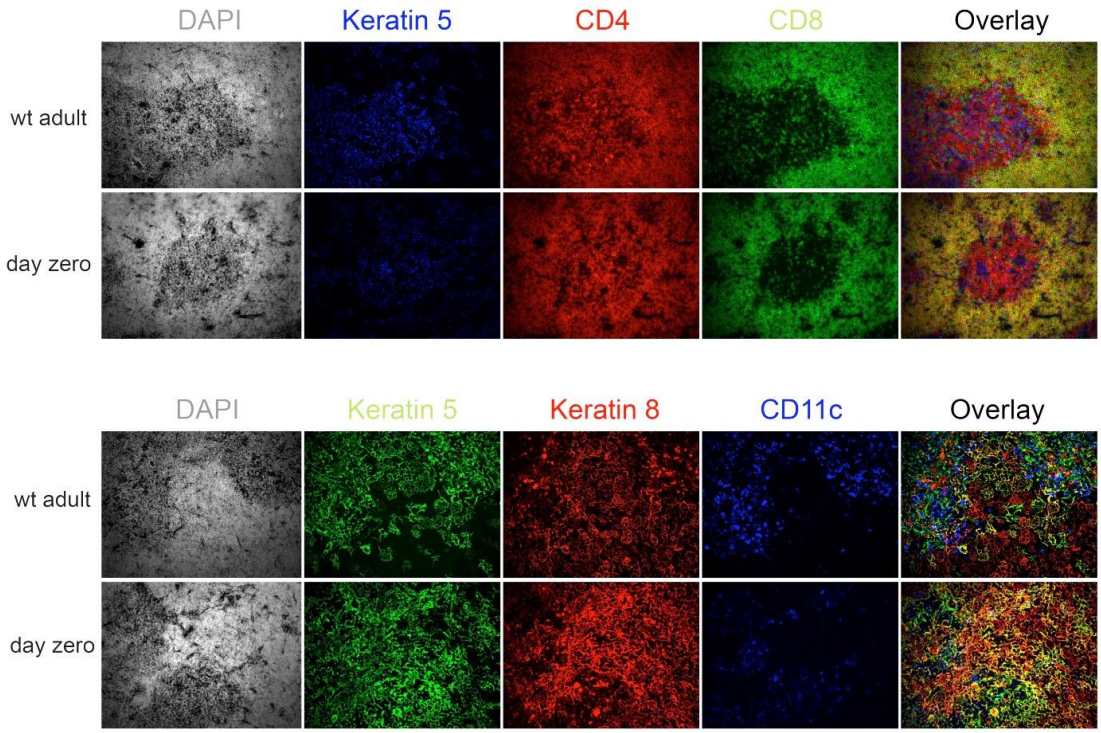

Figure 3- Photos of the split channels from immunohistology of thymus sections of wild type newborn (day 0) and adult thymus, as depicted. In the two upper panels staining for Dapi is represented in grey, for K5-Alexa 488 in blue, for CD4-bio-Streptavidin Cy3 in red and for CD8-APC in green. In the two bottom panels staining for Dapi is represented in grey, for K5-Alexa 488 in green, for K8-Alexa 647 in red and for CD11c-PE in blue In the right columns are the overlays of all channels. Images were acquired in Leica DMRA2 microscope with the software MetaMorph using a 20x magnification.

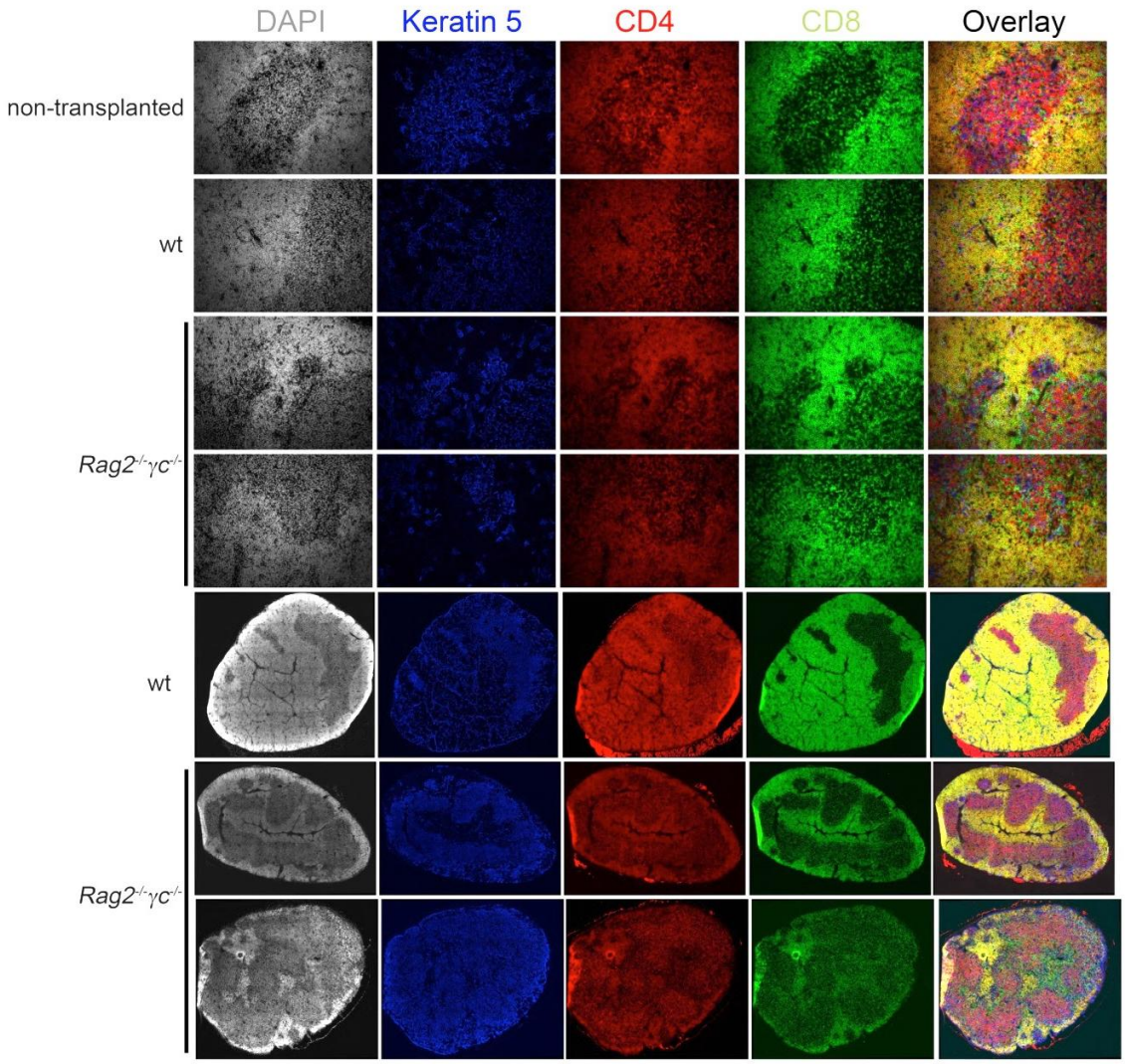

Figure 4- Photos of the split channels from immunohistology of sections from non-transplanted wild type B6 thymus, and of the grafted wild type thymi into wild type and *Rag2*$^{-/-}\gamma c^{-/-}$ recipients, 28 days after transplant. Staining for Dapi is represented in grey, for K5-Alexa 488 in blue, for CD4-bio-Streptavidin Cy3 in red and for CD8-APC in green. In the right column are the overlays of all channels. Images were acquired in Leica DMRA2 microscope with the software MetaMorph using a 20x magnification and in Nikon High Content Screening microscope with the software Nikon Elements also using a 20x magnification

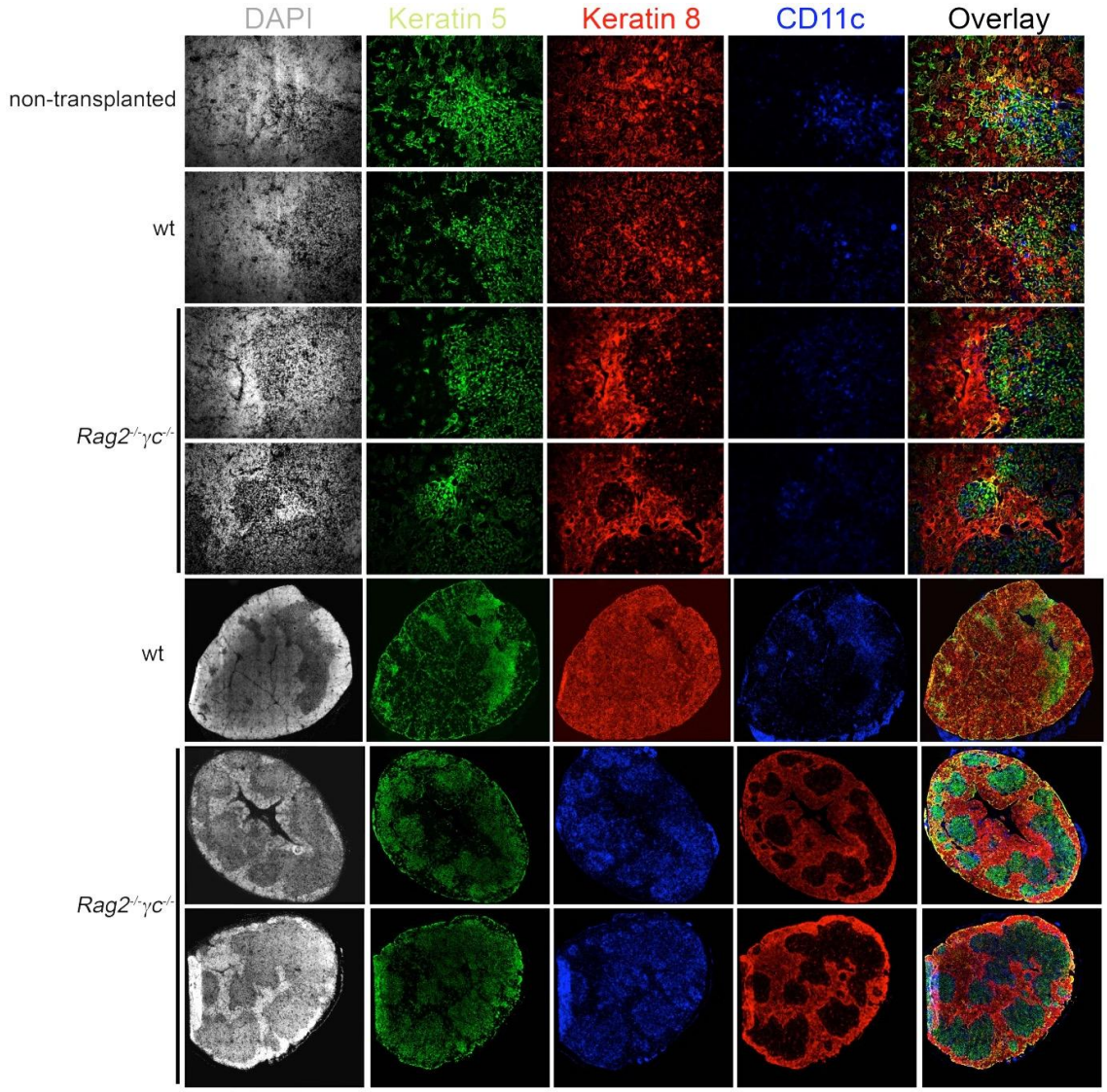

Figure 5- Photos of the split channels from immunohistology of sections from non-transplanted wild type B6 thymus, and of the grafted wild type thymi into wild type and *Rag2*$^{-/-}\gamma c^{-/-}$ recipients, 28 days after transplant. Staining for Dapi is represented in grey, for K5-Alexa 488 in green, for K8-Alexa 647 in red and for CD11c-PE in blue. In the right column are the overlays of all channels. Images were acquired in Leica DMRA2 microscope with the software MetaMorph using a 20x magnification and in Nikon High Content Screening microscope with the software Nikon Elements also using a 20x magnification.

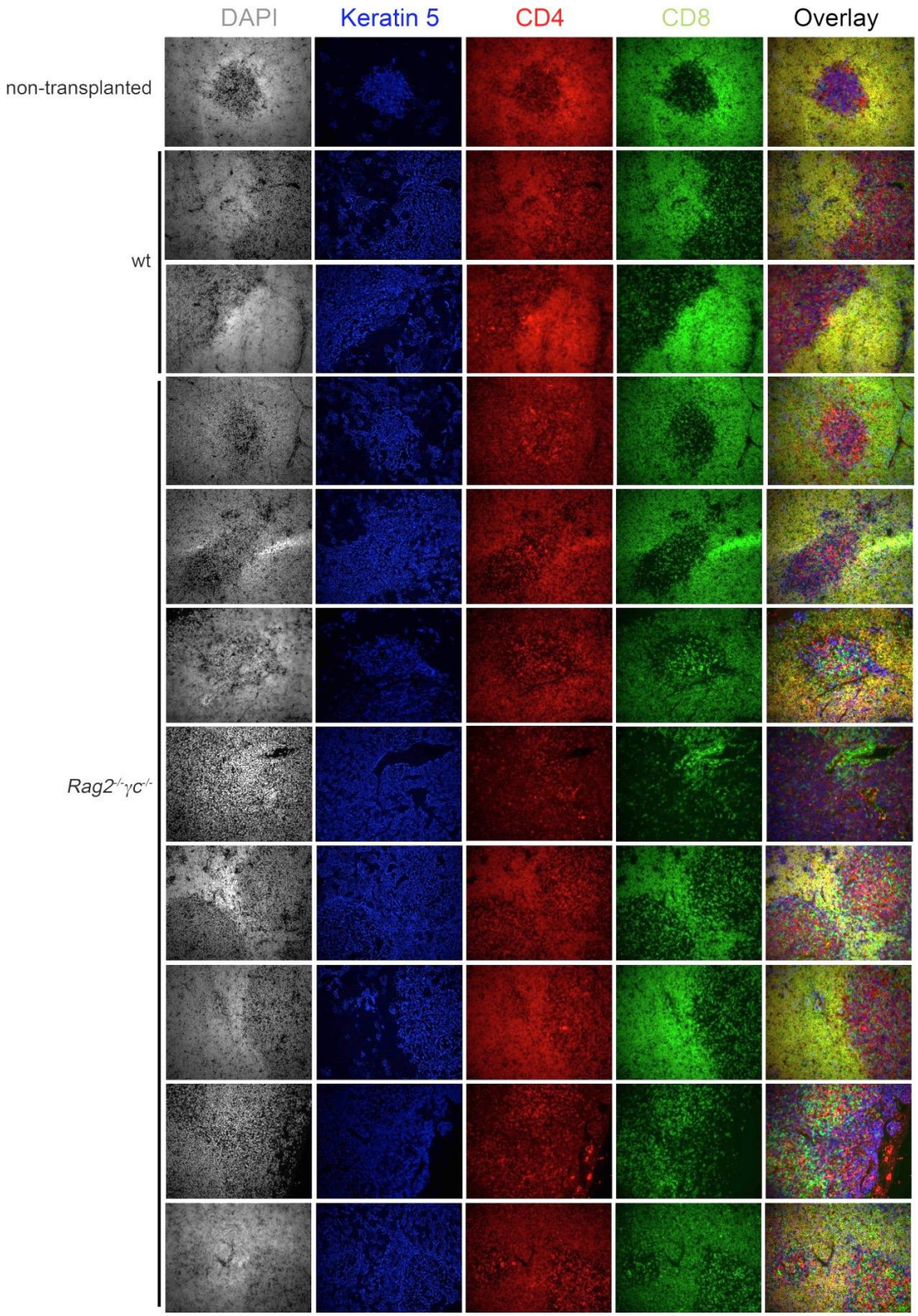

Figure 6- Photos of the split channels from immunohistology of sections from non-transplanted wild type B6 thymus, and of the grafted wild type thymi into wild type and *Rag2*$^{-/-}$*γc*$^{-/-}$ recipients, 9 weeks after transplant. Staining for Dapi is represented in grey, for K5-Alexa 488 in blue, for CD4-bio-Streptavidin Cy3 in red and for CD8-APC in green. In the right column are the overlays of all channels. Images were acquired in Leica DMRA2 microscope with the software MetaMorph using a 20x magnification.

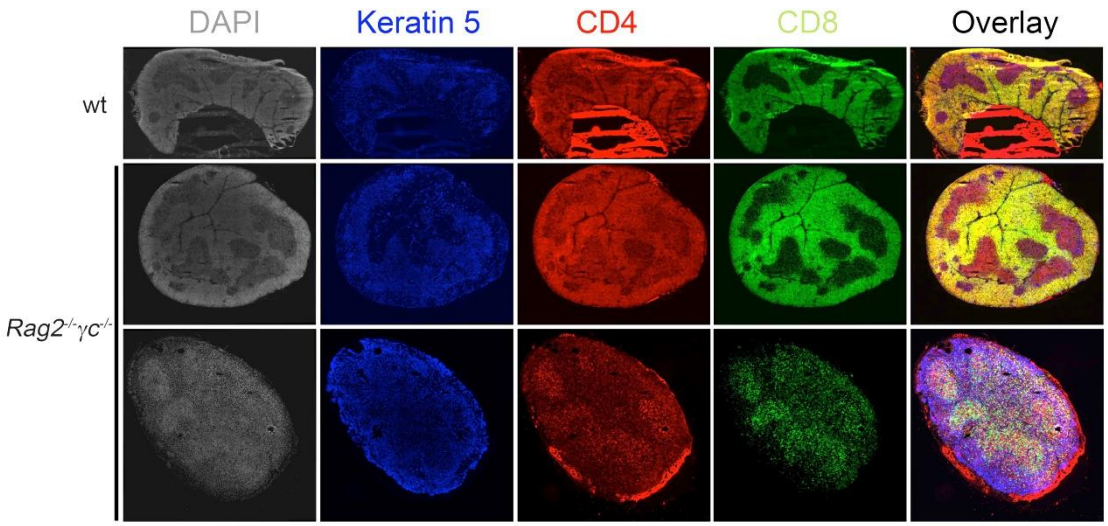

Figure 7- Photos of the split channels from immunohistology of sections from non-transplanted wild type B6 thymus, and of the grafted wild type thymi into wild type and *Rag2*$^{-/-}\gamma c^{-/-}$ recipients, 9 weeks after transplant. Staining for Dapi is represented in grey, for K5-Alexa 488 in blue, for CD4-bio-Streptavidin Cy3 in red and for CD8-APC in green. In the right column are the overlays of all channels. Images were acquired in Nikon High Content Screening microscope with the software Nikon Elements using a 20x magnification.

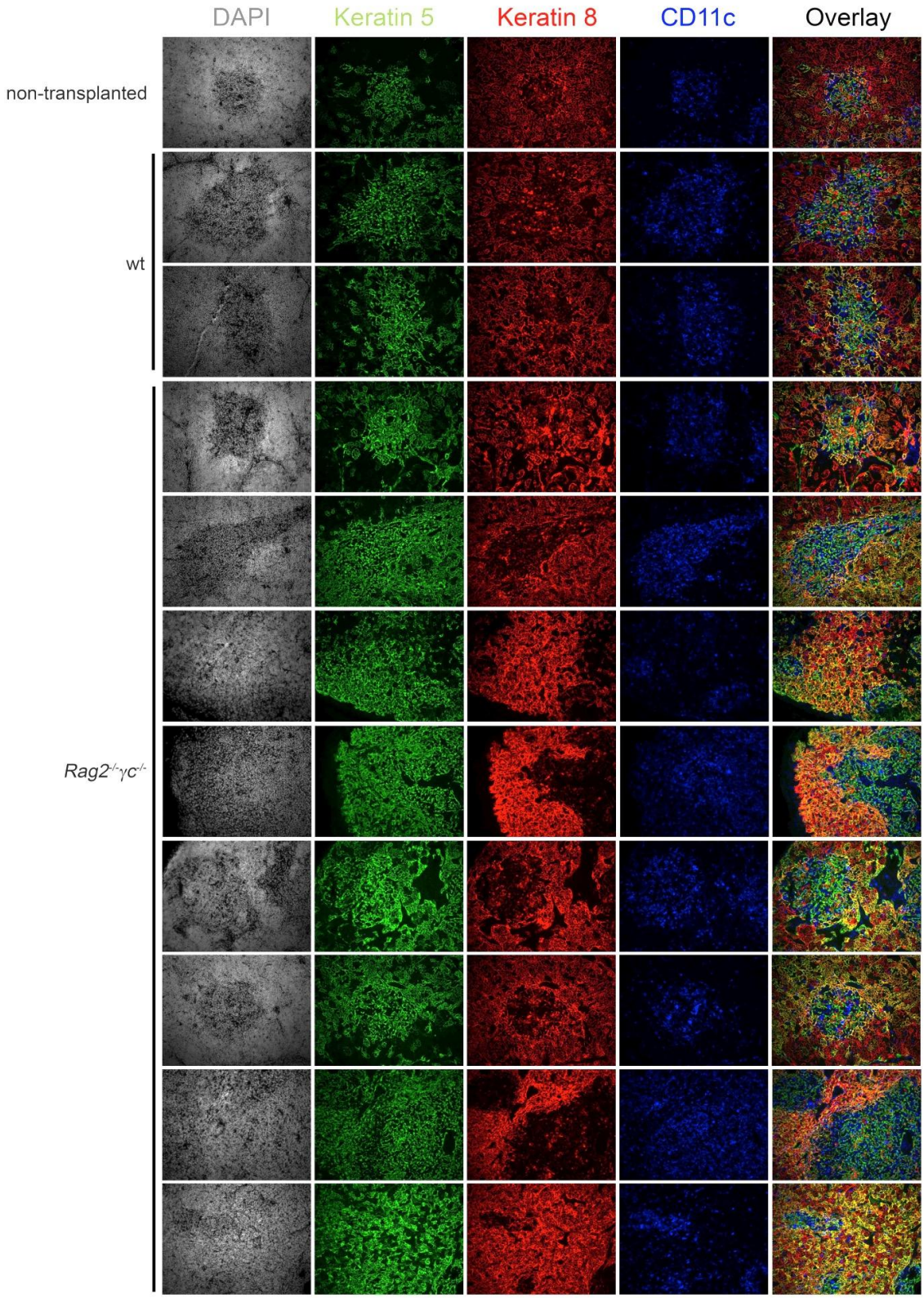

Figure 8- Photos of the split channels from immunohistology of sections from non-transplanted wild type B6 thymus, and of the grafted wild type thymi into wild type and *Rag2*$^{-/-}\gamma c^{-/-}$ recipients, 9 weeks after transplant. Staining for Dapi is represented in grey, for K5-Alexa 488 in green, for K8-Alexa 647 in red and for CD11c-PE in blue. In the right column are the overlays of all channels. Images were acquired in Leica DMRA2 microscope with the software MetaMorph using a 20x magnification.

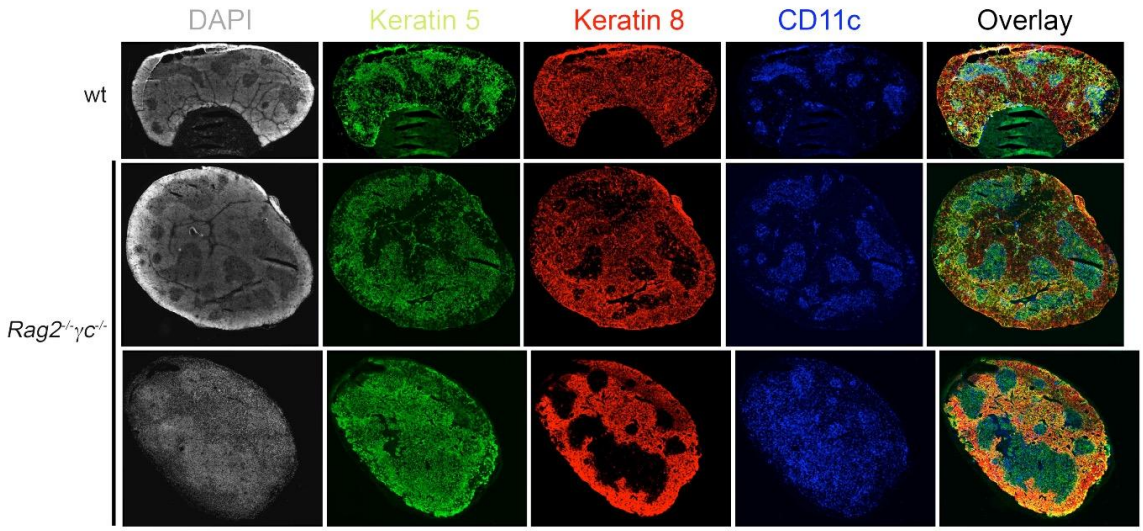

Figure 9- Photos of the split channels from immunohistology of sections from non-transplanted wild type B6 thymus, and of the grafted wild type thymi into wild type and *Rag2*$^{-/-}\gamma c^{-/-}$ recipients, 9 weeks after transplant. Staining for Dapi is represented in grey, for K5-Alexa 488 in green, for K8-Alexa 647 in red and for CD11c-PE in blue. In the right column are the overlays of all channels. Images were acquired in Nikon High Content Screening microscope with the software Nikon Elements using a 20x magnification.

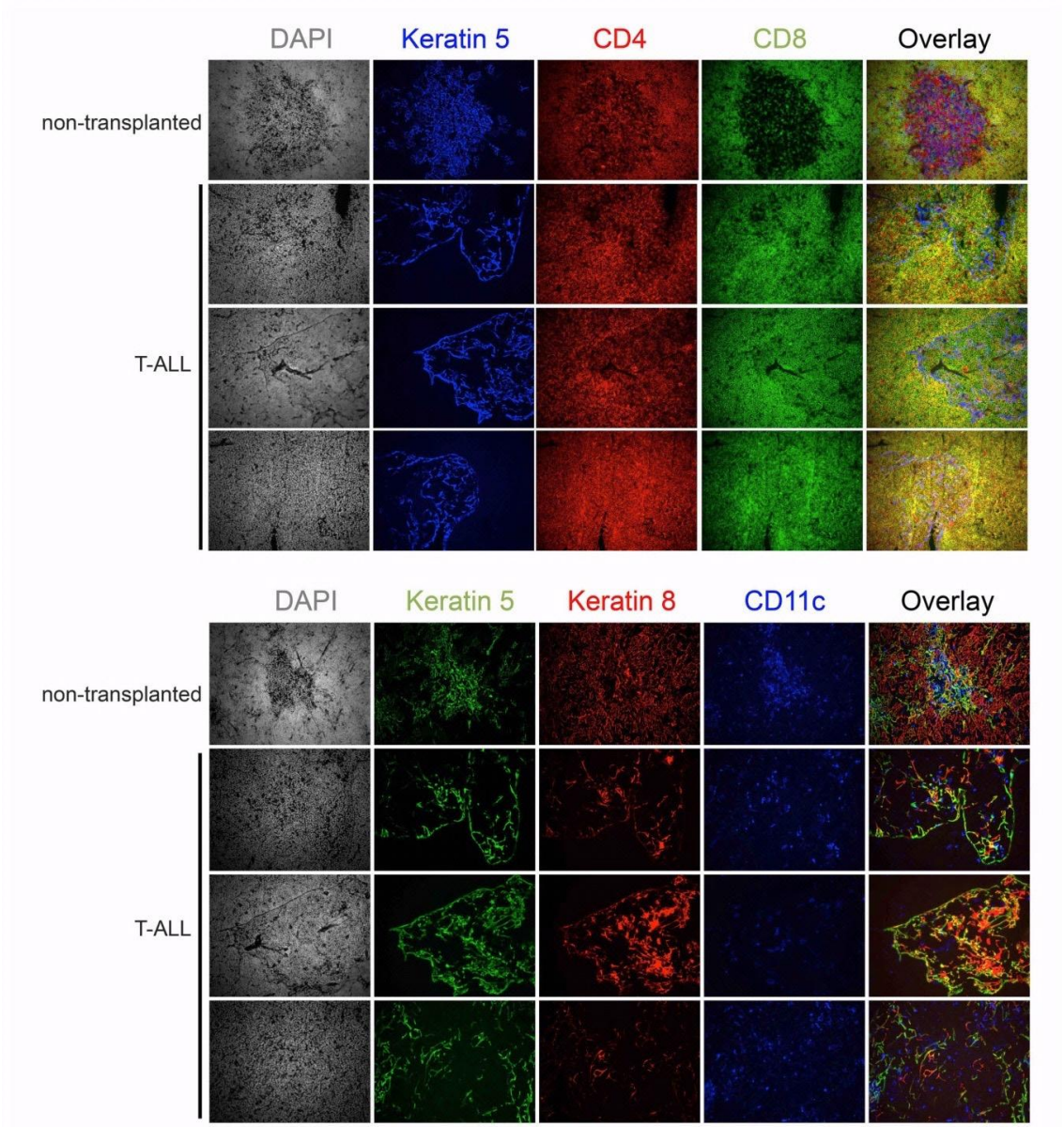

Figure 10- Photos of the split channels from immunohistology of sections of non-transplanted wild type B6 thymus and T-ALL grafts. In the four upper panels staining for Dapi is represented in grey, for K5-Alexa 488 in blue, for CD4-bio-Streptavidin Cy3 in red and for CD8-APC in green. In the four bottom panels staining for Dapi is represented in grey, for K5-Alexa 488 in green, for K8-Alexa 647 in red and for CD11c-PE in blue In the right columns are the overlays of all channels. Images were acquired in Leica DMRA2 microscope with the software MetaMorph using a 20x magnification.

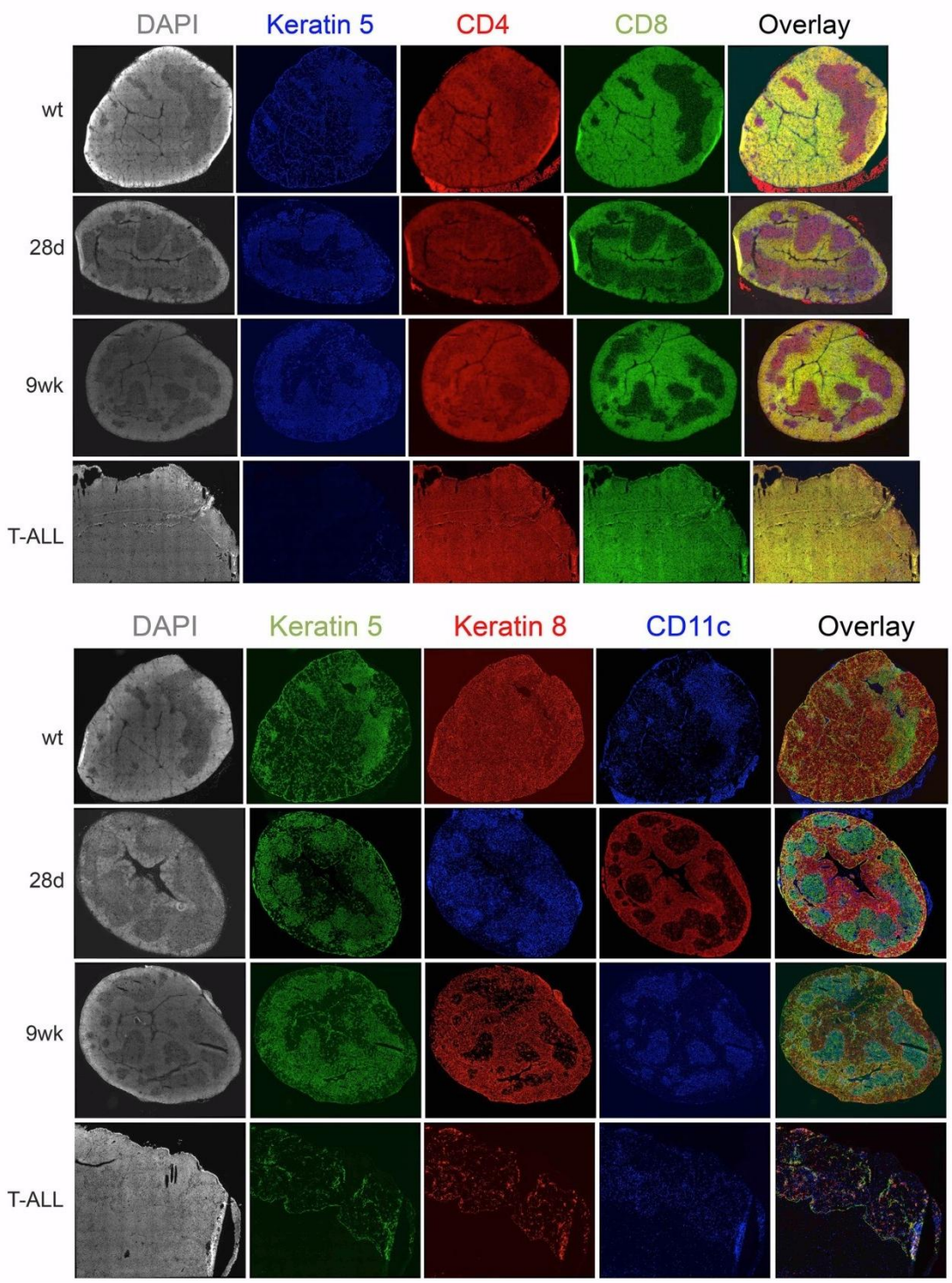

Figure 11- Photos of the split channels from immunohistology in sections of the grafted wild type thymi into wild type and *Rag2*$^{-/-}\gamma c^{-/-}$ recipients (28 days and 9 weeks after transplant), and in a T-ALL situation. In the four upper panels staining for Dapi is represented in grey, for K5-Alexa 488 in blue, for CD4-bio-Streptavidin Cy3 in red and for CD8-APC in green. In the four bottom panels staining for Dapi is represented in grey, for K5-Alexa 488 in green, for K8-Alexa 647 in red and for CD11c-PE in blue. In the right columns are the overlays of all channels. Images were acquired in Leica DMRA2 microscope with the software MetaMorph using a 20x magnification and in Nikon High Content Screening microscope with the software Nikon Elements also using a 20x magnification.

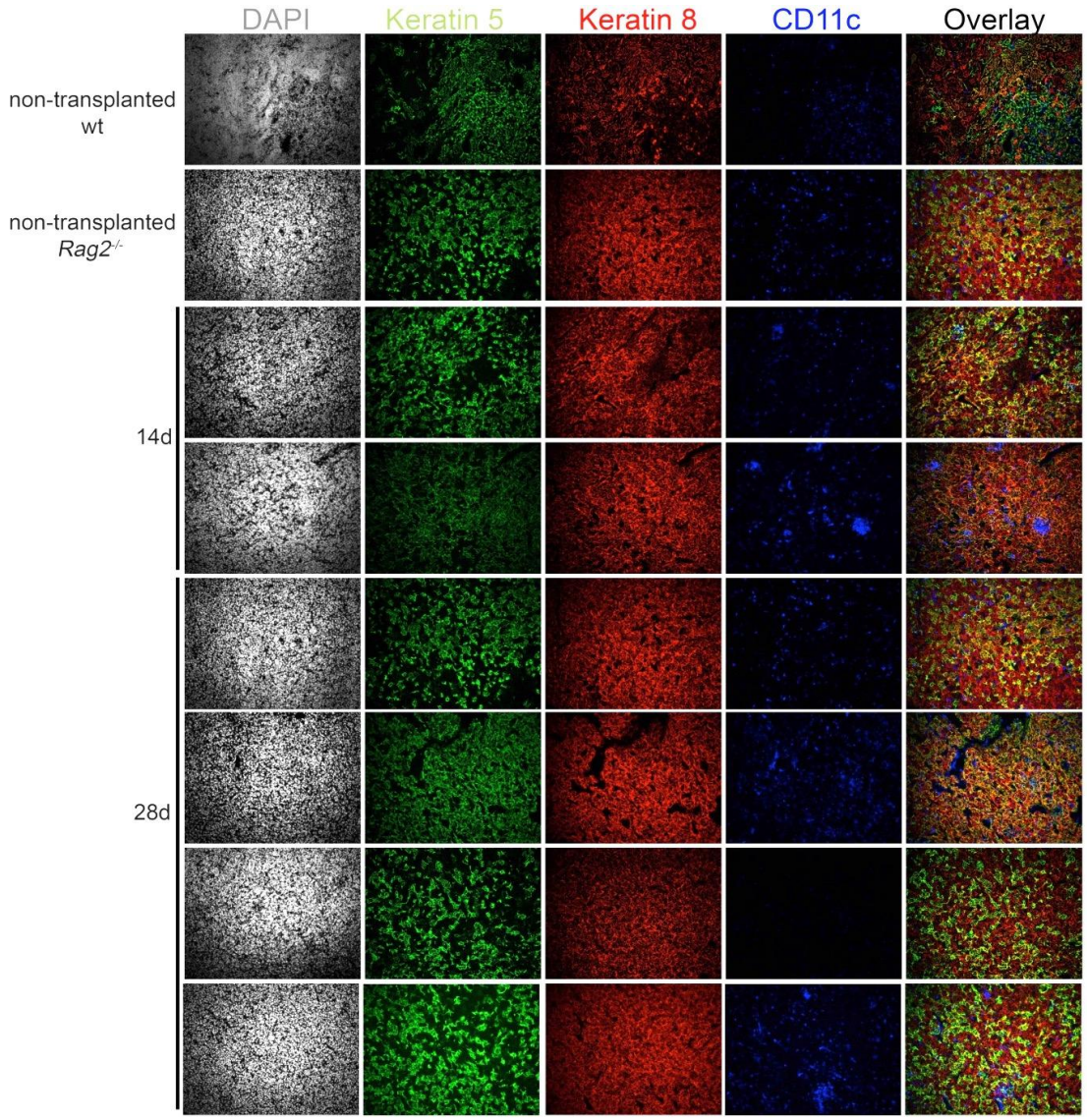

Figure 12- Photos of the split channels from immunohistology of sections from non-transplanted wild type B6 and *Rag2*$^{-/-}$ thymus, and of the grafted *Rag2*$^{-/-}$ thymi into *Rag2*$^{-/-}\gamma c^{-/-}$ recipients, 14 and 28 days after transplant. Staining for Dapi is represented in grey, for K5-Alexa 488 in green, for K8-Alexa 647 in red and for CD11c-PE in blue. In the right column are the overlays of all channels. Images were acquired in Leica DMRA2 microscope with the software MetaMorph using a 20x magnification.

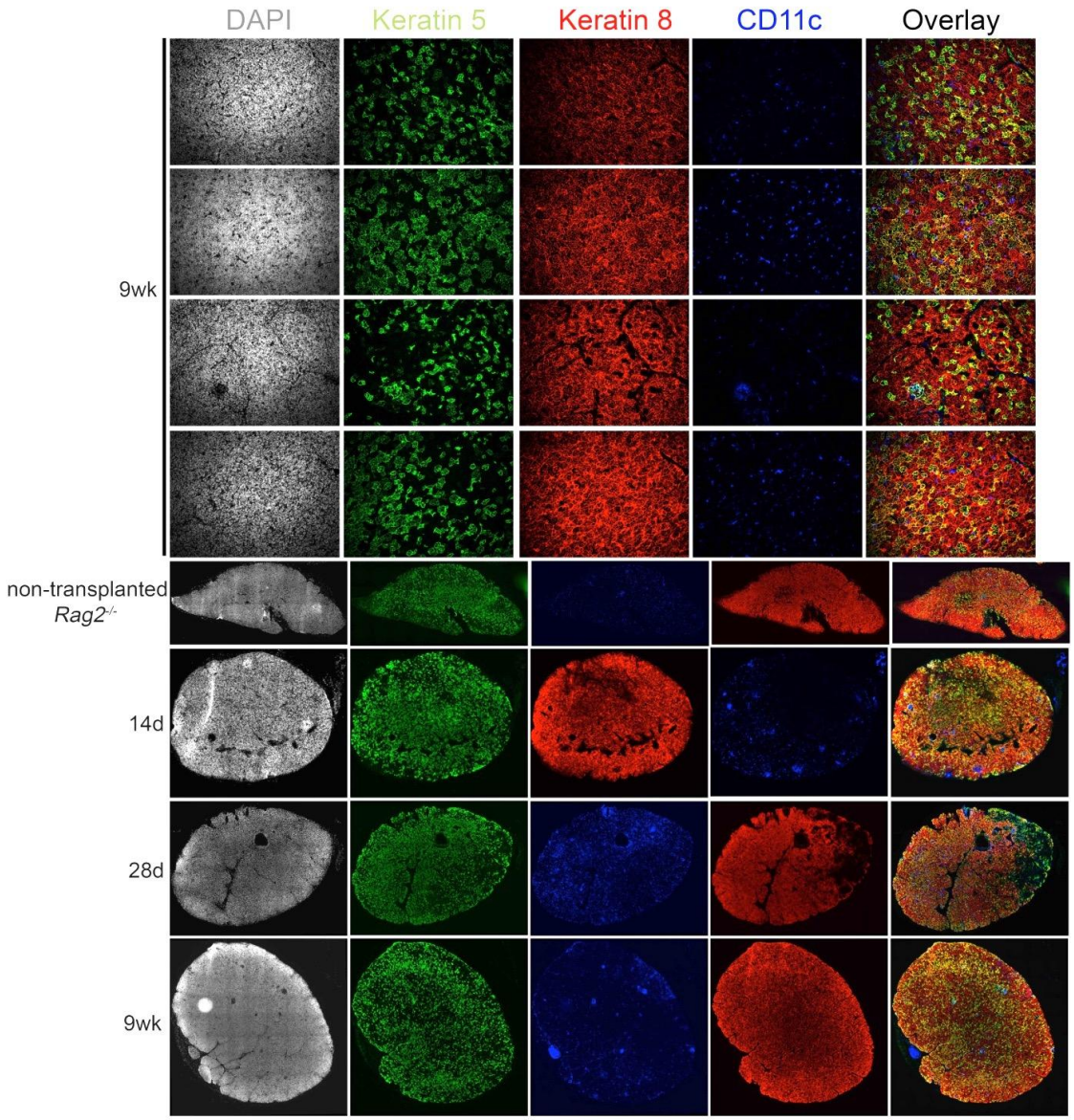

Figure 13- Photos of the split channels from immunohistology of sections from non-transplanted wild type B6 and *Rag2*$^{-/-}$ thymus, and of the grafted *Rag2*$^{-/-}$ thymi into *Rag2*$^{-/-}\gamma c^{-/-}$ recipients, 14, 28 days and 9 weeks after transplant. Staining for Dapi is represented in grey, for K5-Alexa 488 in green, for K8-Alexa 647 in red and for CD11c-PE in blue. In the right columns are the overlays of all channels. Images were acquired in Leica DMRA2 microscope with the software MetaMorph using a 20x magnification and in Nikon High Content Screening microscope with the software Nikon Elements also using a 20x magnification.

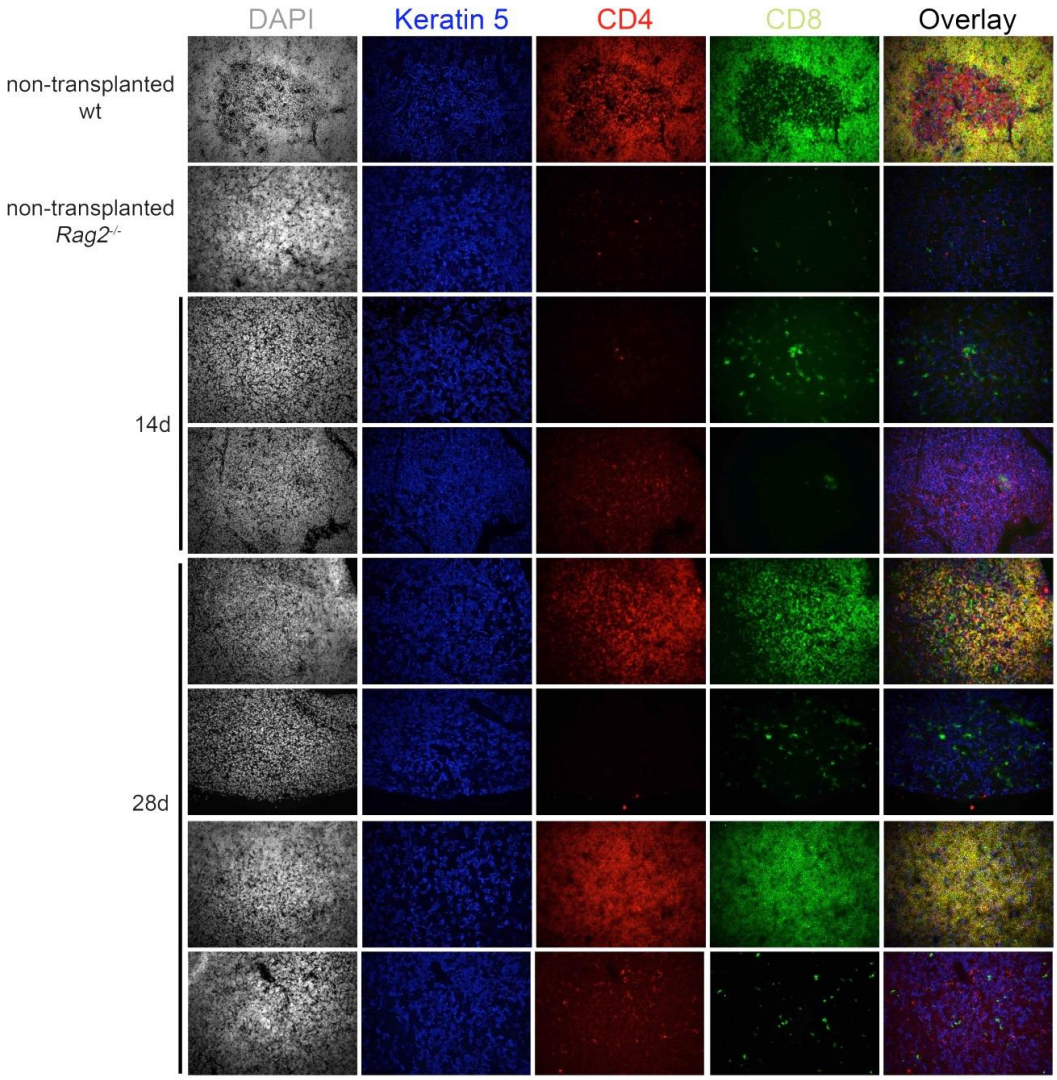

Figure 14- Photos of the split channels from immunohistology of sections from non-transplanted wild type B6 and *Rag2*$^{-/-}$ thymus, and of the grafted *Rag2*$^{-/-}$ thymi into *Rag2*$^{-/-}\gamma c^{-/-}$ recipients, 14 and 28 days after transplant. Staining for Dapi is represented in grey, for K5-Alexa 488 in blue, for CD4-bio-Streptavidin Cy3 in red and for CD8-APC in green. In the right column are the overlays of all channels. Images were acquired in Leica DMRA2 microscope with the software MetaMorph using a 20x magnification.

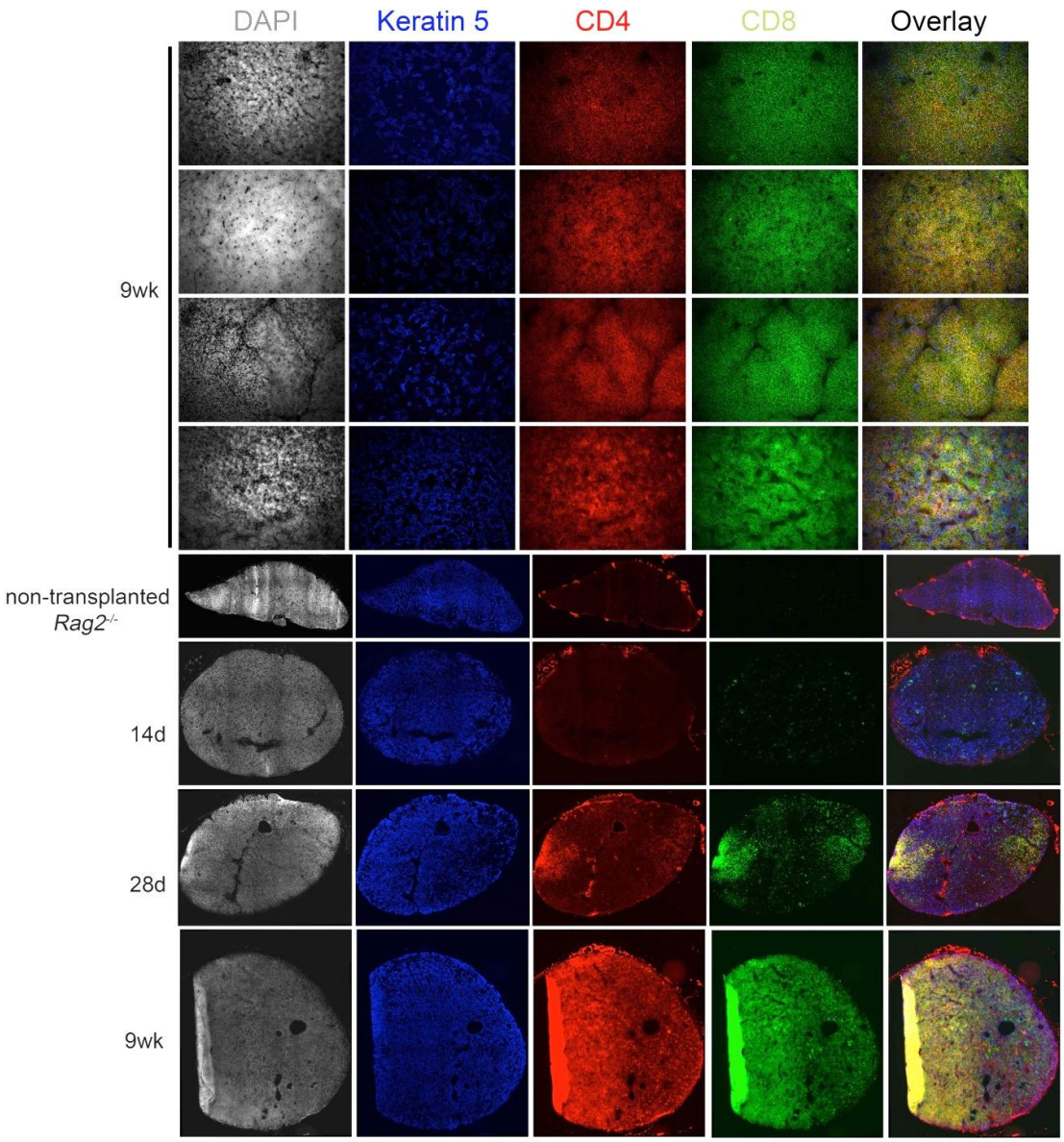

Figure 15- Photos of the split channels from immunohistology of sections from non-transplanted wild type B6 and *Rag2*$^{-/-}$ thymus, and of the grafted *Rag2*$^{-/-}$ thymi into *Rag2*$^{-/-}\gamma c^{-/-}$ recipients, 14, 28 days and 9 weeks after transplant. Staining for Dapi is represented in grey, for K5-Alexa 488 in blue, for CD4-bio-Streptavidin Cy3 in red and for CD8-APC in green. In the right columns are the overlays of all channels. Images were acquired in Leica DMRA2 microscope with the software MetaMorph using a 20x magnification and in Nikon High Content Screening microscope with the software Nikon Elements also using a 20x magnification.

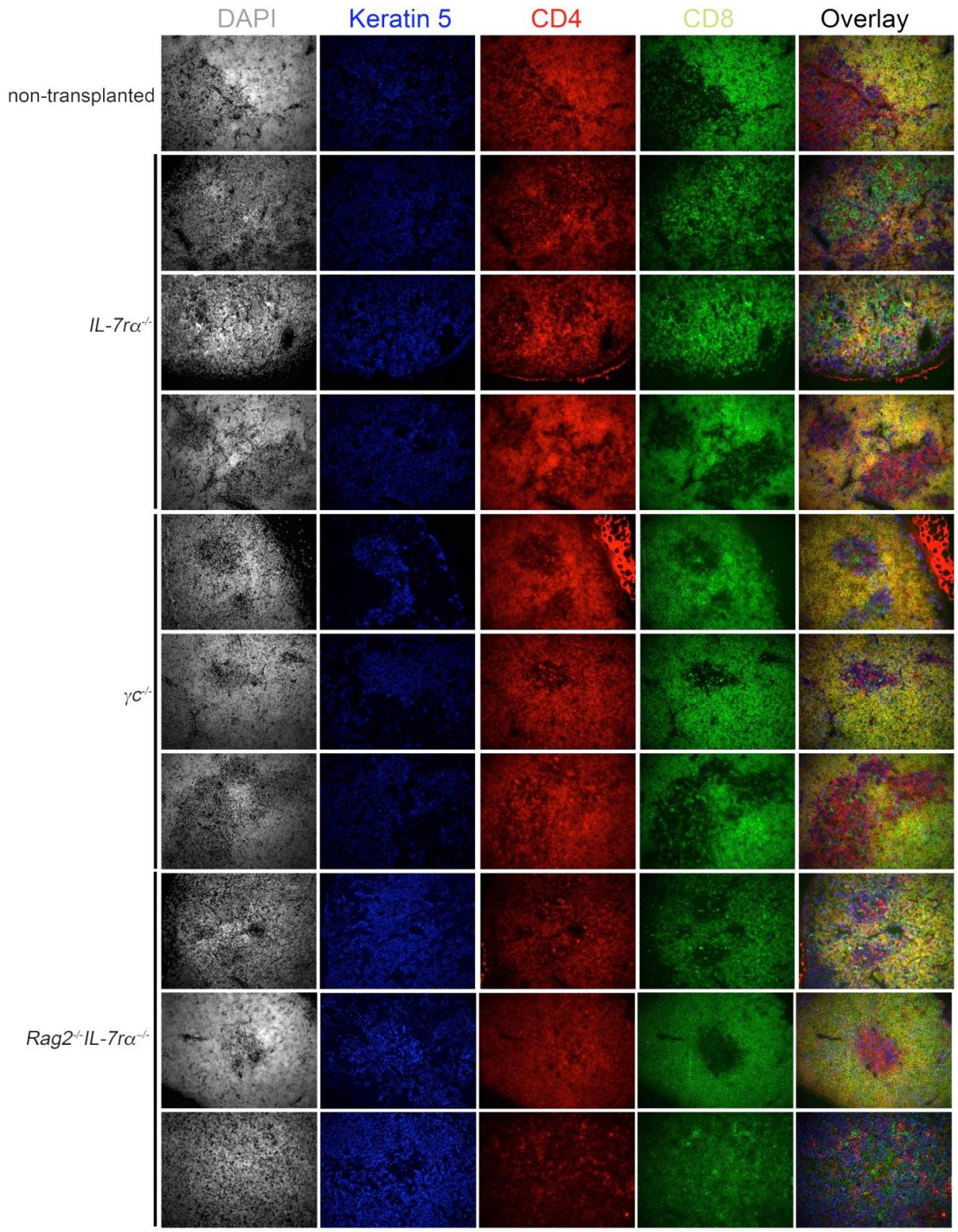

Figure 16- Photos of the split channels from immunohistology of sections from non-transplanted wild type B6 and of the grafted wild type thymi into *IL-7rα*$^{-/-}$, *γc*$^{-/-}$ and *Rag2*$^{-/-}$*IL-7rα*$^{-/-}$ recipients 9 weeks after transplant, as depicted. Staining for Dapi is represented in grey, for K5-Alexa 488 in blue, for CD4-bio-Streptavidin Cy3 in red and for CD8-APC in green. In the right columns are the overlays of all channels. Images were acquired in Leica DMRA2 microscope with the software MetaMorph using a 20x magnification.

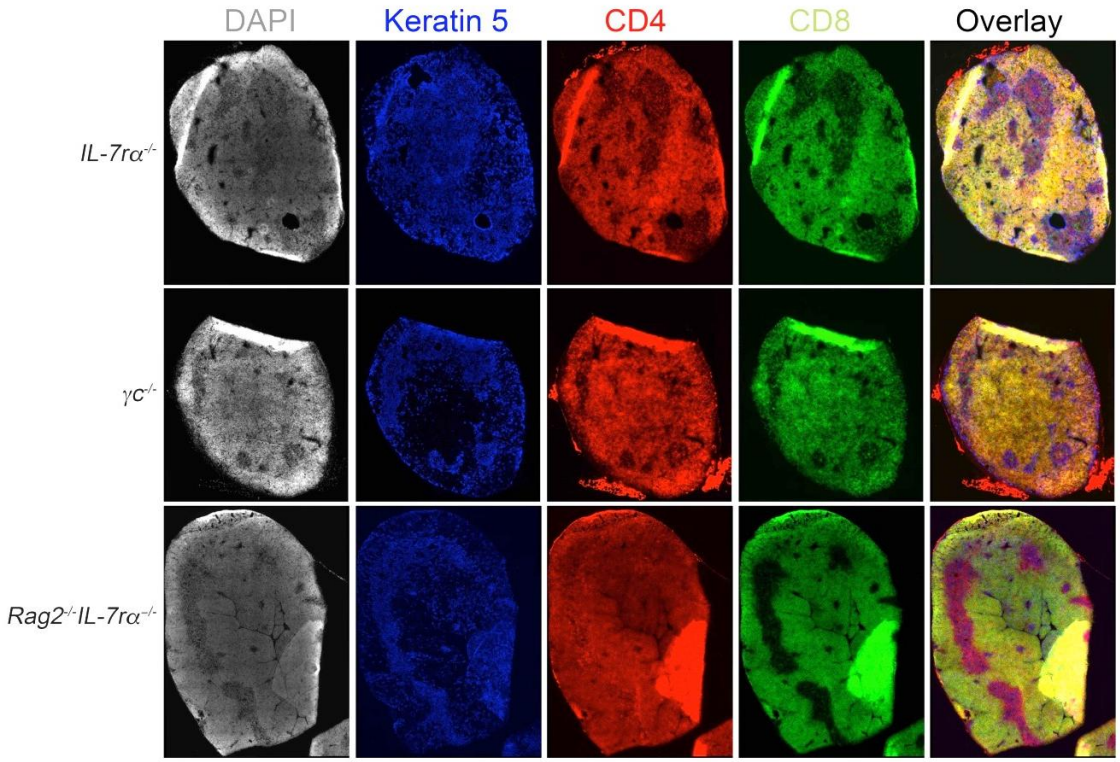

Figure 17- Photos of the split channels from immunohistology of sections of the grafted wild type thymi into *IL-7rα*$^{-/-}$, *γc*$^{-/-}$ and *Rag2*$^{-/-}$*IL-7rα*$^{-/-}$ recipients 9 weeks after transplant, as depicted. Staining for Dapi is represented in grey, for K5-Alexa 488 in blue, for CD4-bio-Streptavidin Cy3 in red and for CD8-APC in green. In the right column are the overlays of all channels. Images were acquired in Nikon High Content Screening microscope with the software Nikon Elements using a 20x magnification.

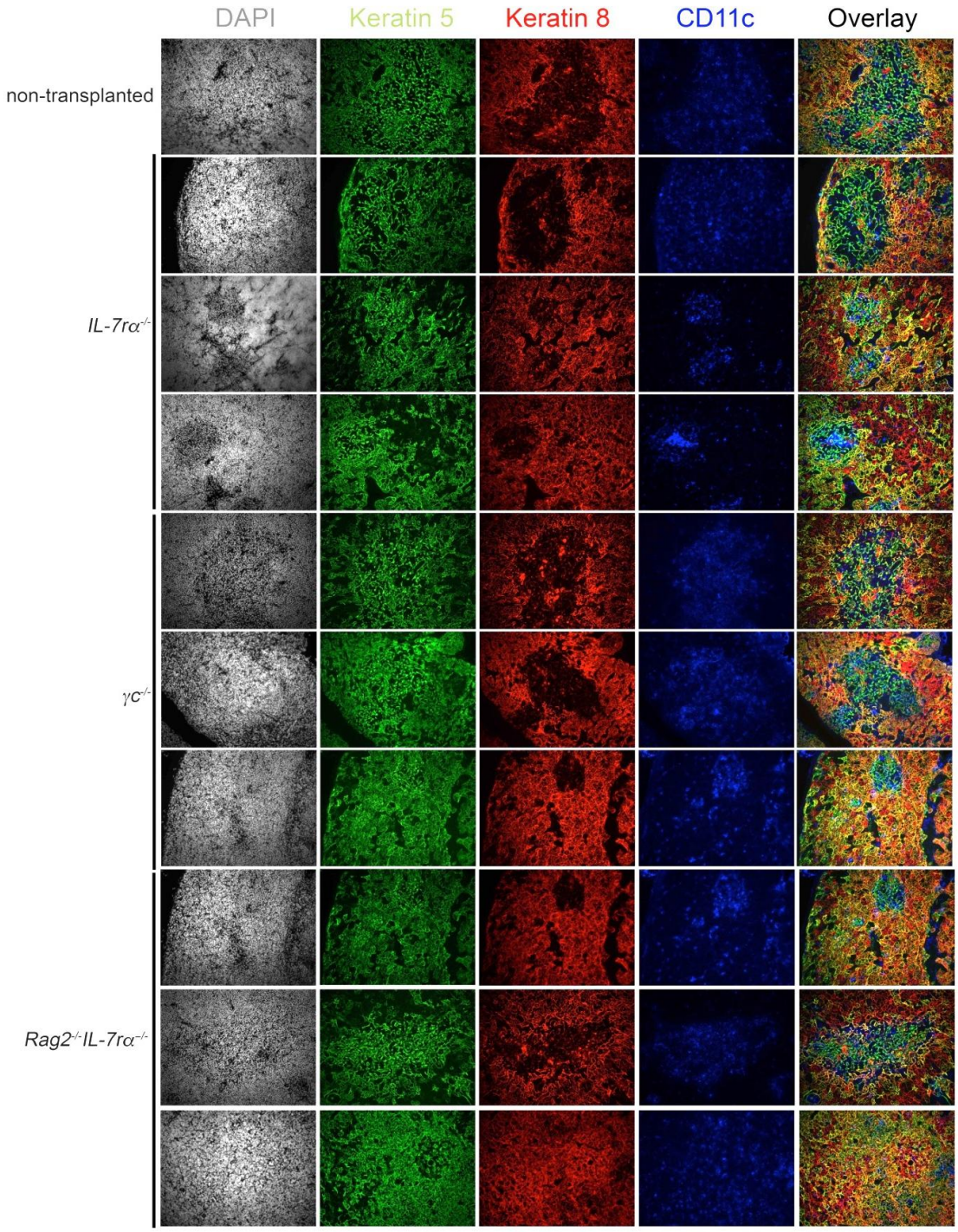

Figure 18- Photos of the split channels from immunohistology of sections from non-transplanted wild type B6 and of the grafted wild type thymi into *IL-7rα*$^{-/-}$, *γc*$^{-/-}$ and *Rag2*$^{-/-}$*IL-7rα*$^{-/-}$ recipients 9 weeks after transplant, as depicted. Staining for Dapi is represented in grey, for K5-Alexa 488 in green, for K8-Alexa 647 in red and for CD11c-PE in blue. In the right column are the overlays of all channels. Images were acquired in Leica DMRA2 microscope with the software MetaMorph using a 20x magnification.

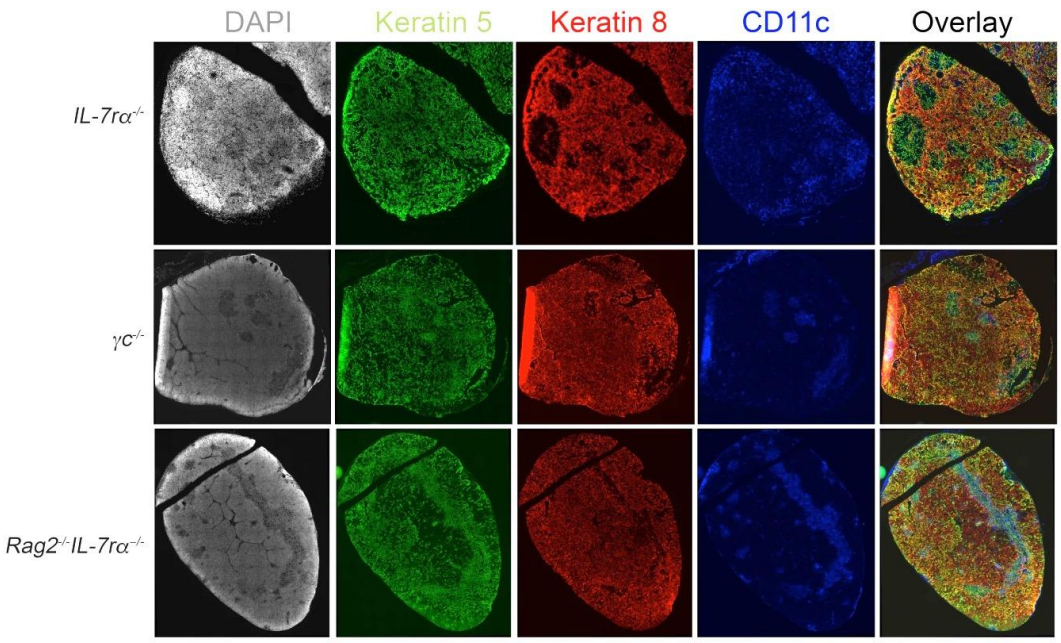

Figure 19- Photos of the split channels from immunohistology of sections of the grafted wild type thymi into *IL-7rα*$^{-/-}$, *γc*$^{-/-}$ and *Rag2*$^{-/-}$*IL-7rα*$^{-/-}$ recipients 9 weeks after transplant, as depicted. Staining for Dapi is represented in grey, for K5-Alexa 488 in green, for K8-Alexa 647 in red and for CD11c-PE in blue. Images were acquired in Nikon High Content Screening microscope with the software Nikon Elements using a 20x magnification.